REPORT NO. P74-438
HAC REF. NO. D0573

ELECTROMAGNETIC RADIATION SCREENING OF MICROCIRCUITS FOR LONG LIFE APPLICATIONS

INTERIM REPORT – NOVEMBER 1973 THROUGH OCTOBER 1974

W. G. BRAMMER
J. J. ERICKSON
M. E. LEVY

OCTOBER 1974

Prepared under Contract No. NAS8-30373 by
Applied Physics Department
Components and Materials Laboratories

AEROSPACE GROUPS
HUGHES
HUGHES AIRCRAFT COMPANY
CULVER CITY, CALIFORNIA

for

GEORGE C. MARSHALL SPACE FLIGHT CENTER
NATIONAL AERONAUTICS AND SPACE ADMINISTRATION
Marshall Space Flight Center, Alabama 35812

FOREWORD

This report is a summary of work performed on NASA contract NAS8-30373 during the period 1 November 1973 to 31 October 1974. This investigation was conducted for the George C. Marshall Space Flight Center, Huntsville, Alabama. The Contracting Officer's Technical Representative was Mr. M. J. Berkebile.

The work was performed within the Component Evaluation Department of Hughes Aircraft Company under the management of Mr. Robert D. Gourlay. Dr. William G. Brammer was the project engineer with Mr. James J. Erickson and Dr. Miguel E. Levy as major contributors. Test specimen examination with the scanning electron microscope was done by Mr. Kim Sandgren. Programming of the Tektronix S3260 microcircuit tester was done by Mr. Hiram L. Lodge.

ABSTRACT

A theoretical and experimental study has been carried out on the utility of X-rays as a stimulus for screening high reliability semiconductor microcircuits. The theory of the interaction of X-rays with semiconductor materials and devices was considered. Experimental measurements of photovoltages, photocurrents, and effects on specified parameters were made on discrete devices and on microcircuits. The test specimens included discrete devices with certain types of identified flaws and symptoms of flaws, and microcircuits exhibiting deviant electrical behavior. With a necessarily limited sample of test specimens, no useful correlation could be found between the X-ray-induced electrical response and the known or suspected presence of flaws.

CONTENTS

CONTENTS (Continued)

LIST OF ILLUSTRATIONS

LIST OF ILLUSTRATIONS (Continued)

LIST OF ILLUSTRATIONS (Continued)

LIST OF TABLES

1.0 INTRODUCTION

The increasing complexity of electronic systems intended for high reliability applications has generated the need for electronic components of unprecedented reliability. In the semiconductor component fabrication and procurement processes, inspection and screening procedures are used to assure the required high degree of reliability by the elimination of faults or errors in materials and processing. The precap visual inspection can be particularly cost-effective by eliminating defective devices before they are put through expensive electrical tests, burn-ins, or system assembly. Unfortunately, this critical inspection step is particularly vulnerable to error since it is performed by human operators applying criteria that are inevitably subjective. Results of visual inspection are never precisely repeatable. Moreover, many reliability hazards and flaws are not detectable either by visual inspection or conventional electrical tests.

Because the need for assuring very high reliability cannot be met economically by conventional testing or screening techniques when they are applied to complex microcircuits, there is a very strong motivation to explore unconventional testing techniques that may complement or supplant present techniques. One class of such innovative techniques would employ electromagnetic radiation to stimulate the uncapped device while the electrical response would be monitored at the device terminals. (Electrical responses could also be monitored at internal points of the circuit with a scanning electron microscope.) A theoretical study of this class of techniques was carried out at Hughes Aircraft Co. for NASA/Marshall SFC in 1972 (Contract No. NAS8-28937). In that study the relative merits of

localized versus flooding excitations were evaluated, and the effectiveness of different regions of the electromagnetic spectrum was explored.

This report presents the results of a program devoted to the evaluation of the use of X-ray flooding for screening microcircuits. The interaction of X-rays with materials and devices was examined both theoretically and experimentally to explore the possibility of enhancing detectability of flaws and reliability hazards. Since the intended application is as an auxiliary screen to accompany or complement precap visual inspection, potential or predictable insensitivity to certain types of flaws was not necessarily deemed a drawback.

Any experimental program to evaluate the effectiveness of a screening procedure for microcircuits must deal with one unavoidable difficulty — namely, that the presence of important kinds of reliability hazards can be established only by a destructive analysis. There are two sources for this problem. Some reliability hazards manifest themselves on finished devices only by a catastrophic failure. Other reliability hazards are detectable by electrical or other means on simple, discrete devices, but in a microcircuit their detectability is obscured by the complexity of the circuit. In either case the result is that microcircuits known to contain identified flaws are just not available in the non-failed condition required for screen evaluation.

The specimen availability problem was addressed in two ways in this program. One approach was to use simple devices with identified flaws or symptoms of flaws to represent the elements of microcircuits. The other approach was to use "maverick" microcircuits selected by testing the electrical specifications of a large number of microcircuits on an automated tester. Specimens believed to be normal or average were used for comparison purposes in both instances.

The more fundamental approach of using simple devices with flaws has the advantage that a meaningful correlation can be attempted between the established presence of flaws and electrical behavior during irradiation. Hypotheses based on device physics can be formulated and tested to explain the effects of different types of flaws on the behavior of the irradiated device. A disadvantage is that the effect of similar flaws on the behavior of

a complex microcircuit must remain undetermined. However, this drawback is more a result of the protean nature of the problem rather than of any inadequacy of the approach. As will be explained further on, an unqualified answer simply cannot be given to the question of the applicability of X-ray irradiation as a microcircuits screen. Electrical responses are too dependent on the circuit configuration and function. The best that this approach can promise is to yield electrical models of flaws for circuit analysis (for use with a computer-aided design and analysis program, if need be) to evaluate the applicability for a given microcircuit.

The alternate approach of using maverick microcircuits addresses the goal of the program directly. The apparent effects of irradiation in enhancing (or suppressing) differences in electrical behavior can be determined in a straightforward manner. However, the results thus obtained must be regarded as tentative, and their interpretation is subject to various pitfalls. The mere observation of a difference in behavior is not necessarily indicative of the presence of faults or reliability hazards. The difference must be evaluated for each type of chip relative to statistically established averages and standard deviations valid for normal chips of the same type. The establishment of statistically significant norms of behavior was beyond the scope of this program, so the experiments with microcircuits were confined to the recording of electrical parameters with and without irradiation.

The difficulty of non-destructively detecting faults that ordinarily manifest themselves by catastrophic device failure could be circumvented ideally by making special faulty test devices in a microcircuit processing facility. For this program that approach was considered impractical. One important type of fault that did seem amenable to available experimental methods is abnormally thin dielectric that can fail catastrophically as a result of an otherwise safe voltage transient. X-ray irradiation could be useful as an enhancing stress if it could be established that the irradiation causes a significant decrease in the breakdown voltage of the dielectric. The irradiation then could be used to induce failure in marginal devices. Exploratory experiments were conducted to determine whether the dielectric

breakdown voltage of SiO_2 was changed significantly during irradiation. The test devices were p-channel MOS transistors having nearly the same threshold voltages and, presumably, the same gate oxide thicknesses. The quantitative applicability of the results to other types of dielectrics is uncertain, although similar qualitative results may be expected for glasses made by doping SiO_2 during growth.

The theory of the mechanisms by which X-rays are expected to affect faulty and normal microcircuits is presented in this report in several stages. First the interaction of X-rays with materials used in microcircuit manufacture is reviewed. Then the effects of X-rays on subelements or features of microcircuits are discussed. The treatment is extended to cover transistors in both operating and inactive states. Finally the expected behavior of microcircuits is discussed. The theoretical treatment is prefaced by a brief review of X-ray sources.

Following the theoretical presentation is a description of the series of experiments that were performed. Each set of experiments is described in turn, and relevant conclusions are given. The report ends with conclusions and recommendations based on an overview of the theoretical and experimental results. Details about the experimental setups and apparatus are given in appendices.

2.0 THEORY OF THE EFFECTS OF X-RAYS ON MICROCIRCUITS

2.1 X-RAY SOURCES

Most X-ray sources generate radiation by the impact of an electron beam on a target anode. The radiation is generated by the acceleration of electrons during collisions and by radiative de-excitation of target atoms excited by electron impacts or by X-ray absorption.

The most widely used X-ray source, both in medical and industrial applications, is the Coolidge tube. It consists of a heated tungsten filament as an electron source or cathode, and a metal anode as the electron beam target. The cathode and the anode are enclosed in a sealed, evacuated envelope that is usually made of glass. X-rays exit from the tube through windows near the anode. The window material is selected to either absorb or transmit low energy X-rays in accordance with the intended application. For industrial applications requiring low energy X-rays the window is often made of beryllium.

The Coolidge tube is normally operated with the anode grounded and the cathode at a large, negative accelerating voltage, typically tens or hundreds of kilovolts. In most applications a steady X-ray output is not necessary, so a high AC voltage is applied to the tube via a step-up transformer. The tube acts as a half-wave rectifier, conducting current only when the cathode is negative with respect to the anode. A tube operated in this self-rectifying mode from 60 Hz power emits 60 X-ray pulses per second, each of about 8.3 msec duration.

The spectral distribution of X-rays from a Coolidge tube consists of a continuum with superimposed emission lines that are characteristic of the anode material. The continuum covers a photon energy range that extends from the maximum electron beam energy (numerically equal in electron-volts

to the accelerating voltage) to the lowest energy effectively transmitted by the tube window. The variation in intensity as a function of photon energy depends in a complicated way on absorption and scattering by the anode material of X-rays generated deep within the anode; it cannot be expressed in closed form by a simple, analytical expression. The emission lines superimposed on the continuum are the result of radiative transitions by atoms in the anode excited by electron collisions or by X-ray absorption. They occur at photon energies characteristic of elements in the anode, and they are labeled by the electron subshell in which a vacancy is filled during the radiative transition. The usual electric dipole transition selection rules apply.

Commonly available Coolidge tubes are intended for imaging or for diffraction, applications which ideally require a point source of radiation. The small source requirement places an upper limit on power dissipation beyond which the anode begins to vaporize or melt. In practice, X-ray tubes that operate at 30-150 KV have electron beam currents in the range of 1 mA to 15 mA, so that the input power to the tube is about 1.5 KW or less. This power limit can be raised by about an order of magnitude by the use of a rotating anode and/or water cooling. In any case, the total X-ray generation efficiency is less than 1 percent. The total intensity in the X-ray continuum produced by a tube with an anode made of a single element is given by

$$I = AiZV^2 .$$

V is the accelerating voltage, i is the tube current, Z is the atomic number of the anode material, and A is a constant of proportionality. The advantage of using a refractory heavy metal with high heat conductivity is evident from these considerations. When an intense X-ray continuum is desired, a tungsten anode is commonly used.

Although a small-source X-ray tube is not desirable for flooding because of power limitations, X-ray tubes with large-area sources are not readily available because there are so few applications for them. Commercial X-ray sources are therefore not optimum for flooding. Other X-ray generators that do not have a significant power limit (linear accelerators,

synchrotrons) are not practical for economic reasons for the purposes of this program.

2-2. THE INTERACTION OF X-RAYS WITH SOLID MATTER

X-rays can interact with solid matter in a variety of ways: X-rays can be scattered, both coherently and incoherently, or they can be absorbed. The absorption of an X-ray quantum by a solid results in the transfer of the energy of the quantum to the solid. The processes of interest here are those that result in a significant energy transfer to the electrons in the solid (i. e. , the photoelectric effect). Although certain specific details about the energy transfer mechanisms are still open questions, an adequate model for this discussion is one in which the absorption of an X-ray quantum results in the excitation of a single electron to a high kinetic energy E_p given by

$$E_p = h\nu - E_b ,$$

where ν is the X-ray frequency, h is Planck's constant, and E_b is essentially the electron binding energy. Since $h\nu$, the X-ray quantum energy, is of the order of several kilo-electron-volts while E_b can be as low as a few electron volts, for an order-of-magnitude estimate it can be assumed that

$$E_p \simeq h\nu .$$

Now, the behavior of the solid under X-ray irradiation depends on the fate of the energetic primary photoelectron. Unless the photoelectron escapes beyond the boundaries of the solid, its excess kinetic energy will be dissipated by collisions with atoms and with other electrons. The physical phenomena that accompany this de-excitation or energy dissipation depend largely on the electrical characteristics of the solid.

In a metal the number of electrons available for electrical conduction per unit volume is very large: of the same order of magnitude as the number of atoms ($\sim 10^{23} cm^{-3}$). With available X-ray intensities, a totally

negligible increase in the conduction electron density results from impact ionizations that accompany the photoelectron de-excitation.

In a semiconductor or insulator the de-excitation of the primary photoelectron can have much more dramatic effects. In these materials the total electron density available for excitation is comparable to that in metals; however, the number of electrons available for electric conduction can be many orders of magnitude smaller. Semiconductors and the inorganic insulators used in microcircuits have a range of energies (the forbidden gap) that, according to quantum-mechanical principles, are inaccessible to mobile electrons. At very low temperatures in pure materials the energy states below the forbidden gap are all occupied, while the states above the gap are empty. Both semiconductors and insulators then have very low electrical conductivity. At room temperature ($300^{o}K$) electrons in semiconductors can be thermally excited across the forbidden gap to the conduction band, so these materials are somewhat conductive. In insulators, however, the forbidden gap is so large that electrons cannot be thermally excited across it to any significant extent. Now, the kinetic energy E_p of the primary photoelectrons is much greater than the forbidden gap (or binding energy E_b) in either semiconductors or insulators, so that as the photoelectron collides with other electrons it excites them across the gap. The energetic secondary electrons collide with other electrons, which are in turn excited across the gap. These impact ionization processes continue until all of the original X-ray quantum energy has been used up. Since the collisions and ionizations are essentially random, the total number of secondary electrons resulting from the absorption of one X-ray quantum of energy $h\nu$ is a random variable. The average value of this number is $\langle n \rangle = h\nu/E_o$, where E_o is a constant that is characteristic of the material. E_o is always greater than the forbidden gap E_g because some of the X-ray quantum energy is used up in thermally exciting the crystal lattice (or network, for glasses). For Si, $E_o = 3.5$ eV, while $E_g = 1.12$ eV. The absorption of a single 140 KeV X-ray quantum in Si generates about 40×10^3 electrons (and an equal number of holes) that are available for electrical conduction.

The electrical effects of the X-ray-induced excess density of charge carriers depends on the carrier mobilities, which are different in different materials. In particular, the mobility of holes in SiO_2 is very low, while the mobility of electrons is significant. The passage of an electric current through SiO_2 during X-ray irradiation can be expected to leave a space charge of immobile positive charges as a result (Andre et al. 1969). Electrical effects in Si will depend on the number of carriers already present as a result of doping and thermal excitation. A given level of incident X-ray intensity therefore will cause a greater relative change in the conductivity of lightly doped regions than in that of heavily doped regions. The most important effects will occur in depleted regions, which have a negligible background density of carriers.

During absorption of sufficiently energetic X-ray quanta, enough energy may be transferred to the lattice or network of atoms comprising the solid that atoms are knocked out of their usual sites. Like impact ionization, such atomic displacement processes are random, and the energy threshold below which they do not occur is not sharp. They can be safely neglected for X-ray energies below 250-300 KeV.

At the other end of the energy scale, the absorption of a low energy photon produces a primary photoelectron that is energetically incapable of causing further ionization. For Si a rough order-of-magnitude estimate for the energy of such a photon is $h\nu < E_o + E_g = 4.62$ eV. This corresponds to a wavelength $\lambda = 268$ nm, in the near ultraviolet. The lowest energy for which a photon absorption process can excite a photoelectron in pure Si is $E_g = 1.12$ eV, for which $\lambda = 1107$ nm, in the near infrared. The absorption of a single light quantum therefore generates a single hole-electron pair.

Up to this point the effects of X-ray absorption have been reviewed in very general terms without consideration of the rate at which the absorption processes occur. The rate at which energy is transferred from an incident X-ray beam to a solid depends on the linear absorption coefficient μ and the intensity I of the beam. For a frequency interval $d\nu$, the spatial rate of decrease of the X-ray beam intensity is described by Lambert's Law:

$$-dI = \mu I \, dx \ ,$$

which can be integrated over a distance x to give

$$I = I_o \exp\left(-\frac{\mu}{\rho}\rho x\right) .$$

The ratio of the linear absorption coefficient μ to the density ρ is known as the mass absorption coefficient. It is particularly convenient because it is essentially independent of the state of aggregation or phase (gas, liquid, or solid) of the element. For a material consisting of n chemical elements:

$$\left(\frac{\mu}{\rho}\right)_{TOTAL} = \sum_{i=1}^{n} \chi_i \left(\frac{\mu}{\rho}\right)_i ,$$

where χ_i is the mass fraction of the i^{th} element.

The mass absorption coefficient for a pure element is a piece-wise continuous function of energy with discontinuities (called "absorption edges") at certain energies that are characteristic of the element. The absorption edges occur at the threshold energies for the excitation of an electron out of an atomic core state to the conduction band or continuum of the solid. Between absorption edges, the dependence of $\frac{\mu}{\rho}$ on energy and atomic number is described by

$$\frac{\mu(E)}{\rho} = \frac{CZ^4}{E^3} .$$

The proportionality constant C changes abruptly at each absorption edge. Now by making use of Lambert's Law, the energy E_o required to produce a hole-electron pair, and the spectral distribution $I_o(E)$ of the X-ray beam, it is possible to deduce the magnitude and spectral distribution of the excess carrier density produced by X-ray absorption. For X-ray intensity I(E)

measured in photons $sec^{-1} sr.^{-1}$ per unit energy interval, the power absorbed in thickness dX is

$$dP = -EdI = E\mu I dX .$$

The carrier generation rate dG is

$$dG = \frac{E}{E_o} \mu(E) I_o(E) \bar{e}^{\mu(E)X} dX$$

per unit energy range. The integal over energy gives the carrier generation ΔG per unit length

$$\Delta G = \int \frac{E}{E_o} \mu(E) I_o(E) \bar{e}^{\mu(E)X} dE .$$

Both $I_o(E)$ and $\mu(E)$ are determined experimentally. The integral over energy is evaluated numerically for a given experimental geometry and apparatus. Once ΔG is known, its effect on conductivities can be computed by noting that the resulting increases in carrier concentrations Δn and Δp are each given by $\tau \Delta G$, where τ is the carrier lifetime.

Insight into the relative efficiencies of different X-ray energies for carrier generation can be gained by integrating dG over X for some particular energy interval dE

$$\Delta G = \frac{E}{E_o} I_o(E) \int_o^L \mu e^{-\mu X} dX = \frac{E}{E_o} I_o(E) \left(1 - e^{-\mu L}\right) .$$

Two extreme cases can be considered:

(a) $$L >> \frac{1}{\mu} , \qquad \Delta G \approx \frac{E}{E_o} I_o (E)$$

as expected since all of the incident power is absorbed.

For

$$L = \frac{4}{\mu} , \qquad \left(1 - e^{-\mu L}\right) \approx 0.982 ,$$

and less than 2 percent of the incident power is not absorbed.

(b) $$L << \frac{1}{\mu} , \qquad \text{so} \qquad \left(1 - e^{-\mu L}\right) \approx \mu L$$

Then

$$\Delta G \approx \frac{E}{E_o} I_o (E) \mu L .$$

$$\mu \propto \frac{Z^4}{E^3} , \qquad \text{so} \qquad \Delta G \propto \frac{Z^4 L}{E^2}$$

Thus for a given element of atomic number Z and specimen thickness L, the lower energy X-rays are more effective in generating carriers. The value of L for which 98 percent of the incident X-ray power is transmitted (and therefore lost for carrier generation purposes) is

$$L = \frac{0.02}{\mu} .$$

For typical microcircuits, the active devices are within 10 μm of the chip surface, so the X-ray energies that are efficient in carrier generation are those for which $\mu >> 20\ cm^{-1}$.

Figure 2-1 shows the linear absorption coefficient (in units of cm^{-1}) for Si over the energy range of 0.5 KeV to 100 KeV. The data were taken from publications by Henke (1969) and Grodstein (1957). The large range of variation — nearly five orders of magnitude — is particularly noteworthy. The K absorption edge is the discontinuity at 1.840 KeV. The figure shows that $\mu > 20\ cm^{-1}$ only for $E \leq 16$ KeV. Figure 2-2 similarly shows the absorption spectrum for Al (from the same publications). Except for the fact that the K absorption edge for Al occurs at 1.559 KeV, it is clear that the absorption coefficients for Si and Al are nearly the same. To a very good degree of approximation, it can be assumed that the effects of absorption by Al metallization (i.e., casting "shadows" on underlying devices) are the same as would result from the same thickness of Si. For SiO_2 the mass absorption coefficient will be roughly the same as that of Si; since the ratio of the densities is ~ 0.945, the linear absorption coefficient also will be roughly the same.

Figure 2-3 shows the spectral distribution of a Coolidge tube equipped with a thick tungsten anode and operated in the self-rectifying mode at 100 KV peak. The data were taken from a published spectrum (Storm et al., 1971) and are believed to be representative of the output expected from one of the X-ray sources used for this program. Output intensity is shown normalized to 1 mA tube current and radiation into 1 steradian. This normalized spectral distribution was experimentally determined (ibid.) to be independent of the tube current, as expected on theoretical grounds.

With the data in Figures 2-1 and 2-3, the carrier generation rate (cm^{-3}) was computed for various depths in Si ranging from 1 μm to 200 μm. An anode-to-specimen distance of 34.6 cm was assumed. (This was the distance used in most of the experimental work for this program.) The results for 1 mA of tube current are shown in Figure 2-4. Taking 10 μm as typical of the maximum depth for active regions of microcircuits, it is apparent that the carrier generation rate has about a 30 percent variation

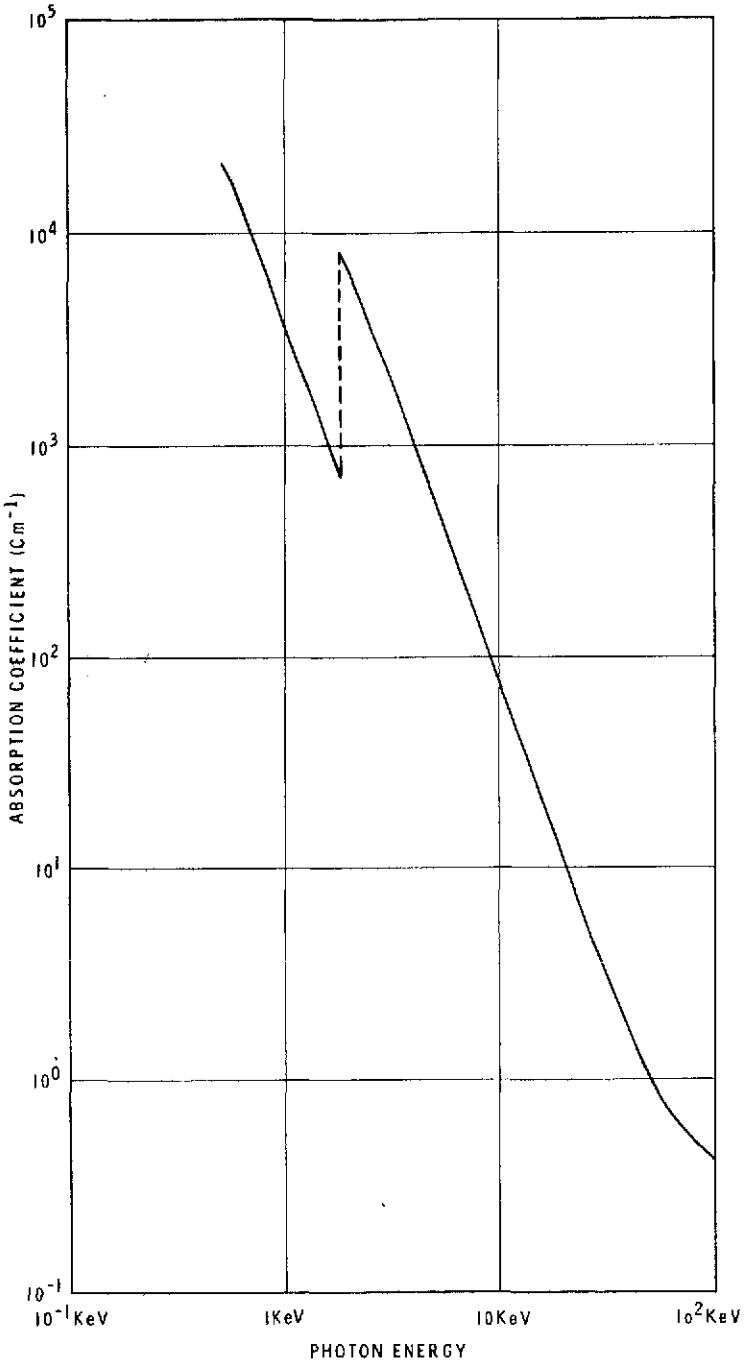

Figure 2-1. X-ray absorption spectrum for Si.

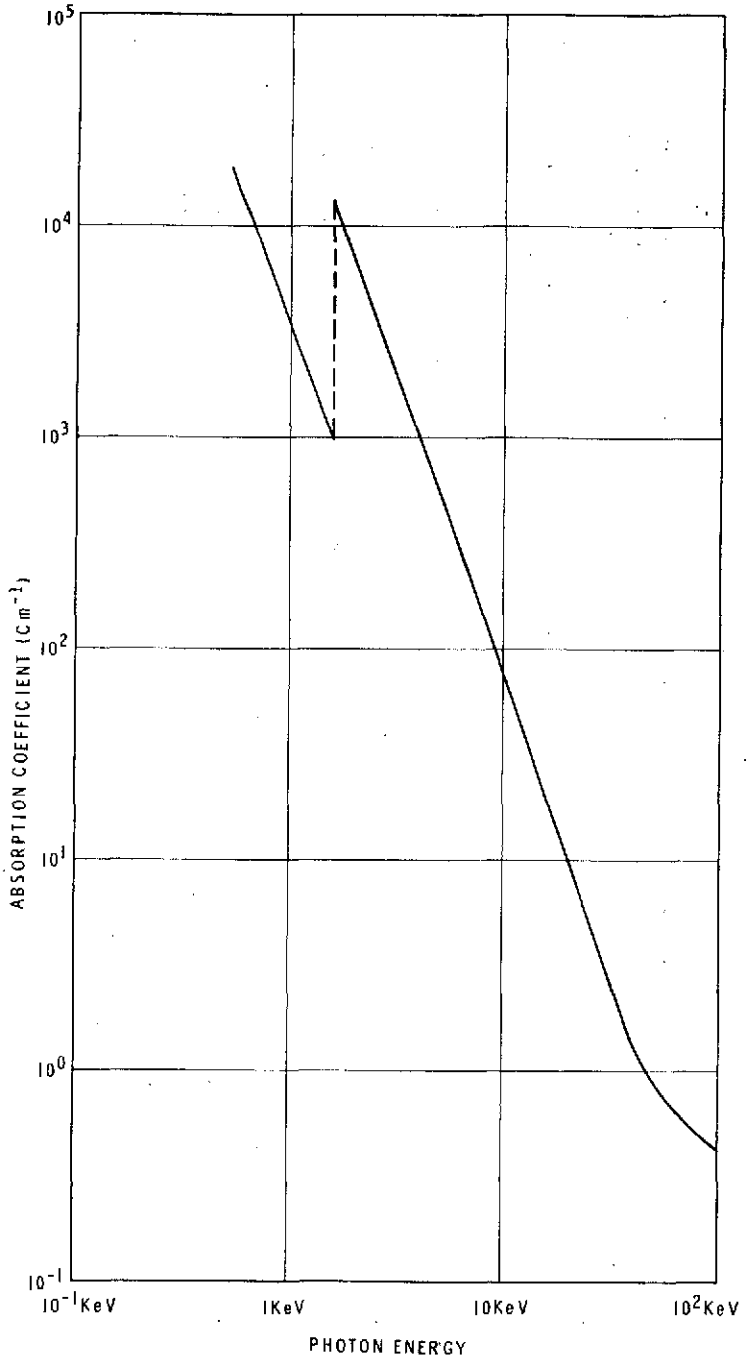

Figure 2-2. X-ray absorption spectrum for Al.

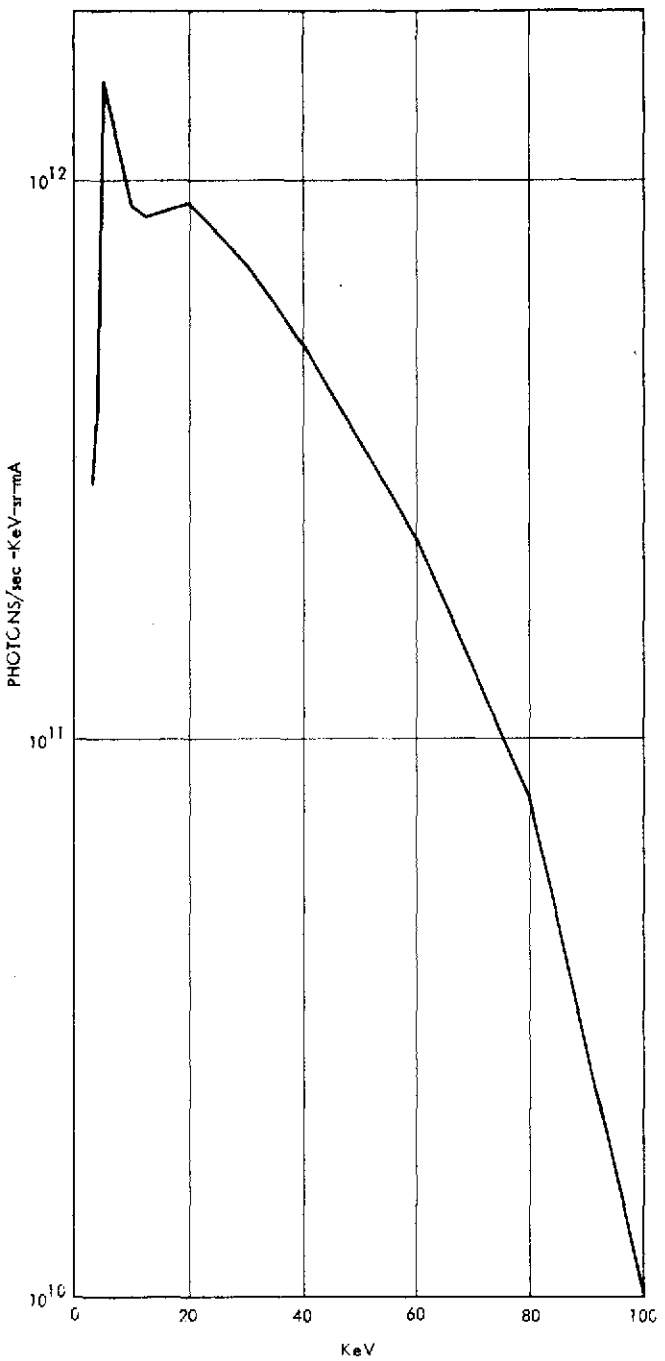

Figure 2-3. Spectral distribution of X-rays from thick tungsten anode Coolidge tube.

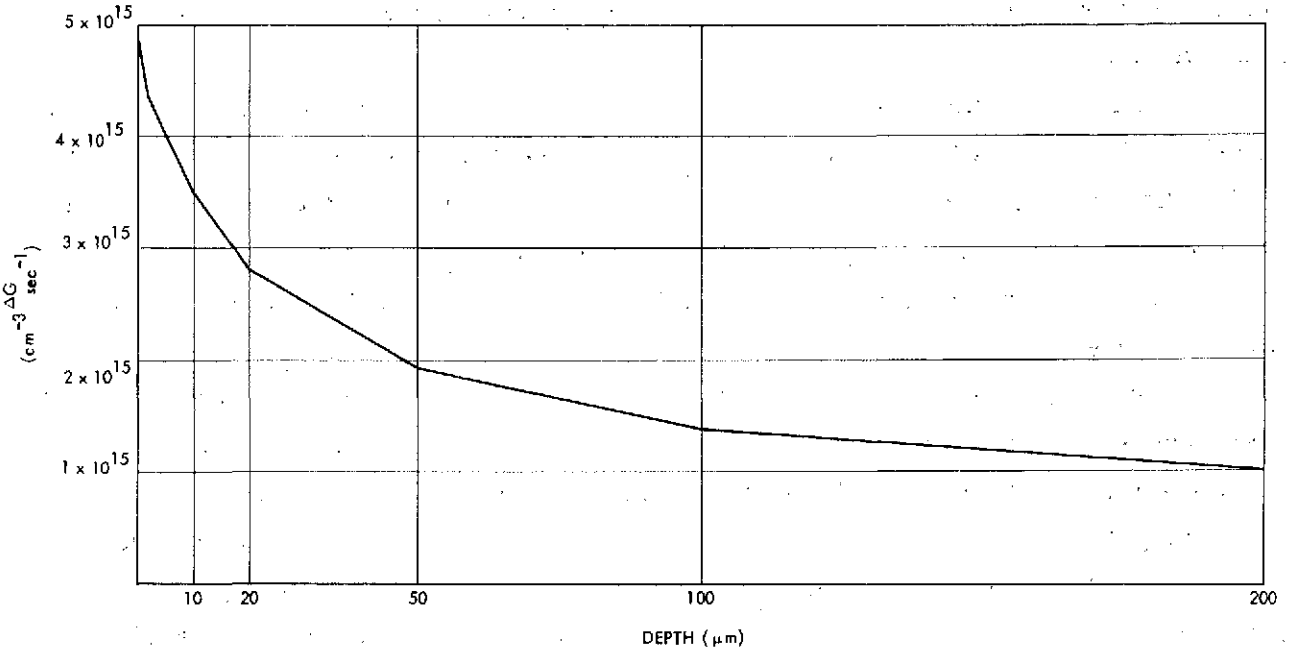

Figure 2-4. Computed carrier generation rate in silicon, normalized to 1 mA tube current, and 34.6 cm anode-to-specimen distance.

over this depth. Near the bottom of the substrate (~ 200 μm) the generation rate has decreased by about a factor of 4. For integrated circuits the carrier lifetime varies from nanoseconds to microseconds. If $\tau \approx 10$ μsec is taken as an approximate upper limit, the results in Figure 2-4 show that even with a tube current of 20 mA only excess densities $An = \Delta p \leq 10^{12}$ cm^{-3} can be achieved. These values are well below normal doping levels in semiconductor devices, so irradiation effects cannot be expected to occur in any phenomena governed by majority carrier concentrations. Only those phenomena that depend on minority carrier concentrations or occur in depleted regions will be affected.

2.3 IRRADIATION EFFECTS ON HETEROGENEOUS INTERFACES — PHOTOELECTRON INJECTION PHENOMENA

When an X-ray absorption event creates an energetic photoelectron near an interface between different materials, one possible outcome is that the primary photoelectron and/or energetic secondaries can cross the interface from one material to the other. The result is that a net transfer of charge takes place. The probability of such an event is governed by, among

other factors, the energy barrier or work function difference between the two materials.

The work functions between different materials are never larger than several electron volts. Compared to the kilo-electron-volt energy of a primary photoelectron generated by X-rays, the work function is negligible. In general, then, it can be expected that X-ray irradiation of a materials interface will result in charge transfer (and, hence, an electric current) between the two materials.

The important heterogeneous interfaces in microcircuits are between dielectrics and the conductive materials (semiconductors or metals). The phenomenon of charge injection into or out of dielectrics (specifically SiO_2) is particularly significant for this study, both during irradiation and after. The discussion on bulk effects showed how irradiation of dielectrics can induce a conductivity enhancement during the irradiation. It was also mentioned that the passage of an electric current through SiO_2 generates a permanent, positive space charge that has been attributed to the immobility of holes. Thus in a powered device the irradiation-induced conductivity in dielectrics (masking and passivating glasses, as well as gate oxides in MOS devices) can result in a permanently charged dielectric. This charging effect is complicated by injection effects at interfaces. Experiments with MOS structures and devices have yielded data that can be explained (Esteve and Buxo 1970) by a mechanism in which there is a net electron current injected out of the SiO_2 into the Si substrate and the Al electrode. The net induced space charge depends on the applied fields, so that MOS transistor threshold voltage shifts are dependent on the gate voltage during irradiation.

One material interface that was found in the present study to introduce experimental complications is that between metal conductors and the ambient atmosphere. As will be explained further on, an empty transistor socket exposed to the X-ray beam was found to produce a detectable photovoltage, presumably as a result of photoelectrons emitted from the metal contact. A similar effect can be expected from the surface of any device under irradiation. That signal, however, will be characteristic of the device and not a completely spurious artifact, as is the signal produced by the device socket.

2.4 IRRADIATION EFFECTS ON P-N JUNCTIONS

The effect of X-ray-induced carrier generation ΔG at a p-n junction is quite unlike what occurs at a heterogeneous interface because the material on either side of the junction is essentially the same. There is no net photoelectron injection. The features of p-n junctions that can lead to special irradiation effects are:

1. The different conductivities and carrier types on each side of the junction and,
2. The depletion layer and its built-in electric field.

In the vicinity of the junction (but not in the depletion region) the semiconductor is essentially in thermal equilibrium. Even in an operating device the non-equilibrium carrier concentrations can be described by introducing suitable modifications (e.g., substitution of Imrefs for the Fermi potential) into the theories for thermal equilibrium. The effects of irradiation-induced carrier generation ΔG are then given by $\Delta n = \Delta p = \tau \Delta G$ as for bulk material.

Within the depletion region, there is an electric field due to the unshielded dopant ions which is directed from the n side to the p side. Electron-hole pairs generated within the depletion region are separated by the field and swept into the non-depleted regions on either side. Electrons are swept into the n side and holes into the p side. Excess carriers generated within a diffusion length on either side of the depletion layer will diffuse close enough to be swept apart by the built-in field. If W is the depletion layer width, and L_n and L_p the diffusion lengths for electrons and holes, respectively, the generated carriers are collected by the built-in field over a width $\sim W + L_n + L_p$.

If the irradiated junction is not forward-biased and has a low resistance shunt across it, the irradiation-generated carriers swept apart by the junction field will cause a short-circuit photocurrent I_{phsc} to flow in the shunt. The current through the junction will flow in the reverse direction since it is, in fact, an X-ray-enhanced generated-recombination current. (In Si, the generation-recombination component of the reverse saturation current predominates over the minority carrier diffusion component). For a planar junction of area A the photocurrent will be

$$I_{phsc} = A(W + L_n + L_p)\,(2\,q\,\Delta G)$$

For a non-planar junction, the factor $A(W + L_n + L_p)$ is replaced by an effective depleted volume V_α.

If the irradiated junction is not forward-biased and is effectively open-circuited, the carriers separated by the junction field will set up a voltage tending to forward bias the junction. The open circuit photovoltage V_{phoc} is obtained from the junction equation as

$$V_{phoc} = \frac{KT}{q} \ln \left(\frac{I_{phsc}}{I_o} + 1 \right) .$$

I_o is the reverse saturation current for an ideal junction.

If the irradiated junction is shunted by a finite, non-negligible load resistance, the photovoltage builds up to some value $V_{phr} < V_{phoc}$. The forward leakage current due to this voltage will subtract from the short-circuit photocurrent to give

$$I_{phr} = I_{phsc} - I_o \left[\exp \left(\frac{qV_{phr}}{KT} \right) - 1 \right] .$$

I_{phsc} varies linearly with ΔG and hence with absorbed radiation intensity. It is directly proportional to the effective junction volume. I_{phr} is also dependent on junction dimensions (area), while V_{phoc} is not.

For irradiation intensity levels being considered here, the effects on forward-biased junctions are negligible. In the junction equation

$$I = I_o \exp \frac{qV}{KT} - I_o ,$$

the exponential term is the injection current, while the second term corresponds to reverse leakage of minority carriers. The injection term depends on majority carrier densities and hence is negligibly perturbed by irradiation.

Reverse leakage depends on minority carrier densities, which are perturbed significantly by irradiation. However, under forward bias the injection current predominates to such an extent that the overall effect of the irradiation is quite minimal.

2.5 EFFECTS OF IRRADIATION ON BIPOLAR TRANSISTORS

A convenient model for a bipolar transistor (biased as an amplifier) is that of a structure in which the reverse saturation current in one p-n junction (the base-collector junction) is controlled by the current through another, forward-biased junction (the emitter-base junction). Within this conceptual framework, the above discussion on p-n junctions can be extended to transistors in a relatively straightforward manner.

When the transistor is not biased, the photovoltage and photocurrents behave qualitatively as for isolated junctions. However, for a given junction, the presence of other junctions at a distance smaller than a carrier diffusion length will cause a decreased response to the X-ray stimulus. In effect, the junctions (base-collector, emitter-base, and isolation) compete with each other for the excess carriers. The outcome of this competition depends on the magnitude of the separation, on the carrier lifetimes on the intervening, non-depleted material, and on the presence of built-in drift-fields. Variations in these and other parameters (e.g., junction areas) therefore will affect the response level.

When the transistor is biased, the effects of the irradiation are very much dependent on the mode of operation. If the transistor is switched on and in saturation, both the base-emitter and base-collector junction are forward-biased. By arguments presented previously, the effects of irradiation will be very small.

If the transistor is biased into cut-off, none of the junctions are forward-biased, and the expected behavior will be qualitatively similar to that of the unpowered device. Differences will arise (1) as a result of the widened depletion regions due to applied voltages; (2) if the number of carriers generated in the base region is enough to turn the device on; or (3) if a large number of carriers generated in the base-collector junction is able to initiate

an avalanche. With the carrier densities that can be generated by a conventional X-ray machine, only the depletion widening effect is likely to be significant.

When the transistor is biased in its active region (emitter-base forward biased and base-collector reverse biased), the amplifying properties of the device come into play. The excess carriers collected by the base-collector junction then are added to the thermally generated reverse leakage current of the base-collector junction. In microcircuits with junction isolated devices, the isolation junction is typically at a distance not much larger (if at all) than a diffusion length from the base-collector junction. Thus some of the carriers generated in the undepleted collector region are collected by the isolation junction.

Figure 2-5 shows an equivalent model of a junction isolated n-p-n transistor. The thermal and irradiation-induced currents are represented by current generators added externally to an ideal transistor and an ideal isolation junction diode. The maximum effect of the irradiation will occur with the base open; then the thermal and irradiation-induced contribution to the emitter current is

$$I = (\beta + 1)\left(I_{ph}^{bc} + I_{th}^{bc}\right) ,$$

while the contribution to the collector current is

$$I_c = (\beta + 1)\left(I_{ph}^{bc} + I_{th}^{bc}\right) + \left(I_{ph}^{cs} + I_{th}^{cs}\right) .$$

β is the current gain of the transistor, while the currents I are as defined in Figure 2-5: the superscript identifies the junction in which the current is collected, while the subscript denotes the driving force for the carrier generation.

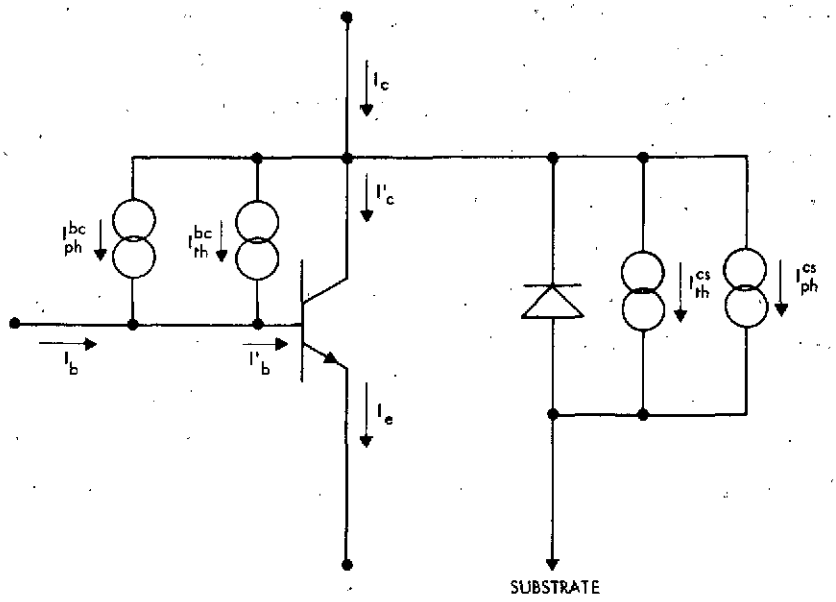

Figure 2-5. Equivalent model of n-p-n junction-isolated transistor under irradiation.

When the base circuit is not open, the effects of I_{ph} and I_{th} must be analyzed for the circuit configuration of interest. It is clear, however, that with the transistor in the active region, some portion of $\left(I_{ph}^{bc} + I_{th}^{bc}\right)$ will be amplified by the current gain of the transistor. The magnitude of the effect will depend on three device parameters $\left(I_{th}^{bc}, I_{th}^{cs}, \text{and } \beta\right)$, on the device and irradiation dependent responses I_{ph}^{bc} and I_{ph}^{cs}, and on the circuit.

2.6 MANIFESTATIONS OF FLAWS IN THE RESPONSES OF MICROCIRCUIT ELEMENTS TO IRRADIATION

Flaws in microcircuit elements can affect the irradiation response, either because they directly alter structural parameters that determine the response or because they interfere with the response. The effects of structural variations caused by flaws can be deduced from an analysis of the dependence of the response on structure. The manner in which flaws interfere with the response cannot be treated quite as generally, so it is discussed here on a case-by-case basis.

The fundamental responses of unpowered devices are the open circuit photovoltage V_{phoc} and the short circuit photocurrent I_{phsc}. At a given, fixed irradiation intensity the photocurrent is proportional to an effective depleted volume V_d, which can be approximated by $A(W + L_n + L_p)$ for isolated junctions. Any structural variation or flaw that affects V_d therefore will affect the photocurrent directly. More subtle effects can be expected in transistors, where the junctions in effect compete for generated carriers. Variations in the thickness of the undepleted base region will affect the way in which irradiation-induced excess carriers are distributed between the base-emitter and base-collector junctions. Similar effects will arise from variations in the distance from the base-collector junction to the collector-substrate isolation junction.

Doping levels and doping profiles can affect the magnitude of the photocurrent by affecting the size of the volume over which excess carriers are collected. The doping levels affect carrier lifetime τ, and hence diffusion length, since $L = (D\tau)^{1/2}$ (D is the diffusion constant). The lifetime τ is especially sensitive to the presence of deep-lying recombination centers, such as Au, which are intentionally introduced into some devices to lower lifetime and thereby increase frequency response. Gradients in the densities of ionized (i. e., shallow) impurities contribute built-in electric fields to the non-depleted regions of devices. These doping profile-dependent drift-fields affect the volume over which carriers are collected by either aiding or hindering diffusion of carriers from non-depleted material towards the depletion layer.

The irradiation-induced response of a powered transistor operating in its active region is essentially the photocurrent induced in the base collector junction as amplified by the device. The flaws that affect the photocurrent may, in addition, affect the small-signal current gain β, so that the detectability of flaws may be enhanced. However, β is a highly variable parameter that can be affected by numerous factors that cannot be classified as flaws. Any enhancement in detectability is obtained at the cost of possibly introducing irrelevant effects.

Unlike the photocurrent, the open circuit photovoltage V_{phoc} of a p-n junction is independent of the junction area:

$$V_{phoc} = \frac{KT}{q} \log_e \left[\frac{(I_{phsc} + I_o)}{I_o} \right],$$

so if I_{phsc} and I_o have the same dependence on area, the term in brackets is independent of area.

$$\frac{I_o}{A} = q \left(\frac{D_p p_{no}}{L_p} + \frac{D_n n_{po}}{L_n} \right)$$

V_{phoc} depends on doping levels and doping profiles through their effects on I_o, as shown by this expression, and on I_{phsc}, as discussed above. However, the logarithmic dependence does make V_{phoc} an insensitive indicator of doping variations.

The open circuit photovoltage can be expected to be sensitive to interference from extraneous effects, especially flaws that tend to load the junction with some sort of shunt conductance. A number of important device flaws fall in that category. Crystal defects, such as dislocations or stacking faults, that penetrate through the junction are known to increase leakage currents. Similarly, an excess of recombination centers, either in the depleted bulk or at the surface (surface contaminants), also will increase leakage. One effect that was initially believed to be causing experimental difficulties in this program was irradiation-induced conductivity in oxide layers overlaying the junction. Such conductivity could be expected to considerably decrease photovoltage by its shunting effect. Although the problem was later shown to be inconsequential for the X-ray intensities used for this program, it could turn out to be significant at much higher intensities. (The shunting conductance will increase linearly with intensity, while the voltage increases only logarithmically).

In addition to affecting recombination rates at the surface, ionized contaminants on the device surface can modulate the surface conductivity via the field effect. In extreme cases, the semiconductor type at the surface can be inverted, so that contaminated bipolar transistors act as if they had a parasitic MOSFET between the emitter and the collector. This phenomenon, known as channeling, drastically increases collector-emitter leakage. However, it also effectively increases the total area of the base-collector and base-emitter junctions, which increases I_{phsc} for these junctions. The net effect on the photocurrent response of an unpowered transistor will be an increase proportional to the increase in effective junction volume. The effect on a powered device could be analyzed only on an individual basis. On the one hand, the depletion layer between the channel and the base region will collect an additional component of photocurrent that is amplified by the transistor; on the other hand, the transistor with a channel is so leaky that the amplified photocurrent may be completely obscured by the leakage current.

2.7 EXPECTED EFFECTS OF X-RAYS ON GOOD AND FLAWED MICROCIRCUITS

The manner in which various microcircuit elements contribute to the X-ray-induced response of the entire circuit is completely dependent on the circuit configuration. For each type of circuit chip there will be a characteristic response or "signature" that in principle can contain contributions from every point on the chip. However, in practice the signature at the output terminal will contain detectable contributions only from a small number of microcircuit elements, and also from other sources that are not readily recognizable as such in circuit schematics. For example, resistors in microcircuits are often diffused regions isolated from the substrate by a p-n junction. Under irradiation it is the effective depleted volume of this junction that collects generated carriers. As mentioned in the previous section, the isolating junctions of transistors will play a similar role. Photoelectron emission from metallization and wire bonds can in principle be expected to contribute to the signal; quantitatively the contribution is probably negligible.

Because of the widespread use of TTL digital microcircuits, they will be used here to exemplify the expected effects. Figure 2-6 is the

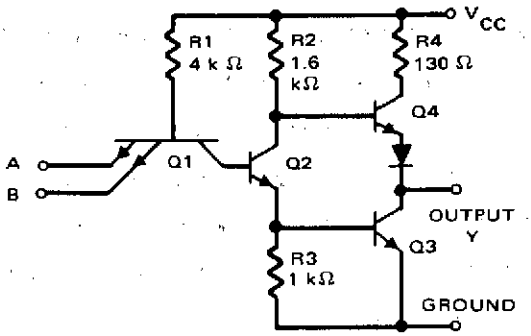

Figure 2-6. Schematic diagram of typical NAND gate in a TTL microcircuit.

schematic for a typical TTL NAND gate. When both inputs A and B are at a high voltage, the base-emitter junctions of Q1 are back-biased. All the Q1 base current is directed out the collector into the base of Q2. Both Q2 and Q3 are turned on and saturated, while Q4 is turned off. The irradiation will have little effect on saturated transistors, so at the output terminal Y the irradiation-induced signal will contain contributions from a series-parallel combination of non-forward-biased junctions: all the junctions of Q4, D, and the isolating junctions of R2 and R4. The photocurrent collected by this combination of junctions is shunted to ground through Q3. A portion of it will be detectable only with a current amplifier having an input impedance that is very small compared to the "on" resistance of Q3. Alternatively, a voltage amplifier would have to be able to detect the voltage drop of the photocurrent across Q3. Alterations of this signal as a result of flaws would have to be quite large to be detectable at all.

When either input A or B is at a low voltage, the base current of Q1 is directed to the low emitter (A or B). Q1, Q2, and Q3 then are off, and Q4 is turned on. Again a transistor at the output is saturated and hence unaffected by irradiation. Significant photocurrents are collected only at non-forward-biased junctions. In this case they are the junctions of Q3, Q2, R3, R2, and the base-collector junction of Q1. Whatever portion of the collected photocurrent flows through Q3 is shunted through Q4 and R4 to the power supply rail. In practice, what would be detected would be the voltage drop of the photocurrent across R4.

Estimates of excess carrier generation rates due to X-rays were shown in Section 2.2 to be of the same order of magnitude as thermal generation rates under the most favorable conditions. Thus a very generous estimate of the photocurrent through R4 would be in the tens of nanoamperes. The voltage drop across R4 would then be on the order of a microvolt. If faults caused relatively small changes (10 percent) in this irradiation-induced response, the ability to make voltage measurements with resolution of tens or hundreds of nanovolts would be required. The measurements would have to be insensitive to power supply ripple and noise as well as noise induced by stray electromagnetic fields.

This brief analysis of a simple, typical microcircuit illustrates two significant difficulties. One is that signals at internal points of the circuit can be buffered by the output stage, so that variations in the irradiation-induced signals that might arise from faults may be externally inaccessible. The other is that the use of a flooding stimulus causes the effects of faults, if any, to be diluted in a signal that is a superposition of many effects from many sources.

The problem of limited access to internal points of the circuit caused by buffering can be partly circumvented by irradiating unpowered microcircuits and detecting induced photovoltages and photocurrents from the power supply terminal to ground. Then the microcircuit can be regarded as a complex network connected between the power supply and ground terminals. Each branch of the network will, in general, contain a series combination of non-forward-biased junctions. Since every active device in the circuit must ultimately be connected to the power supply, this approach does allow access (in principle) to all points of the microcircuit. The problem of diluting the effects of faults, however, does remain.

3.0 EXPERIMENTAL RESULTS

3.1 INTRODUCTION

The experimental part of this program essentially consisted of observing the electrical responses of semiconductor devices when irradiated with X-rays produced by an industrial radiography machine of conventional design.

Experiments were also performed with a flash X-ray source to explore the effects of device flaws on transient X-ray response. The possibility of enhancing detectability of certain types of flaws by combining X-ray and optical irradiation was also investigated by interposing a fluorescent screen between the X-ray source and the device under test. The possibility of using X-rays as a failure-inducing stimulus for thin dielectric was also explored briefly.

The main X-ray source used for the experiments was a Faxitron Model 8060 radiography unit manufactured by Field Emission Corporation. It is equipped with a tungsten anode Coolidge tube operated in the self-rectified mode at up to 110 KV peak and a current of 2.8 mA. The X-ray window is 0.635 mm (25 mils) thick beryllium.

The flash X-ray source was Fexitron Model 8030 unit, also manufactured by Field Emission Corporation. It is equipped with a special X-ray tube that uses multiple pointed cold cathodes operating as field emission sources. The power supply is a Marx generator that can provide as many as 100 pulses at 100 KVp or 150 KVp. The X-ray pulse shape has a very steep rise with an approximately linear decay, so it resembles a time-reversed sawtooth waveform. Pulse width at half of maximum is ~100 ns.

Irradiation-induced responses were measured using mostly conventional instrumentation, which is described individually for each set of experiments. A current-to-voltage converter with a 1MΩ transfer resistance was assembled with a FET-input I. C. operational amplifier; it was used for all short circuit photocurrent measurements. For the flash x-ray experiments, a Biomation Model 610 digital transient recorder was used to circumvent difficulties imposed by the short duty cycle (1-minute cool down for each 25 pulse train) of the flash X-ray source. (Further details on the X-ray sources and unconventional instrumentation are given in Appendix A.)

The measured responses included photovoltages and photocurrents from separate junctions in unpowered, discrete devices, and selected, specified parameters for powered microcircuits.

Specimens were selected by various conventional and unconventional techniques. Leaky transistors believed to have incipient channels were discovered and made available as a result of electrical tests alternated with HTRB (High Temperature Reverse Bias) treatments. Power transistors with diffusion flaws or irregularities at the base-emitter junction periphery were selected by imaging the junction periphery by the Electron Beam Induced Current (EBIC) mode in a Scanning Electron Microscope (SEM). The technique is described in detail in Appendix B. Other power transistors used for the initial experiments were examined after the fact by this technique, and junction irregularities were also found in some of them. "Normal" and "maverick" microcircuits were selected by testing a large number of microcircuits for their specified parameters with a Tektronix S3260 IC tester. Only a small number of maverick or deviant microcircuits was found, so it was not practical to impose a rigid criterion based on standard deviations to define abnormal behavior. The selection of mavericks was carried out simply by looking for devices whose parameters were noticeably different from the majority in the tester print-out. Abridged specifications and other detailed information on all test specimen types are given in Appendix C.

A few experimental problems had to be resolved before meaningful data could be taken. A sample holder was constructed to hold the specimens at a well-defined, repeatable distance from the X-ray source. Subminiature

coax cable was used to conduct the photovoltages and photocurrents to the instrumentation outside the X-ray machine chamber. Since it was anticipated that the X-ray machine power supply could induce undesired signals in the specimen holder and associated cables, the complete photovoltage measurement instrumentation was tested without a specimen in the specimen holder. A signal voltage was detected when the X-ray source was turned on. The fact that this spurious signal voltage was directly induced in the specimen holder by the X-rays was verified by placing a small sheet of lead (Pb) over the empty device socket. With the Pb sheet in place, the signal disappeared. Although adequate for stopping X-rays, the Pb sheet was too small to effect any kind of electrical shielding. To avoid having this spurious photoelectric signal superimposed on the specimen response, a Pb shield with an aperture was added to the specimen holder to confine the irradiated area to the specimen chip and its immediate vicinity. In particular, the device package and socket were not exposed directly to the X-ray beam.

One unavoidable difficulty involved the low signal levels that had to be measured. Since a self-rectified X-ray source was used, a-c coupled amplifiers were used, so that drift problems associated with low level d-c amplifiers could be avoided. As explained in the section on X-ray interactions with solid matter, the X-ray intensity, and hence the response, could not have been increased by more than a couple of orders of magnitude.

One order of magnitude increase could be obtained by decreasing the source to specimen distance from 34.6 cm to ~10 cm. Another order of magnitude increase would result from increasing the tube input power from ~300 W to 3 KW - a practical upper limit for conventional, fixed anode X-ray tubes. Signal levels 100 times larger than those that were recorded in this program would still present practical measurement problems. For devices irradiated and measured under power, the residual noise and ripple in power supplies would have to be accounted for by making comparative measurements, with and without irradiation.

An implicit assumption in the measurement of X-ray responses with an oscilloscope is that the incident X-ray intensity remains constant. It was discovered early in the first experimental series that the output intensity of the self-rectified source (Faxitron 8060) had an oscillating 10 percent

variation at a frequency of ~ 4 Hz super-imposed on the normal, half-wave rectified sine waveform. The cause for this unexpected variation is unknown. A true RMS voltmeter with a long time constant was therefore used to average out the variations and yield a steady reading. The RMS readings that were recorded are directly proportional to the average peak amplitude. (The constant of proportionality is 0.5.)

3.2 X-RAY INDUCED RESPONSES IN UNPOWERED TRANSISTORS

These experiments were performed with unpowered transistors in an attempt to correlate photovoltages and photocurrents with measured leakage currents. Some of the devices were known to have diffusion flaws or irregularities along the base-emitter junction periphery. Others were examined after irradiation, and some of them were also found to have similar junction irregularities. The experiments involved power transistors and individual transistors in monolithic transistor arrays. The power transistors were used for the initial experiments when the X-ray sources and other instrumentation were being checked out. The large area junctions in these devices were helpful in minimizing anticipated difficulties caused by low signal levels. Moreover, devices with identified flaws were available. The transistors in the monolithic transistor arrays were then measured to establish the signal amplitudes that could be expected from devices having the dimensions and electrical characteristics of microcircuit elements. Unlike the power transistors, the transistors in the monolithic arrays are junction-isolated, so any anomalous effects that might be due to the isolating junction were looked for. (None were found.)

Each series of experiments was undertaken with a specific goal in mind, so the motivation and interpretation are discussed in the individual descriptions of the experiments.

3.2.1 Suspected Oxide Conductivity Effects

Initial estimates of the photovoltages and photocurrents that could be expected from discrete transistors were made by rough calculations based on the input power delivered to the X-ray tube and on the fraction of that

power that would be available to create hole-electron pairs in irradiated devices. The calculations showed that photovoltages of at least several tens of millivolts could be anticipated. The measurements performed while checking out the equipment did not bear this out. Measured photovoltages were lower than 10 mV, and they varied considerably among nominally identical devices. In the absence of any other plausible explanation, it was hypothesized that conductivity induced by the irradiation in the oxide overlaying the device was acting as a shunt to reduce the photovoltage. A literature search was started to see if the conductivity induced in SiO_2 by X-rays was of the correct order of magnitude to account for the observed results. Unfortunately, no reports were found on the electrical properties of SiO_2 under irradiation. The reports that were found all dealt with MOS structures. At first these reports were disregarded because photoelectron injection phenomena at the metal-oxide interface would make the data inapplicable to non-metallized SiO_2. Since the required data was just not available, the reports on MOS structures were reviewed. For a dose rate, approximately 1/4 of that delivered by the Faxitron 8060 machine, Esteve and Buxo (1971) reported an induced conductivity (in SiO_2) $\sigma = 0.499 \times 10^{-12}\ \Omega^{-1}m^{1}$. This would give an equivalent shunting resistance in the hundreds of megohms for the micron-thick oxide layers on devices.

An experiment then was performed to verify that the induced conductivity hypothesis was not correct. Photovoltages from the base-emitter and base-collector junctions of a 2N3810 dual transistor were measured with an oscilloscope across whose input various shunting resistances were connected. If the irradiated junctions did have a conductive glass shunt across them, the shunts added to the oscilloscope input would have a negligible effect as long as the net input impedance of the oscilloscope amplifier remained large compared to the resistance of the conductive glass. A Tectronix 53/54E oscilloscope amplifier with a 10 MΩ input impedance was used for these experiments, and peak voltages were read directly off the oscilloscope screen. The results (see Table 3-1) show that any glass shunting resistance would have to be large compared to 10 MΩ. Since oscilloscope plug-ins with 1 MΩ or 10 MΩ input impedances were to be used to measure photovoltages, irradiation-induced conductivity in the SiO_2 was shown by these experiments to be negligible.

TABLE 3-1. PHOTOVOLTAGE DEPENDENCE ON OSCILLOSCOPE INPUT IMPEDANCE

Input Impedance	Transistor A		Transistor B	
	C-B	B-E	C-B	B-E
10 MΩ	12.8 mV	1.5 mV	8.3 mV	1.3 mV
4.6 MΩ	3.7 mV	0.38 mV	3.4 mV	0.34 mV
0.91 MΩ	0.9 mV	0.09 mV	0.84 mV	0.08 mV
0.1 MΩ	0.09 mV	0.02 mV	0.08 mV	0.02 mV

3.2.2 X-ray Responses of Power Transistors with Junction Irregularities

Photovoltages and photocurrents were measured in the base-emitter and base-collector junctions of two different kinds of Planar n-p-n power transistors. Although these two kinds of transistors were electrically equivalent and of the same type (2N3767), they were made by different manufacturers — Solitron and Fairchild — using different chip designs. Not surprisingly, both the X-ray responses and the junction characteristics (leakage currents and breakdown voltages) were very different.

The Solitron chips were of a conventional interdigitated design. The Fairchild chips utilized a multiple emitter structure with integral, ballasting emitter resistors. Further details are given in Appendix C.

The photovoltages, photocurrents, junction breakdown voltages and leakage currents were measured for a total of eleven transistors; the results are shown in Table 3-2. Photovoltages were measured with an RMS voltmeter in conjunction with a Tektronix 1A7A high sensitivity plug-in, which has a 1 MΩ input impedance. The results for the preceeding experiment showed that a 1 MΩ load caused a significant decrease in the photovoltage, so the photovoltages measured in this way are not open circuit voltages. Photocurrents were measured with a FET-input operational amplifier current-to-voltage converter connected between the device and the 1A7A plug-in. All measurements were done with the Faxitron 8060 X-ray machine operated at 110 KVp with the device at a distance of 34.6 cm from the device. Breakdown voltages were measured conventionally on a Tektronix 576 curve tracer; the

TABLE 3-2. X-RAY RESPONSES OF 2N3767 TRANSISTORS

2N3767 Fair-child	Vph (mv rms)		Iph (nA rms)		Breakdown Voltages		Leakage Currents	
	B-E	B-C	B-E	B-C	E-B V	C-B V	B-E	C-B
1	1.48	17.2	0.93	14.2	8.2	110	25 nA	13 nA
2*	2.88	16.8	1.60	14.6	9.5	150	20 nA	8 nA
3*	2.62	18.2	1.66	15.2	9.4	156	20 nA	9.5 nA
4*	3.84	21.6	1.78	21.0	10.0	130	5.0 nA	6.0 nA
5	1.96	16.2	1.04	12.0	8.8	150	27 nA	7.5 nA
6	1.27	17.2	0.58	13.4	9.0	155	85 nA	16 nA
7*	1.40	15.2	0.54	11.8	9.8	165	370 nA	18 nA
Solitron								
8*	17.0	21.8	13.4	27.2	12.1	220	96 pA	0.26 nA
9*	16.0	19.6	14.6	23.2	11.4	205	92 pA	0.72 nA
10	15.0	21.6	12.8	29.6	12.0	230	44 pA	0.82 nA
11*	15.2	21.0	13.6	26.4	11.0	175	160 pA	0.30 nA

*Device with irregularities in the base-emitter junction periphery.

base-emitter leakage was measured with 6 V reverse bias, while the base-collector leakage was measured with 50 V reverse bias.

For all these measurements, the unused terminal was left unconnected (i.e., floating).

Comparison of the data for the Fairchild transistors and the Solitron transistors discloses a few trends. The junctions in the Solitron devices have significantly higher breakdown voltages than the corresponding junctions in Fairchild devices; the Solitron devices also have significantly higher photocurrent response from both junctions. If all other parameters (i.e., junction areas) were the same, the junctions with higher breakdown voltages (which indicate lower doping levels), would be expected to have the higher photocurrent response. (Junctions with lower doping levels also would have wider depletion layers and, possibly, longer carrier diffusion lengths. The effective volume for carrier collection then would be larger.)

Unfortunately, within each group of transistors made by the same manufacturer, there appears to be no correlation among measurements that can be shown to have a counterpart in the other group of transistors. For example, device No. 10 has the lowest base-emitter leakage of the Solitron transistors, and it also has the lowest base-emitter junction photovoltage and photocurrents. However, for the Fairchild transistors, the device with the lowest base-emitter leakage (No. 4) also has the highest X-ray responses for that junction.

Devices shown to have base-emitter junction irregularities are indicated in Table 3-2 by an asterisk. EBIC images of the flawed junctions and conventional secondary electron images of the regions around the flaws are shown in Figures 3-1 through 3-7. The presence of this type of flaw was recently shown by a Hughes Aircraft Co. IR&D study to be well correlated with the appearance of localized hot spots in power transistors. The junction irregularities are therefore indicators of real flaws and not just cosmetic defects. However, the X-ray response data clearly show that there is no correlation between the magnitudes of the responses and the presence of junction irregularities.

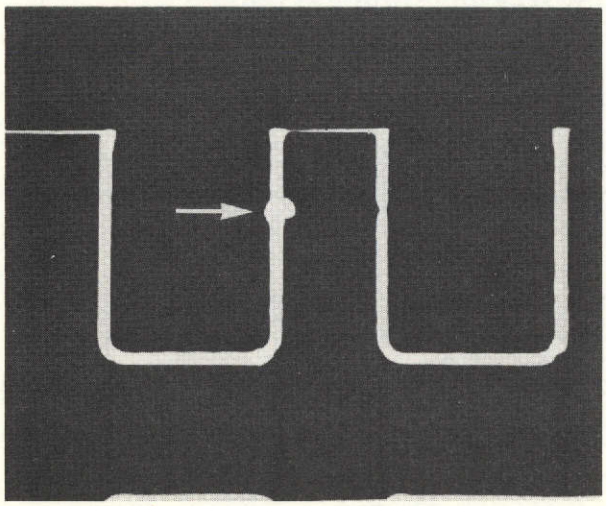

Figure 3-1a. SEM-EBIC image of flaw in base-emitter junction of transistor 2N3767 No. 2. Arrow points to junction irregularity (magnification: 392X).

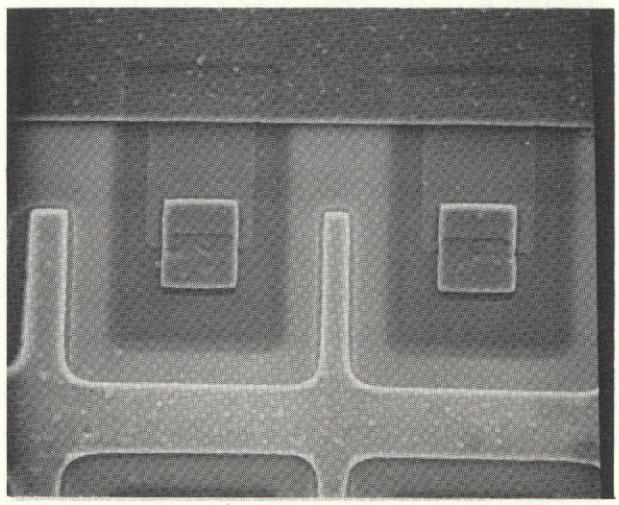

Figure 3-1b. SEM micrograph of flawed area on 2N3767 No. 2, made with base-emitter junction reverse-biased (magnification: 392X).

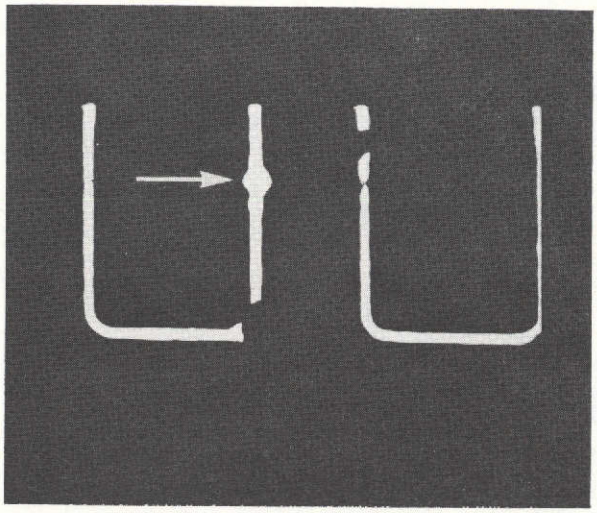

Figure 3-2a. SEM-EBIC image of flaw in base-emitter junction of transistor 2N3767 No. 3. Arrow points to junction irregularity (magnification: 392X).

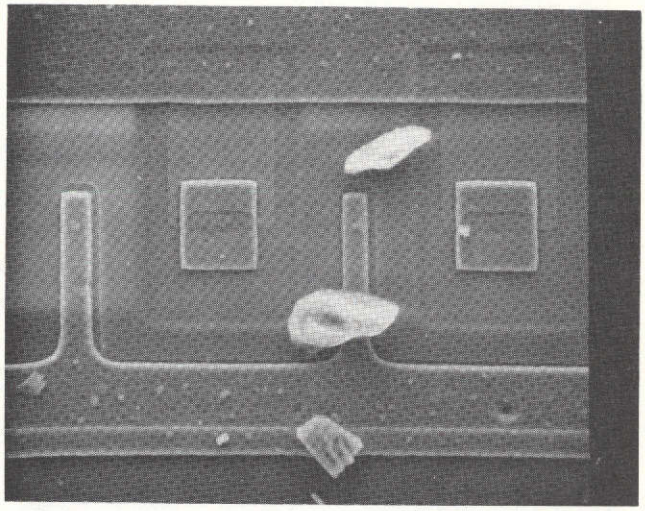

Figure 3-2b. SEM micrograph of flawed area on 2N3767 No. 3, made with base-emitter junction reverse-biased (magnification: 392X).

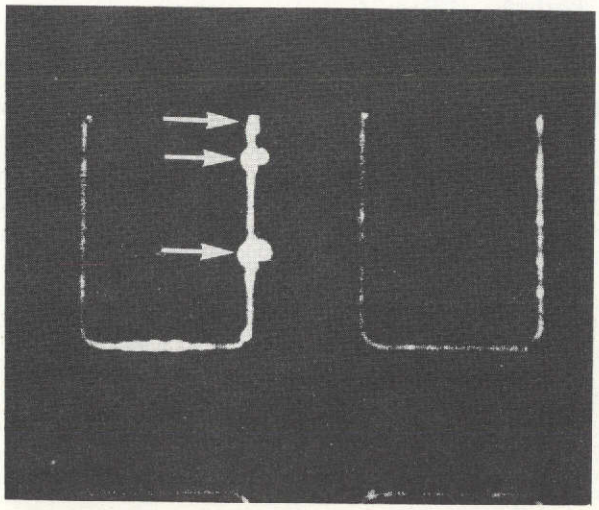

Figure 3-3a. SEM-EBIC image of several flaws in base-emitter junction of transistor 2N3767 No. 4. Arrows point to junction irregularities (magnification: 392X).

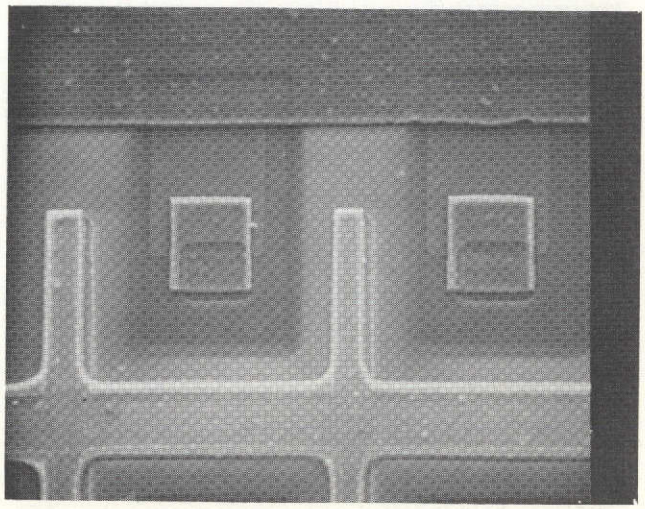

Figure 3-3b. SEM micrograph of flawed area on 2N3767 No. 4, made with base-emitter junction reverse-biased (magnification: 392X).

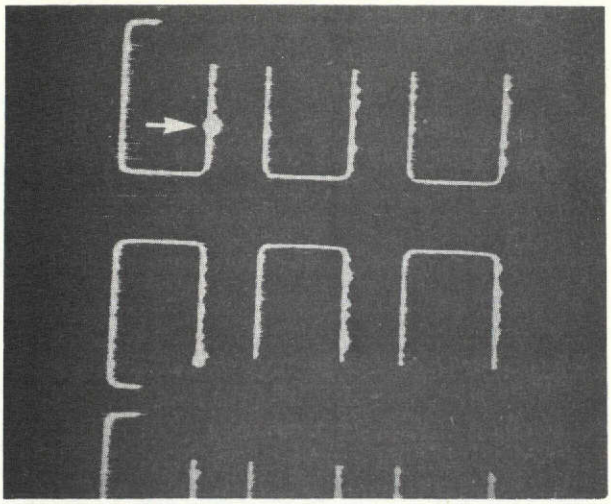

Figure 3-4a. SEM-EBIC image of irregularities in base-emitter junction of transistor 2N3767 No. 7. Arrow points to most prominent irregularity (magnification: 192X).

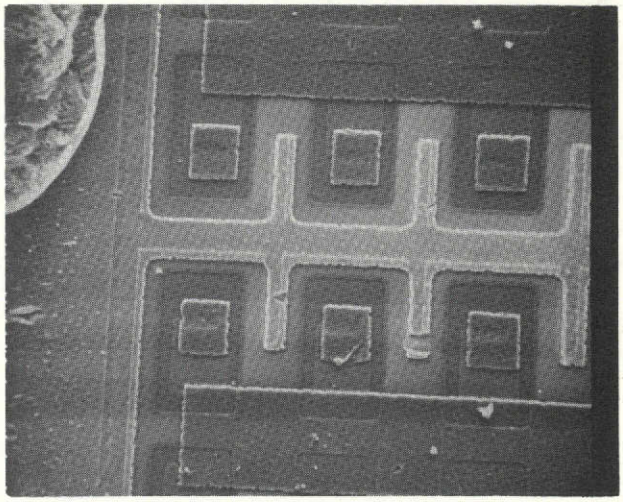

Figure 3-4b. SEM micrograph of flawed area of 2N3767 No. 7, shown in Figure 3-4a. Micrograph made with reverse bias applied to base-emitter junction (magnification: 192X).

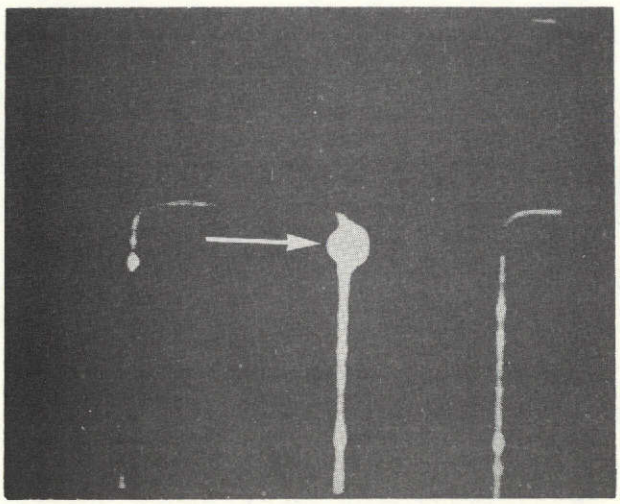

Figure 3-4c. Higher magnification SEM-EBIC image of flaw (designated by arrow) in base-emitter junction of transistor 2N3767 No. 7. This flaw does not appear in Figure 3-4a. (magnification: 481X).

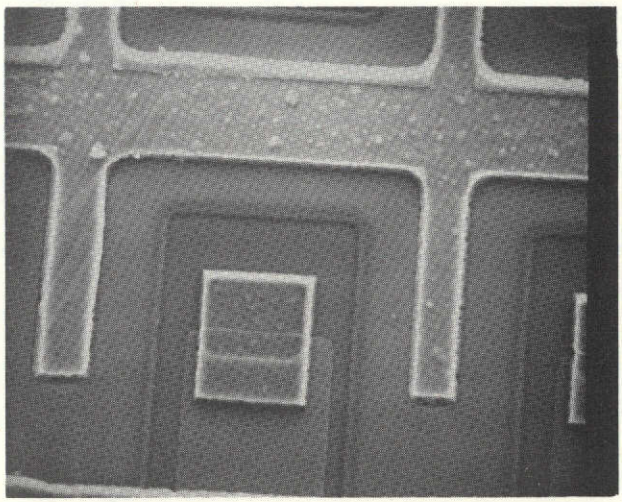

Figure 3-4d. SEM micrograph of flawed area corresponding to Figure 3-4c, made with reverse-biased base-emitter junction (magnification: 481X).

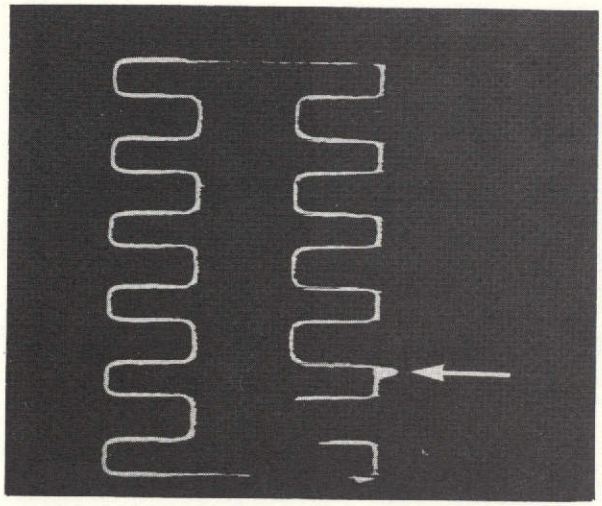

Figure 3-5a. SEM-EBIC image of base-emitter junction of transistor 2N3767 No. 8. Arrow points to flaw (magnification: 50X).

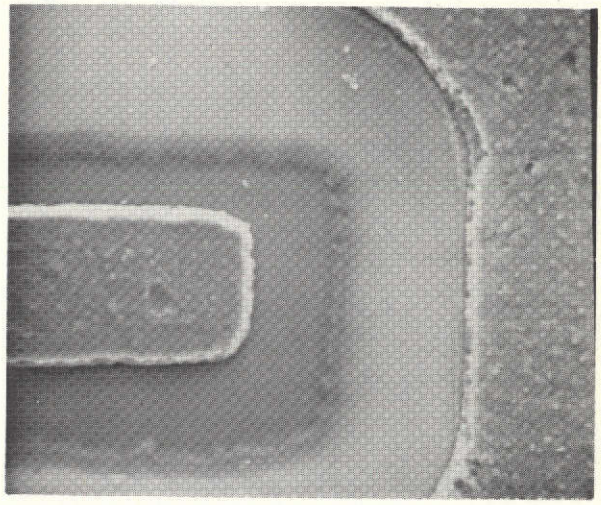

Figure 3-5b. High magnification (503X) SEM micrograph of flawed area shown in Figure 3-5a. Micrograph made with reverse bias applied.

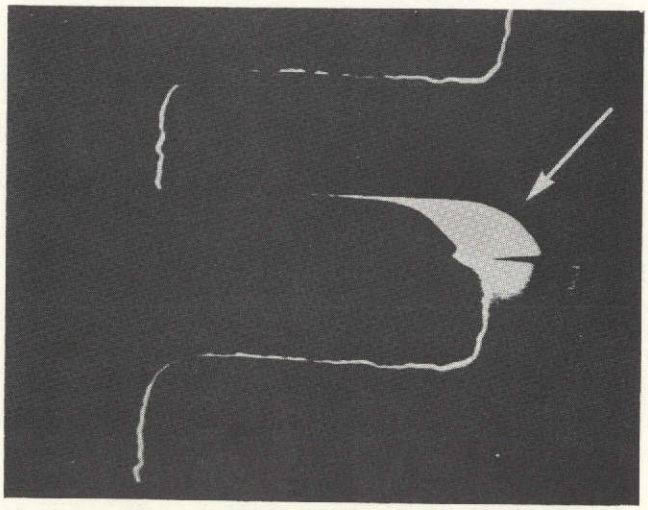

Figure 3-6. SEM-EBIC image of large irregularity in base-emitter junction of transistor 2N3767 No. 9 (magnification: 195X).

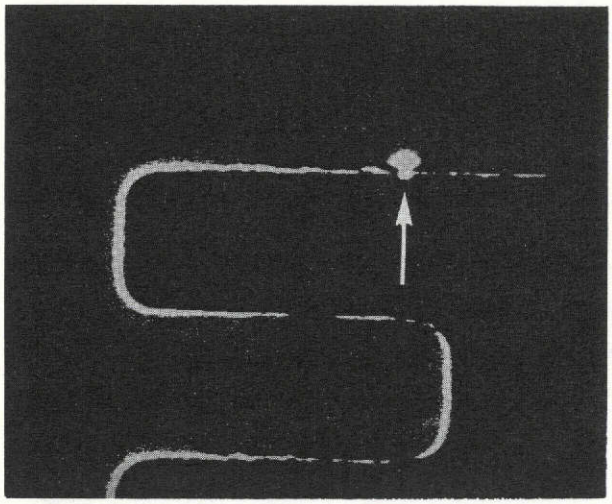

Figure 3-7a. SEM-EBIC image of junction irregularity in base-emitter junction of transistor 2N3767 No. 11. Arrow points to irregularity (magnification: 192X).

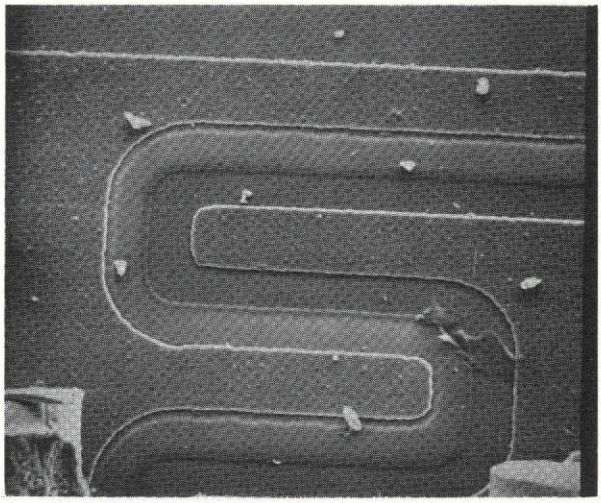

Figure 3-7b. SEM micrograph of flawed area of 2N3767 No. 11. (magnification: 192X).

3.2.3 Transient Photovoltage Responses of Power Transistors with Junction Irregularities

A problem that has been anticipated with a flooding approach, as opposed to a localized stimulus, is that the signals originating from flaws are superimposed on signals originating from normal, unflawed regions of the specimen. One way that this difficulty might be avoided is to spread out the various signals in time: if the transient response of a flawed region to a brief radiation pulse differs from that of normal regions, the net effect may be to alter the decay time of the overall X-ray response.

In order to check this hypothesis, the photovoltage response of the 2N3767 transistors to short duration X-ray pulses (produced by the Fexitron 8030 flash X-ray source) was measured with the goal of finding decay time differences that could be correlated to the presence of detected flaws. Four additional transistors of a different type – Solitron MHT 6424 – were added to the test group. Two of these transistors were known to have junction irregularities, and one of these flawed transistors (MHT 6424 No. 1) also had numerous other defects, including cracked dielectric, poorly delineated metallization and incomplete coverage of the emitter contact windows.

Figures 3-8a through 3-8f are micrographs of MHT 6424 No. 1. Figure 3-8a shows the EBIC image of the base-emitter junction, which appears as a nearly continuous curve. Following the contours of this curve is another image made up of spots. These spots are parts of the emitter contact window left uncovered by the metallization. The electron beam can penetrate through the emitter at the uncovered spots into the depletion layer of the base-emitter junction. Figures 3-8b and 3-8c are conventional secondary electron images showing the poorly delineated metallization. Figure 3-8d shows an irregularity in the base-emitter junction periphery. Figures 3-8c and 3-8f are conventional scanning electron and optical micrographs, respectively, of cracked glass in the vicinity of the base-emitter junction. Figure 3-9a shows an EBIC image of an irregularity in the base-emitter junction of MHT 6424 No. 4. Figures 3-9b and 3-9c are scanning electron and optical micrographs, respectively, of the flawed region.

The devices were irradiated with 150 KV and 100 KV X-ray flashes, and the photovoltages from the base-emitter and base-collector junctions were recorded with a Biomation Model 610 digital transient recorder. The transient recorder has 1 MΩ input impedance and a maximum sensitivity setting of 50 mV full scale. Resolution is 6 bits, and the 10 MHz word conversion rate was more than ample for the decay times that were observed. The sensitivity was inadequate only for the signal from the base-emitter junctions of the Fairchild 2N3767 transistors. All of the transient responses were viewed and photographed on an oscilloscope.

Figures 3-10a and 3-10b show the photovoltage responses of the base-emitter junction of a normal (MHT 6424 No. 3) and a flawed (MHT 6424 No. 1) transistor. The different voltage scales of the two oscillograms should be noted in making comparisons. From these and similar photographs for the other transistors, the response duration time, defined as the decay time to 10 percent of the peak value, was obtained. (See Figure 3-11 for a graphic definition of the response duration time.) The peak photovoltage and response duration times for all the transistors are listed in Table 3-3.

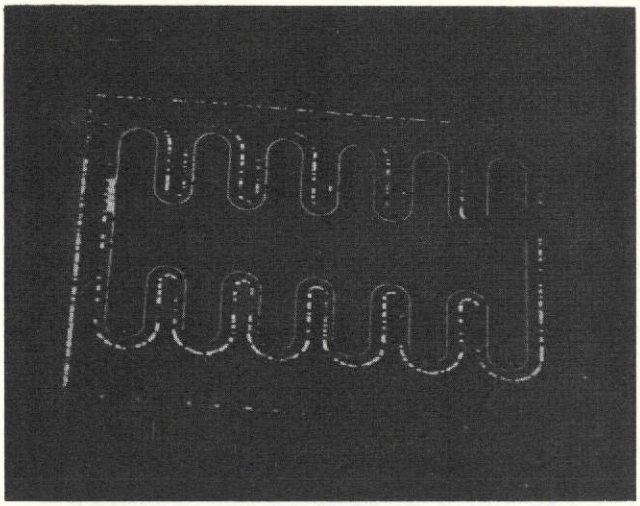

Figure 3-8a. SEM-EBIC image of base-emitter junction of transistor MHT 6424 No. 1 (magnification: 38X).

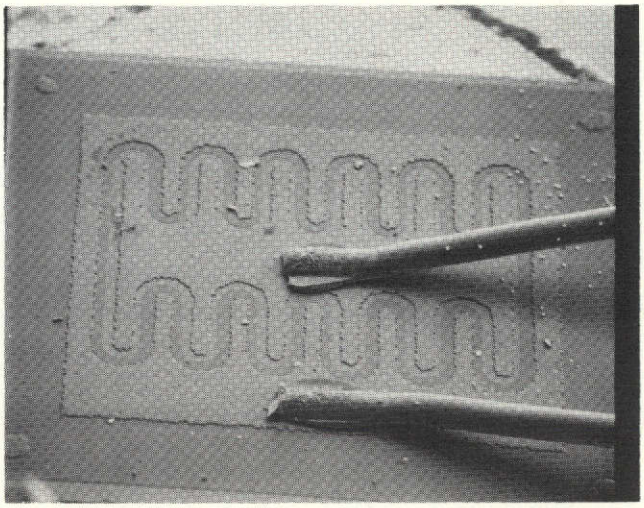

Figure 3-8b. Overall SEM micrograph of MHT 6424 No. 1 die, corresponding to EBIC image in Figure 3-8a. Note ragged metallization edges (magnification: 38X).

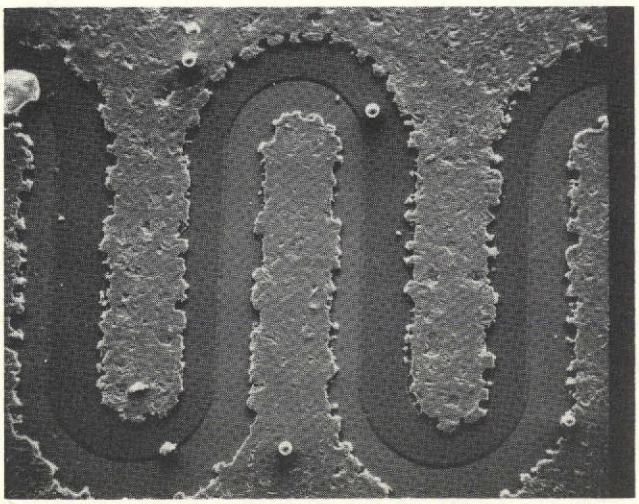

Figure 3-8c. SEM micrograph of metallization of MHT 6424 No. 1, showing poorly delineated metallization (magnification: 141X).

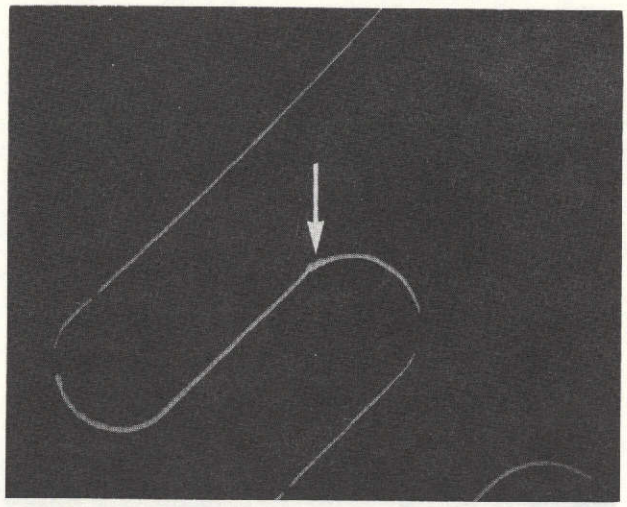

Figure 3-8d. SEM-EBIC image of base-emitter junction of MHT 6424 No. 1, showing junction irregularity designated by arrow (magnification: 141X).

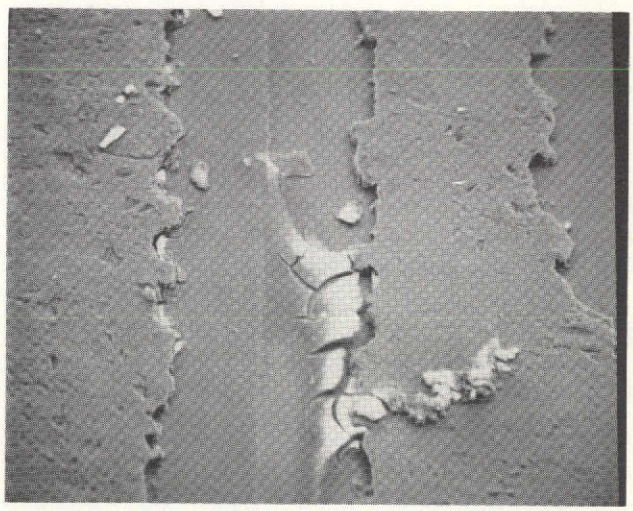

Figure 3-8e. SEM micrograph of cracked glass near base-emitter junction periphery of MHT 6424 No. 1 (magnification: 340X).

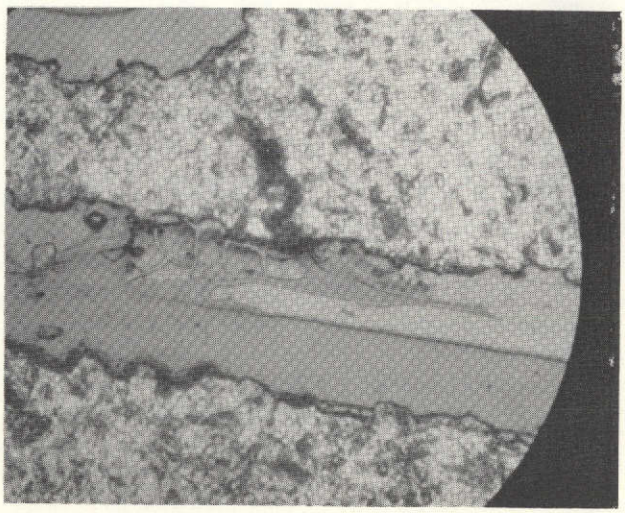

Figure 3-8f. Optical micrograph of cracked glass. Same flaw shown in Figure 3-8e, but image is rotated counter-clockwise 90 degrees (magnification: 241X).

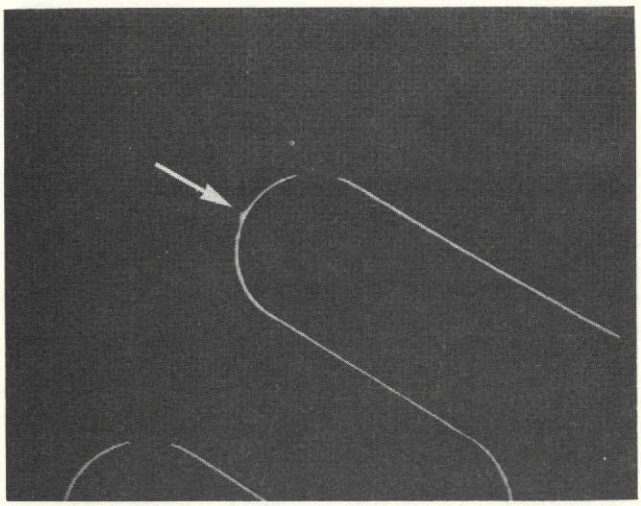

Figure 3-9a. SEM-EBIC image of irregularity (designated by arrow) in base-emitter junction of transistor MHT 6424 No. 4 (magnification: 148X).

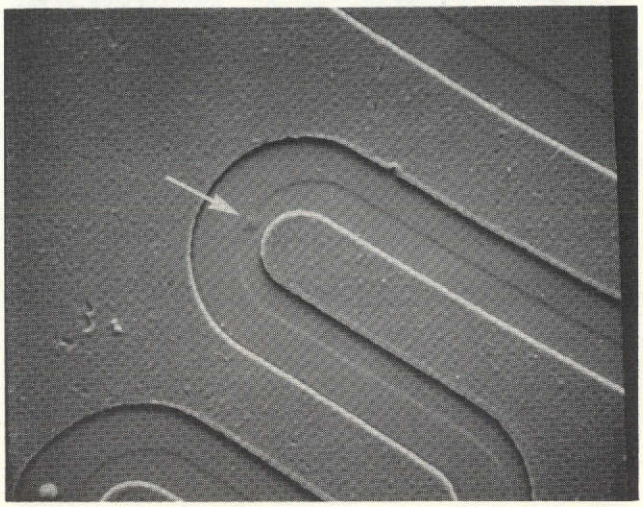

Figure 3-9b. SEM micrograph of flawed area in MHT 6424 No. 4. Arrow points to barely discernible surface feature coincident with junction flaw shown in Figure 3-9a (magnification: 148X).

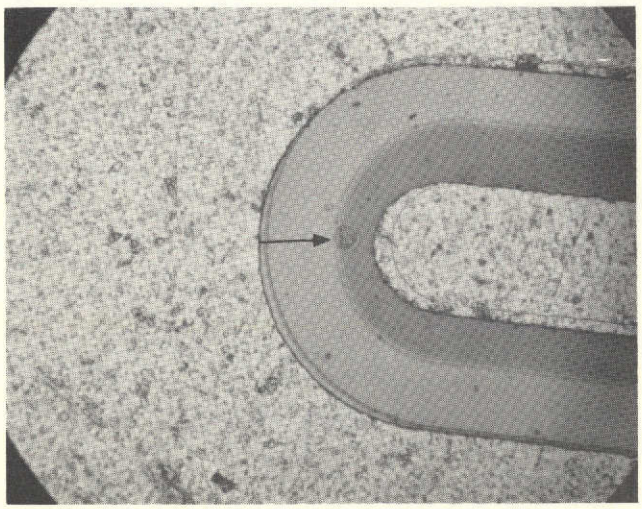

Figure 3-9c. Optical micrograph of surface feature associated with junction flaw in MHT 6424 No. 4 (magnification: 219X).

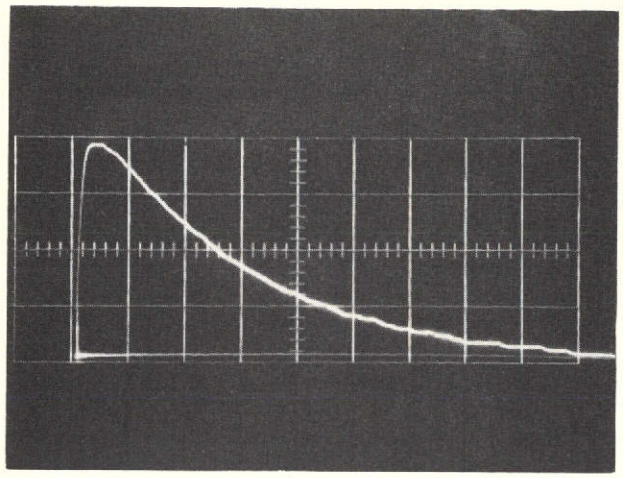

Figure 3-10a. Flash X-ray photovoltage response of base-emitter junction of normal (MHT 6424 No. 3) transistor. Vertical scale - 0. 1V/div; Horizontal scale - 5 ms/div.

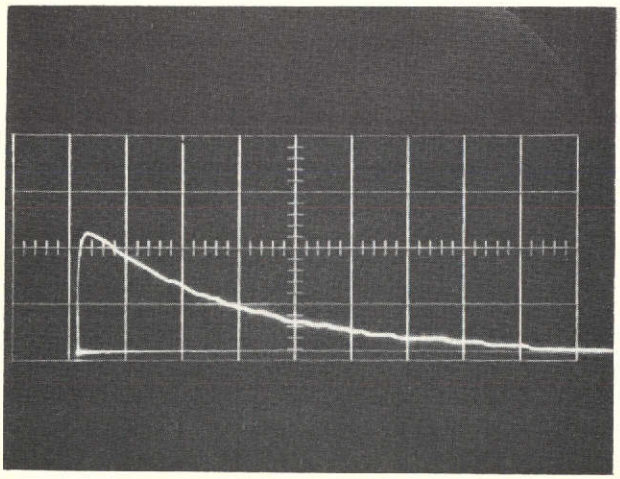

Figure 3-10b. Flash X-ray photovoltage response of base-emitter junction of flawed (MHT 6424 No. 1) transistor. Vertical scale - 0. 2 V/div; Horizontal scale - 5 ms/div.

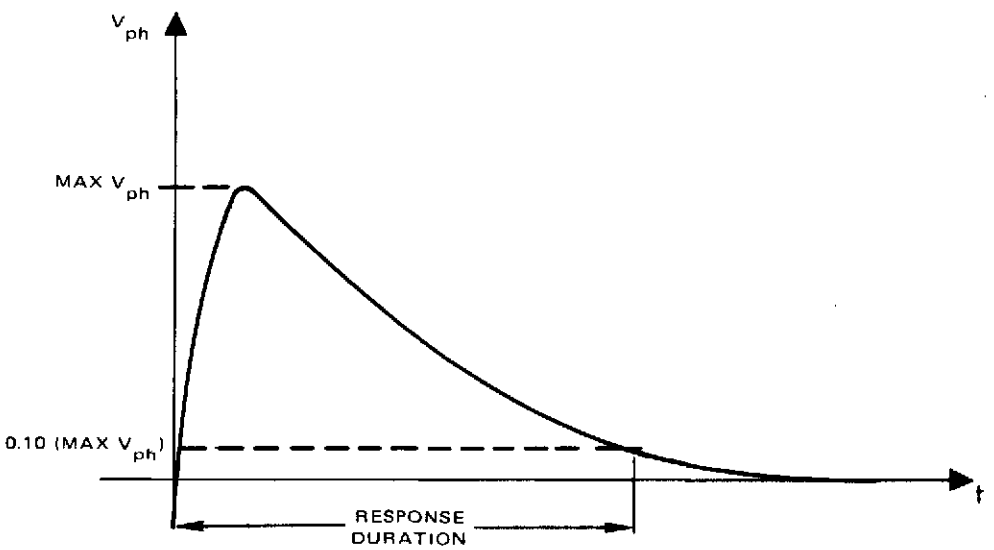

Figure 3-11. Definition of response duration for transient photovoltage response to X-ray flashes.

TABLE 3-3. FLASH X-RAY RESPONSES OF 2N3767 AND MHT 6424 TRANSISTORS

		MHT6424							
	Device No.	Max Vph		Response Duration		Max Vph		Response Duration	
		B-E V	B-C V	B-E ms	B-C ms	B-E V	B-C V	B-E ms	B-C ms
Solitron	1*	0.105	0.25	2.85	1.60	0.015	0.155	3.33	1.50
	2	0.009	0.165	1.95	1.85	very small	0.085	4.45	1.35
	3	0.093	0.281	3.15	1.42	0.021	0.158	4.6	1.36
	4*	0.031	0.185	3.33	1.00	0.003	0.125	5.0	1.36
		2N3767							
Fairchild	1		0.12		1.0		0.046		0.94
	2*		0.13		0.98		0.065		0.99
	3*		0.14		0.95		0.0575		0.92
	4*		0.158		0.93		0.0775		0.99
	5		0.115		0.98		0.046		1.06
	6		0.12		0.89		0.055		0.96
	7*		0.93		0.84		0.043		0.89
Solitron	8*	0.053	0.275	1.6	0.73	0.0131	0.155	2.2	0.85
	9*	0.043	0.288	1.78	0.88	0.0097	0.14	2.6	0.86
	10	0.059	0.281	1.98	0.82	0.0125	0.158	2.4	0.83
	11*	0.041	0.244	2.5	0.52	0.0119	0.145	3.15	0.615
		← 150 KV →				← 100 KV →			

*Device with irregularities in the base-emitter junction periphery.

One particularly important feature of the response duration data is the relatively narrow spread in values for transistors of the same type. As a parameter to characterize the junctions, the response duration does not seem to be any more sensitive to structural variations than the more commonly measured parameters.

Another noteworthy result is the fact that response duration data does not appear to reflect in any way the presence of junction irregularities. Although the absence of data for the base-emitter junction response of Fairchild 2N3767's does minimize the data base for base-emitter junctions (i. e., the function directly affected by the observed flaws), there is no evidence of a significantly different response that could be a useful, reliable indicator of the presence of faults. Only the reduced response of the base-emitter junction of MHT 6424 No. 2 can be said to be significantly different, and that could not be attributed to or correlated with the presence or absence of flaws.

3.2.4 X-ray Responses of Transistors in Monolithic Arrays

The photocurrent and photovoltage responses were measured for the base-emitter and base-collector junctions of transistors in RCA CA3018A monolithic transistor arrays. Unlike discrete devices used in this study to represent microcircuit elements, the transistors in these arrays have dimensions and electrical characteristics that are typical of microcircuit elements. The X-ray responses obtained, therefore, are of the same order of magnitude that can be induced in individual microcircuit transistors. Since no faulty devices had been identified, the breakdown voltages, leakage currents, and current gains for the transistors were measured in an attempt to find faulty devices. Measurements of these parameters were made both before and after irradiation to monitor radiation damage effects, if any.

The results of electrical characterization and of X-ray response measurements are listed in Table 3-4. (The two values listed for each electrical characteristic were measured before and after irradiation.)

Particularly striking in the listing of electrical parameters was the very narrow spreads, both within a chip and from chip to chip. Only the leakage currents show a moderate degree of variability. Except for the leakage currents, the electrical parameters are also essentially unchanged

TABLE 3-4. X-RAY RESPONSES OF TRANSISTORS IN CA3018A MONOLITHIC ARRAYS

(Two sets of measurements are shown, which were taken before and after irradiation, respectively.)

Array No.		Breakdown Voltages				Gain (h_{fe}) V_{CE} = 3.0 V			Leakage Currents		Photovoltages		Photocurrents	
		C-E V	E-B V	C-B V	C-Subs V	I_c = 10 mA	1 mA	100 μA	(50V) C-B nA	(5V) E-B nA	C-B mV rms	B-E μV rms	C-B nA rms	B-E pA rms
1	Q1	23	6.8	59	93	73	81	72	1.3	0.37	0.148	29.2	0.078	8.2
		23	6.8	58	89	72	79	69	2.5	0.38				
	Q2	30	6.6	58	93	70	80	70.5	2.5	0.79	0.172	29.2	0.088	13.7
		32	6.6	58	90	68	78	69	3.6	0.76				
	Q3	26	7.0	58	92	77	85	81	1.4	0.22	0.170	26.4	0.089	18.4
		26.5	7.0	58	89	76	86	77.5	6.0	0.22				
	Q4	19	6.8	58	92	72	82	75	2.7	0.19	0.174	27.6	0.084	15.8
		19	6.8	58	89	71	82	73.5	2.6	0.34				
2	Q1	29	7.2	62	97	70	80	68	0.81	0.40	0.180	33.2	0.094	10.9
		33	7.15	60.5	98	70	76	60	0.29	0.05				
	Q2	28.5	7.1	61	96	66	80	72	1.8	0.38	0.192	35.6	0.102	12.2
		29	7.1	61	97	68	79	66	8.0	0.53				
	Q3	29	7.2	61	95	68	80	69	1.4	0.35	0.182	10.9	0.082	10.6
		32	7.15	61	92	69	75	61.5	2.0	0.40				
	Q4	29	7.2	61	96	72	78	68	1.5	0.17	0.198	31.2	0.124	29.6
		30	7.1	60.5	92	68	76	62.5	2.2	0.15				
3	Q1	27	7.0	59	94	81	94	84	1.1	0.26	0.129	25.8	0.069	11.0
		28.5	7.0	59	92	79	88	74	3.9	0.176				
	Q2	27	7.0	59	94	84	97	87	2.9	0.23	0.140	12.9	0.073	11.7
		28.0	7.0	59	92	82	94	80	2.55	0.27				
	Q3	26.5	7.0	59	94	84	97	86	2.0	0.17	0.140	11.1	0.074	8.48
		28.0	7.0	59	92	81	92	76	6.1	1.25				
	Q4	28.0	7.0	59	94	80	92	80	2.0	0.25	0.160	12.9	0.071	11.2
		29.0	7.0	59	93	79	88	72	6.9	0.54				
4	Q1	29.0	7.1	61	96	71	79	67	5.5	0.85	0.174	22.0	0.099	8.8
		30.0	7.05	60	94	70	76	60	8.2	0.66				
	Q2	29.5	7.1	61	96	68	78	67	4.1	0.19	0.168	20.4	0.083	8.16
		31.0	7.1	61	96	56	76	61	4.2	0.245				
	Q3	29.0	7.2	61	96	70	78	67	2.5	0.33	0.166	21.2	0.088	13.2
		31.0	7.1	60	94	69	76	59	3.0	0.50				
	Q4	29.0	6.8	61	96	66	74	64	4.4	1.4	0.186	26.0	0.083	13.6
		30.0	6.8	60	94	66	72	56	2.25	2.1				
5	Q1	32	6.8	70	93	73	86	75.5	27.0	0.73	0.176	38.0	0.97	15.6
		32.5	6.8	63	98	73	84	72	11.50	4.4				
	Q2	30.5	6.8	52	72	74	88	74	25.5	1.15	0.192	39.2	0.104	17.4
		34.0	6.8	53	76	74	87	73	14.0	0.80				
	Q3	32	6.8	60	92	72	84	72	11.0	1.1	0.186	16.0	0.097	15.5
		33.5	6.8	60	94	72	82	68	15.0	1.65				
	Q4	30	6.8	58	78	76	92	79	11.0	1.0	0.238	41.6	0.129	15.3
		31	6.8	58	80	76	85	75.5	15.5	1.41				

by the irradiation. There is a trend for leakage currents to increase following irradiation, although counter examples can be found in the tabulation. The leakage current changes cannot be ascribed to irradiation with certainty: such changes can be caused by exposure of the uncapped device to the ambient atmosphere.

The measured responses to irradiation show a degree of variability comparable to that of the leakage currents. However, there is no significant correlation between leakage currents and X-ray responses. (The X-ray responses are also uncorrelated with the other electrical parameters.) The magnitude of the responses are, as expected, much lower than for larger, discrete devices. The photovoltages fall in the range of ~10-20 μV, while photocurrents vary from ~ 8-130 pA.

3.2.5 Effects of Selective Filtering on X-ray Response

The photovoltage induced in the base emitter junction of a 2N3767 transistor (specimen No. 8) was measured with different thicknesses of different metal foils interposed between the X-ray source and the device. As discussed in Section 2.2, the absorption coefficient varies as Z^4/E^3, when Z is the atomic number of the absorber and E the X-ray photon energy. The use of filter foils of successively higher atomic numbers therefore selectively removes a greater proportion of the softer, lower energy X-rays. The discussion in Section 2.2 showed that it is these lower energy photons that are effective in stimulating the devices. Accordingly the rate of decrease of response should be steeper for the higher atomic number filters.

Figure 3-12 shows the responses obtained with Al (Z = 13), Ni (Z = 28), and Cu (Z = 29) filters. The data was obtained with the Tektronix 1A7A plug-in, which has 1 M ohm input impedance. (Since they are not open-circuit photovoltages, they do not vary logarithmically with effective intensity, which is why the figures are not straight lines. The data nevertheless are a valid representation of the decreased X-ray responses.) The fact that the X-ray response decreased slowly with Al filters shows that shadowing effects due to Al metallization in devices are negligible. (Each Al filter foil thickness used was 30.48 μm. Typical metallization thickness is on the order of 1 μm.)

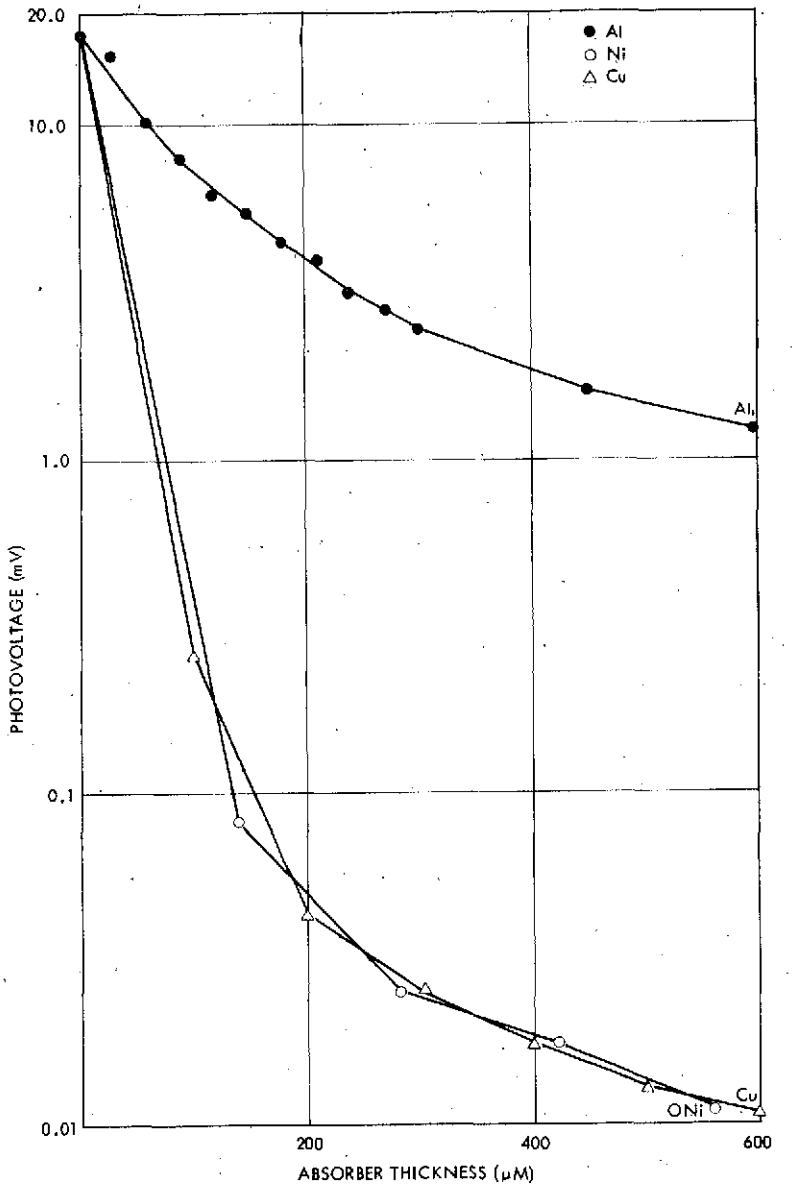

Figure 3-12. Responses obtained with Al, Ni, and Cu filters.

The data indicates no advantage to the use of filtering to remove lower energy X-rays, as it aggravates a low signal level problem.

3.2.6 Effects of Combined X-ray and Light Excitation

As discussed in Section 2.2, the effects of light and X-rays in generating hole-electron pairs in Si are qualitatively similar. They differ mainly in the number of hole-electron pairs created per absorbed photon and in the magnitude of the absorption coefficient. For light of 550 nm wave length, for example, the absorption coefficient is $\sim 10^4$ cm^{-1}, so most of the energy is absorbed on the top 4 μm of a Si specimen. A comparison of X-ray response versus combined X-ray and light response for a device therefore might disclose the presence of surface faults. Since junction irregularities in transistors appear to be surface faults, selected specimens of 2N3767 transistors, with and without faults, were used as test devices. The photovoltages and photocurrents from the base-emitter junctions were measured.

The light was produced by a fluorescent screen placed between the device and the X-ray source. Since the 11.4 x 15.2 cm screen intercepts a large amount of X-ray radiation that would not normally be available for stimulating the device, the low conversion efficiency of the fluorescent material was partially offset. Measurements were made with the light emissions alone by placing a small (1 x 1 cm) Pb shield on the screen to cast an X-ray shadow on the device. The signal level produced by the light alone was comparable to that produced by X-rays.

The data obtained in this experiment are listed in Table 3-5. The screen absorbs a fixed amount of X-ray intensity, so the behavior of interest is the change in radiation response with and without the fluorescent screen. It is evident from the tables that this change is quite variable from one device to another. However, there is no internal consistency with either the flawed device group (No. 3 and 9) or within the control group (No. 1, 5, and 10). Two chip types are represented here. Within the Fairchild group (1, 3, 5) the flawed device showed behavior opposite to that of the control group. Within the Solitron group (9, 10), this behavior pattern did not appear. The different behavior of the flawed Fairchild device could be due to causes unrelated to the presence of junction irregularities.

TABLE 3-5. EFFECTS OF COMBINED X-RAY AND LIGHT STIMULUS ON DEVICES WITH SURFACE FLAWS

Device No.	X-rays and Light		X-rays without screen		X-rays trans thru screen		Light only	
	Iph (nA)	Vph (mV)	Iph (nA)	Vph (mV)	Iph (nA)	Vph (mV)	Iph (nA)	Vph (mV)
1	1.46	2.52	0.800	1.26	0.041	0.080	1.38	2.40
3*	0.984	1.74	1.26	1.74	0.034	0.064	0.880	1.65
5	0.968	1.94	0.768	3.86	0.033	0.062	0.708	1.82
9*	1.31	1.44	3.24	3.60	0.036	0.070	0.670	1.28
10	2.00	2.14	4.92	4.64	0.037	0.082	0.820	1.92

*Devices with junction irregularities.

The fluorescent screen that was employed was made with a ZnS-CdS phosphor. Attempts were made to use a higher efficiency material — a commercial scintillation phosphor called Pilot B, which has a proprietary composition that its manufacturer will not disclose. (Pilot B is manufactured by Nuclear Enterprises of San Carlos, CA.) Unfortunately, the radiative decay time of this material was so long that its light output was unable to follow the X-ray pulses produced by the self-rectified X-ray tube. Since a-c coupled amplification was used to detect electrical responses, the phosphor was unfortunately not useful.

3.2.7 X-ray Responses of Transistors with Incipient Channels

Discrete transistors with high emitter-to-collector leakage were irradiated and photovoltage and photocurrent responses from both junctions were measured. A high emitter-to-collector leakage is indicative of surface contamination causing an incipient channel by inversion of the base region. Since the inverted material and the adjacent depleted region increase the effective depleted volumes for carrier collection of both the base-emitter and the base-collector junctions, the presence of a channel may cause an appreciable increase in the collected photocurrents.

Five 2N2222A leaky transistors and five control specimens were irradiated and measured. Both sets of transistors were manufactured by

Motorola. Unfortunately, when the control transistors were uncapped and examined, it was found that they were made with a chip design that was quite different from that of most of the leaky transistors. Only one leaky device, No. 5, had the same chip design. Since matching control specimens could not be located, the specimens on hand were irradiated and measured in an attempt to find a self-consistent correlation between some electrical parameter and the X-ray responses.

The measured electrical parameters and X-ray responses for the two groups of transistors are shown in Table 3-6. Transistors 1 through 5 are the leaky devices, as can be determined from the measurement of I_{CEO}. Transistors 6 through 10 are the control specimens. Only transistor 5, of the leaky devices, has the same type of chip as the control specimens.

The only positive observation that can be made concerning these measurements is that the device with the highest I_{CBO} and I_{EBO} leakage currents – device No. 1 – also has the highest photocurrent collected in the base-emitter junction. However, for the other devices these measurements are not correlated. On the basis of this isolated data point, the hoped-for correlation between leakage and collected photocurrents cannot be said to exist.

3.3 IRRADIATION EFFECTS ON TTL MICROCIRCUIT

As explained in the introduction, the difficulty of obtaining microcircuits with identified faults in a non-failed state makes it necessary to use microcircuits in which the presence of faults is suspected, but cannot be verified. For this study, three different types of TTL microcircuits were irradiated, both under power and unpowered. The test specimens were selected by testing a large number of circuits of each type and picking out those that appeared to have deviant behavior. A set of "normal" control specimens were tested along with the "mavericks". While the specimens were under power, certain specified electrical parameters were tested with and without irradiation in an attempt to see a change. Specified voltages were measured with a 4 digit DVM in order to insure high sensitivity to small, irradiation-induced changes.

TABLE 3-6. ELECTRICAL CHARACTERISTICS AND X-RAY RESPONSES OF LEAKY TRANSISTORS

Part No.	BV_{CEO}	BV_{CBO}	BV_{EBO}	h_{FE} V_{CE}=10V I_C=0.1 mA	h_{FE} V_{CE}=10V I_C=1.0 mA	h_{FE} V_{CE}=10V I_C=10 mA	h_{FE} V_{CE}=10V I_C=100 mA	I_{CEO} V_{CE}=50V	I_{CBO} V_{CB}=50V	I_{EBO} V_{EB}=5.0V	V_{ph} B-E'	V_{ph} B-C	I_{ph} B-E	I_{ph} B-C
1	57V	108V	7.2V	120	180	230	310	52 μA	6 μA	5 μA	0.41mV	1.23mV	0.225nA	0.85nA
2	58V	100V	7.8V	108	132	156	260	54 μA	35 nA	2.60nA	0.097mV	1.58mV	0.125nA	0.79nA
3	56V	99V	6.8V	92	122	153	220	62 μA	940 pA	1.20nA	0.104mV	1.46mV	0.16nA	0.75nA
4	56V	96V	7.4V	106	134	164	225	55 μA	880 pA	760 pA	0.097mV	1.49mV	0.14nA	0.74nA
5	64V	122V	8.5V	93	124	154	175	15 μA	17.0 nA	340 pA	0.51mV	1.83mV	0.49nA	0.89nA
6	98V	108V	7.4V	80	112	152	196	0.5 nA	55 nA	270 pA	0.41mV	2.26mV	0.45nA	1.18nA
7	84V	103V	7.4V	120	148	180	240	1.3 nA	1.7 nA	110 pA	1.08mV	2.74mV	0.82nA	1.43nA
8	86V	110V	7.3V	119	140	168	220	2.0 nA	4.2 nA	250 pA	0.25mV	2.20mV	0.29nA	1.18nA
9	88V	108V	7.0V	84	109	140	182	0.4 nA	200 pA	1.30 nA	0.35mV	2.26mV	0.38nA	1.19nA
10	87V	119V	7.3V	106	124	145	184	1.2 nA	21 nA	550 pA	0.18mV	2.12mV	0.32nA	1.11nA

All parameters measured before irradiation were also measured after irradiation in an attempt to detect possible radiation damage effects.

Since the brief analysis of a TTL NAND gate and its expected behavior under irradiation (presented in Section 2.7) indicated that irradiation effects might be undetectable, measurements of photovoltages and photocurrents were also made at the power (V_{cc}) and ground terminals.

The microcircuits tested were: DM 54L00F Quad Two-input-NAND gate, manufactured by National (a total of 150 tested); RSN 5400H radiation-hardened quad two-input NAND gate, manufactured by TI (a total of 100 tested); SN 5473W dual J-K master-slave flipflop, manufactured by TI (a total of 50 tested). Device specification sheets, as well as test results for the "maverick" and typical "normal" microcircuits, are shown in Appendix C.

One of the DM 54L00F gates, part No. 41, failed to pass its functional test on the automatic IC tester, so the procedure used to test it manually under irradiation differed from that for other parts of the same type.

Tables 3-7 through 3-9 list the results of measurements on powered devices. The results on the non-functional part (DM 54L00F No. 41) are as follows:

VoH tested at all 4 outputs —

0.129V at pin 14
0.125V at pin 3
0.128V - 0.129V at pin 5 No change detected under irradiation
0.129V at pin 8

Icc (0) = 1.129 mA, changes to 1.128 — 1.129 mA under irradiation.
Icc (1) = 0.402 — 0.403 mA; no change detectable under irradiation.

The other parameters were monitored on an x-y oscilloscope with 60 Hz a-c connected to the horizontal amplifier and with the appropriate pin on the microcircuit connected to the vertical amplifier. Since the X-ray machine operates the tube in the self-rectifying mode, the X-ray source emittted radiation during half of the horizontal sweep time. It was expected that a parameter change caused by the irradiation would appear as an oscilloscope trace with a non-zero slope. In practice, a complicated Lissajous

TABLE 3-7. IRRADIATION EFFECTS ON TTL MICROCIRCUITS: PART TYPE DM54L00F – QUAD TWO INPUT NAND GATE

Parameter Tested	Part Number 6 (Normal)		
	Before	During	After
V out (0)	0.123V avg. for each output	no change	no change
V out (1)		not tested	
V in (1)	1.330V avg. (1.335 high 1.328 low)	no change	no change
V in (0)	1.252V avg. (1.277 low, 1.297 high)	no change	no change
I in (1) at V in = 2.4V	1.17 μA	1.16 μA no scope change	1.16 μA no scope change
I in (1) at V in = 5.5V	1.50 μA	no change	no change
I in (0) at V in = 0.3V	-10.63 μA	no change	-10.62 μA no scope change
I cc (0)	1.178 mA	no change	no change
I cc (1)		not tested	

TABLE 3-8. IRRADIATION EFFECTS ON RADIATION-HARDENED TTL MICROCIRCUITS: PART TYPE RSN5400H – QUAD TWO INPUT NAND GATE

Parameter Measured	Part No. 4 (Normal)			Part No. 56 (Maverick)		
	Before	During	After	Before	During	After
V_{OH}	2.993V to 2.994V	no scope change	2.995V	2.989V to 2.992V	no scope change	same fluctuation in meter
V_{OL}	0.271V	no change	no change	0.239V	no change	no change
$V_{Thres.}$	goes 0.5 to 9 mA at 1.300V, 9 mA to 16 mA at 1.684V	no change	no change	0 to 7 mA at 1.294V, 7 to 16 mA at 1.50V	no change	no change
I_{CCH}	10.12 mA on digital, 10.5 mA on meter	no change	no change	12.71 mA on digital, 13.1 mA on meter	no change	no change
I_{CCL}	12.93 mA on digital, 13.4 mA on meter	no change	no change	16.0 mA on meter, 13.52 mA on digital	no change	no change
I_{H2}	0.00295 mA on meter, 0.00298 on digital	no change	no change	0.0115 mA on meter	no change	no change
I_{H1}	0.00245 mA on ammeter, 0.00238 mA on digital	no change	no change		no change	no change
I_{IL}	1.08 mA on ammeter, 1.100 mA on digital	no change	no change	1.05 mA	no change	no change

TABLE 3-9. IRRADIATION EFFECTS ON TTL MICROCIRCUITS: PART TYPE SN5473 – MASTER SLAVE J-K FLIP-FLOP

Parameter Measured	Part No. 20 (Maverick)			Part No. 43 (Maverick)		
	Before	During	After	Before	During	After
V in (1)	1.184V	1.182V no scope change	1.182V no scope change	voltage not recorded	no change	no change
V in (0)	1.228V	no change	no change	voltage not recorded	no change	no change
V_{OH}	$\overline{Q}$ = 3.371V at J=1, K=1	no change	no change	voltage not recorded	no change	no change
	$\overline{Q}$ = 3.367V at J=1, K=0	3.365V no scope change	3.365V no scope change			
V_{OL}	Q = 0.256V at J=1, K=1	no change	no change	voltage not recorded	no change	no change
	Q = 0.098V at J=1, K=0	no change	no change			
1 in (0) J	-1.20 mA	no change	no change	-1.05 mA	no change	no change
K	-1.20 mA	no change	no change	-1.05 mA	no change	no change
clear	-1.20 mA	no change	no change	-1.05 mA	no change	no change
clock	-2.20 mA	no change	no change	-1.95 mA	no change	no change
I_{H2} J	0.0026 mA	no change	no change	0.0037 mA	no change	no change
K	0.0016 mA	no change	no change	0.0021 mA	no change	no change
clear	0.0295 mA	no change	no change	0.032 mA	no change	no change
clock	0.0048 mA	no change	no change	0.0062 mA	no change	no change
I_{H1} J	0.0019 mA	no change	no change	0.0026 mA	no change	no change
K	0.0012 mA	no change	no change	0.0015 mA	no change	no change
clear	0.22 mA	no change	no change	0.0225 mA	no change	no change
clock	no data	no data	no data	no data	no data	no data
I_{os}	-5.5 mA	no change	no change	-5.0 mA	no change	no change

no change - no change on scope, ammeter, or digital VOM; no meter change, no digital change, no scope change - refer to individual pieces of equipment.

figure was observed because of strong a-c noise. However, the figure remained completely unchanged when the X-ray source was turned on and off.

The measurements of photovoltages and photocurrents from unpowered devices were performed from the power supply terminal to ground. The results for the radiation hardened NAND gates are shown in Table 3-10, while results for the regular NAND gates appear in Table 3-11.

TABLE 3-10. X-RAY RESPONSES OF RADIATION-HARDENED TTL PART TYPE RSN5400H

Mavericks			Average		
No.	V_{ph}	I_{ph}	No.	V_{ph}	I_{ph}
5	30.4 μV	0.034 nA	1	26.8 μV	0.034 nA
56	21.3 μV	0.028 nA	4	23.2 μV	0.026 nA
93	25.4 μV	0.030 nA	6	28.9 μV	0.036 nA
99	25.4 μV	0.030 nA	12	27.2 μV	0.036 nA

TABLE 3-11. X-RAY RESPONSES OF TTL MICROCIRCUITS: PART TYPE DM54L00F

Mavericks			Average		
No.	V_{ph}	I_{ph}	No.	V_{ph}	I_{ph}
67*	1.20 mV	3.22 nA	6	1.32 mV	1.79 nA
116	1.40 mV	2.09 nA	8	1.27 mV	1.71 nA
123	1.38 mV	-	9	1.41 mV	1.92 nA
125	1.32 mV	1.91 nA			
41Δ	1.40 mV	2.02 nA			

*67 - had slightly different metallization pattern.

Δ 41 - failed functional testing.

The results in Tables 3-10 and 3-11 show that the radiation-hardened devices have X-ray responses that are nearly two orders of magnitude lower than for conventional devices.

Device No. 67 in Table 3-11 had a slightly different metallization pattern from the rest of the same type number. The photocurrent response from this device is somewhat higher than from the others.

The results listed in Tables 3-7 through 3-11 give no indication whatsoever that X-ray-induced signals could have been used to detect the deviant behavior disclosed by the Tektronix 3260 tester. The devices under power exhibited no response at all to the irradiation. Without power there was a measurable response. However, the maverick and the normal devices had essentially similar responses. The fact that DM 54L00F No. 41, had an X-ray response that was very similar to that of No. 9 is particularly significant: No. 41 failed functional tests when tested manually and with the automatic tester, while No. 9 was one of the "normal" devices from the control group.

3.4 EFFECT OF IRRADIATION ON DIELECTRIC BREAKDOWN

This experiment was designed to look at the effects of irradiation on the dielectric breakdown strength of thin oxides. The experiment consisted of taking thirty-two HD1G 1030 insulated gate MOSFET devices in three groups and measuring the dielectric breakdown strength of a group either before, during, or after irradiation. The HD1G 1030 was chosen because of the controlled thickness of the gate oxide. Threshold voltages were measured to verify that the devices had similar gate oxides. The groups were chosen such that the mean and standard deviation of the threshold voltages would be similar in each group.

It was hoped that a decrease in dielectric breakdown under irradiation would be observed. If so, devices with thin or weak oxides could be screened out by applying a predetermined voltage stress during exposure to radiation. Good devices would be unaffected, others would be destroyed. The application of this effect could be extended to any device with metal stripes separated from other circuit components by a dielectric glass. Unfortunately, the results were negative.

Results of this experiment are tabulated in Table 3-12. Note that in several devices tested during or after irradiation non-destructive breakdown occurred, while in the control samples all devices broke down catastrophically. This indicates that irradiation produces irreversible changes in MOS devices and possibly should not be considered further. Means and standard deviations were calculated for the gate-to-source breakdown voltage of each group of devices.

For the control group, $\overline{BV}_{GS}$ = 120.0V with a large standard deviation of 20.76V. For the devices broken down during irradiation, the values were 104.9V and 3.9V respectively. For the devices tested after radiation exposure, the values were 103.9V and 6.01V. Note that the values obtained after irradiation are very similar to those obtained during irradiation. Also note that change caused by irradiation is less than one standard deviation of the control group. This indicates that such a screen would be inconclusive even if it worked in principle, because the changes effected by irradiation are smaller than the normal device tolerances.

In summary, then, a number of MOSFET devices were tested to determine the effect of irradiation on dielectric breakdown. It was found that while irradiation adversely affects device characteristics, the desirable changes are not large enough to be useful.

TABLE 3-12. RESULTS OF SiO_2 BREAKDOWN EXPERIMENT

Device No.	$\lvert V_{threshold} \rvert$ Volts	Gate-to-Source Breakdown Voltage (Volts)		
		No Radiation	During Radiation	After Radiation
0	2.25		106*(2)	
1	2.25		100	
2	1.82		shorted (3) out	
3	2.22		108*	
4	2.58		96	
5	2.30		106*	
6	2.15		106*	
7	2.11		106	
8	2.28		108*	
9	2.68		108*	
10	2.08	104		
13	2.50	126		
14	2.00	107		
18	2.32	78		
19	2.28	120		
21	2.38	128		
22	1.94	144		
23	2.30	138		
26	2.30	132		
28	2.00	148		
31(1)	2.24	95		
11	1.90			100*(2)
12	2.20			112
15	1.73			106
16	2.28			88
17	2.70			104
20	2.30			105*
24	2.20			106*
25	2.26			108*
27	2.25			106
29	2.28			108*
32	2.37			100

(1) There was no device No. 30.

(2) * Indicates breakdown was not catastrophic and is repeatable.

(3) Gate damaged before test.

4.0 SUMMARY AND CONCLUSIONS

The study project described in this report investigated the possibility of using X-rays as a stimulus for screening microcircuits during precap visual inspection. The tasks that were performed and results that were obtained are as follows:

1. A theoretical analysis and a literature search were carried out on the subject of X-ray interactions with semiconductor materials and devices. Calculations showed that X-ray-induced carrier generation rates are limited to being no greater than thermal generation rates for conventional X-ray machines. It was also determined that certain types of flaws could alter the X-ray response of microcircuit elements, although no dramatic enhancement of flaw detectability by the irradiation could be predicted. The possibility of radiation damage to dielectrics was investigated, but the sparse literature on the subject yielded few qualitative results.
2. The X-ray-induced photovoltages and photocurrents from both junctions of 2N3767 power transistors were measured. Some of the test devices were known to have irregularities in the base-emitter junctions. No correlation was found between the presence of flaws and the X-ray responses.
3. The flash X-ray-induced transient photovoltages from the same transistors, plus four other transistors of a different type, were measured. No correlation could be found between response decay time and the presence of flaws.
4. Photovoltages and photocurrents were measured in transistors in CA3018A monolithic transistor arrays. In three devices, comparable to microcircuit elements, photovoltages were measured in the range of tens of hundreds of microvolts; photocurrents were in the range of about ten to one hundred picoamperes. No correlations with electrical parameter variations were found, and no anomalies or faults were indicated by unusual X-ray responses. Breakdown voltages, leakages, and current-gain measured before and after irradiation showed little or no damage attributable to the irradiation.

5. The effects of using metal foils to filter out soft X-rays were observed. The results were as expected from theoretical considerations.

6. The effects of combining a fluorescent screen with X-ray stimulus were studied. Since irregularities in the base-emitter junction periphery occur at the surface (where light is strongly absorbed), the possibility of enhancing their detectability by this technique was explored; the results of the experiment were negative.

7. X-ray responses of transistors with incipient channels were measured to see if channels would affect (i. e. , increase) the amount of collected carriers. The results for the base-collector junction were negative; for the base-emitter junction there were suggestions of a correlation with high I_{EBO}, but on the basis of a small sampling the result is not conclusive.

8. Effects of irradiation on measured parameters of powered TTL microcircuits (two types of NAND gates, one type of flip-flop) were investigated; during irradiation no effect at all was detectable with a four-digit DVM on major parameters. No unusual effects on "maverick" microcircuits were detected.

9. Photovoltage and photocurrents from selected maverick and normal microcircuits were measured from the power supply terminal to ground. No correlation with deviant performance was found. In particular, a device that had failed functional testing was not detected by an unusual X-ray response.

10. The possibility of using X-rays as a failure-inducing stress for thin dielectrics was explored briefly. It was hoped that the irradiation would cause a significant decrease in the breakdown voltage of SiO_2. Measurements of gate oxide breakdown on MOSFET's showed no such decrease; however, the irradiated devices showed a significant tendency to break down reversibly. Non-irradiated devices failed catastrophically.

In summary, the theoretical and experimental results of this project do not indicate that X-rays can be used to enhance in any practical way the detectability of flaws in semiconductor devices. Moreover, X-rays are particularly difficult to handle experimentally. They cannot be focused (either by reflection or refraction), produced efficiently in intense beams, polarized, reflected or refracted, scanned or otherwise localized, or monochromatized.

They are also a potential health hazard. In view of these drawbacks and the negative results obtained in this study, it cannot be recommended that work on the use of X-rays as a microcircuit screen be continued. However, the theoretical phase of this study has indicated that the energy range between 1.1 ev and 4.0 ev (11,000 to 3100 Angstroms) does have potential as a microcircuit screen. The low energy end of this region is established by the need to exceed the bandgap energy of silicon, while the upper limit avoids undesirable photoemission charging of SiO_2. An effort to apply this portion of the EM spectrum as a low cost screen to augment present visual and electrical processes is recommended.

5.0 LITERATURE CITED

B. Andre, J. Buxo, D. Esteve, and H. Martinot, "Effects of Ionizing Radiation on MOS Devices," Solid State Electron, 12, p. 121 (1969).

D. Esteve and J. Buxo, "Degradation Mechanism of MOS Structures and Transistors Under Ionizing Radiation," Electronics Letters, 6, #7, p. 198 (April 1970).

D. Esteve and J. Buxo, "On the Behaviour of Currents Going Through MOS Structures Under Ionizing Radiations," Solid State Electron, 14, p. 257 (1971)

G. W. Grodstein, "X-ray Attenuation Coefficients from 10KeV to 100MeV," Circular 583, National Bureau of Standards. (1957)

B. L. Henke and R. L. Elgin, "X-ray Absorption Tables for the 2 to 200 Å Region," Advances in X-ray Analysis, 13, p. 639 (1969).

E. Storm, H. I. Israel, and D. W. Lier, "X-ray Spectral Distributions from Thick Tungsten Targets in the Energy Range of 12 to 300KV," Advances in X-ray Analysis, 15, p. 339 (1970).

APPENDIX A. EQUIPMENT DESCRIPTIONS

A.1 FAXITRON 8060

One of the X-ray sources used in this work, the one used for most of the photocurrent and photovoltage measurements, was the Faxitron Model 8060. The Model 8060 is a continuous exposure X-ray system employing a self rectifying X-ray tube. The tube uses a tungsten filament and a tungsten target. The inherent filtration of the system is due to a beryllium window. The machine generates X-rays of up to 110 kV. A source-to-target distance of 34.6 cm was used for most measurements. Chamber construction prevented the use of shorter working distances. Refer to Figure A-1.

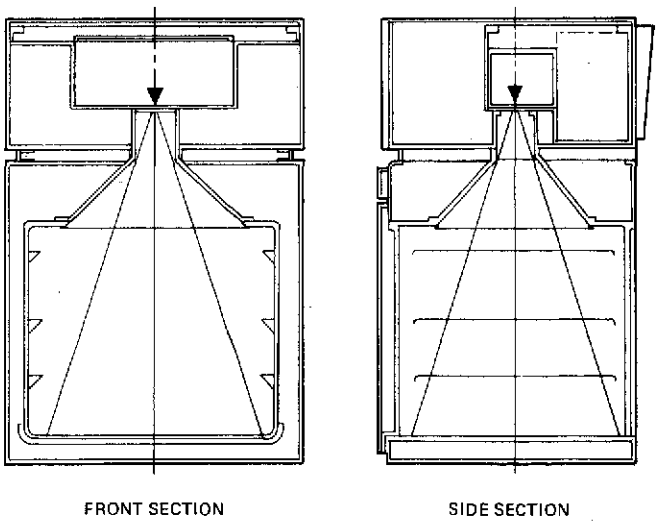

Figure A-1. Chamber arrangement of Faxitron 8060

Specifications of the Faxitron Model 8060

Power Input Requirements:	Voltage: 110-120 V ac (230 V ac optional)
	Frequency: 60 (50 Hz optional)
Power Output to X-ray Tube:	Voltage: 10-110 kV peak
	Current: 3 mA at 110 kVP
Duty Cycle (Expose on Time):	Continuous
X-ray System Type:	Self rectified.
Spot Size:	0.5 mm (as measured by Fed. Std. No. 83).
Target Angle:	20^{o}
Beam Half Angle:	15, +1-1/2 degrees
Inherent Filtration:	0.635 mm Beryllium max. – provisions in exposure chamber for slide-in filter.
Penetration:	A minimum of 6.25 mm steel or 51 mm aluminum w/type M film.
Film-to-Source Distance:	610 mm with exposure shelf in place. 650 mm maximum. Dual cabinet configuration allows 1.260 m FTSD.
Beam Size at Floor:	340 mm diameter.

A.2 FEXITRON 8030

The use of a pulsed X-ray system was explored. For this experimental work a Fexitron Model 8030 was used. The Model 8030 produces a train of high energy, high intensity X-ray pulses of 60 nanoseconds duration. Up to ninety-nine pulses may be produced in a single pulse train. The unit uses a Fexitron Model 532 cold cathode X-ray tube with an effective spot size of 1.8 mm.

Specifications of the Fexitron 8030

X-ray tube voltage	150 kv 100 kv
Effective MAS/pulse	0.06 MAS at 150 kv 0.03 MAS at 100 kv
MAS/99 pulse train	6 MAS at 150 kv 3 MAS at 100 kv

Pulse duration	60 nanoseconds
Pulse rate (at nominal 120 VAC or 240 VAC input)	14 per second at 100 kv 7 per second at 150 kv
Pulse number selection	1 to 99 pulses
Effective X-ray source size	1.8 mm diameter
Inherent filtration	exceeds 2.5 mm aluminum equivalent

A.3 BIOMATION TRANSIENT RECORDER

The Biomation Model 610 Transient Recorder was used to digitize and store data from the pulsed X-ray experiments until the data could be recorded on an oscilloscope. The Model 610 Recorder utilizes a high speed six bit analog-to-digital converter combined with a shift register memory to capture and hold an analog signal. The signal is outputted through a smoothing network to an oscilloscope or an x,y plotter where the data are recorded. Refer to Figure A-2.

A.4 CURRENT AMPLIFIER

The photocurrents expected in the experiments were smaller than could be accurately be observed with available equipment. In order to facilitate measurement a current amplifier suitable for this work was constructed. The amplifier consists of an LH0032 current amplifier hybrid microcircuit and an LH0002 line driver with appropriate discrete components. The LH0032 is an FET input, high input impedance, low noise, precision current amplifier suitable for picoamp measurements. The LH0002 provides the power capability of driving cables, an oscilloscope, and/or a current meter. The amplifier circuit was housed in a lead-shielded container to provide for its use within an X-ray machine.

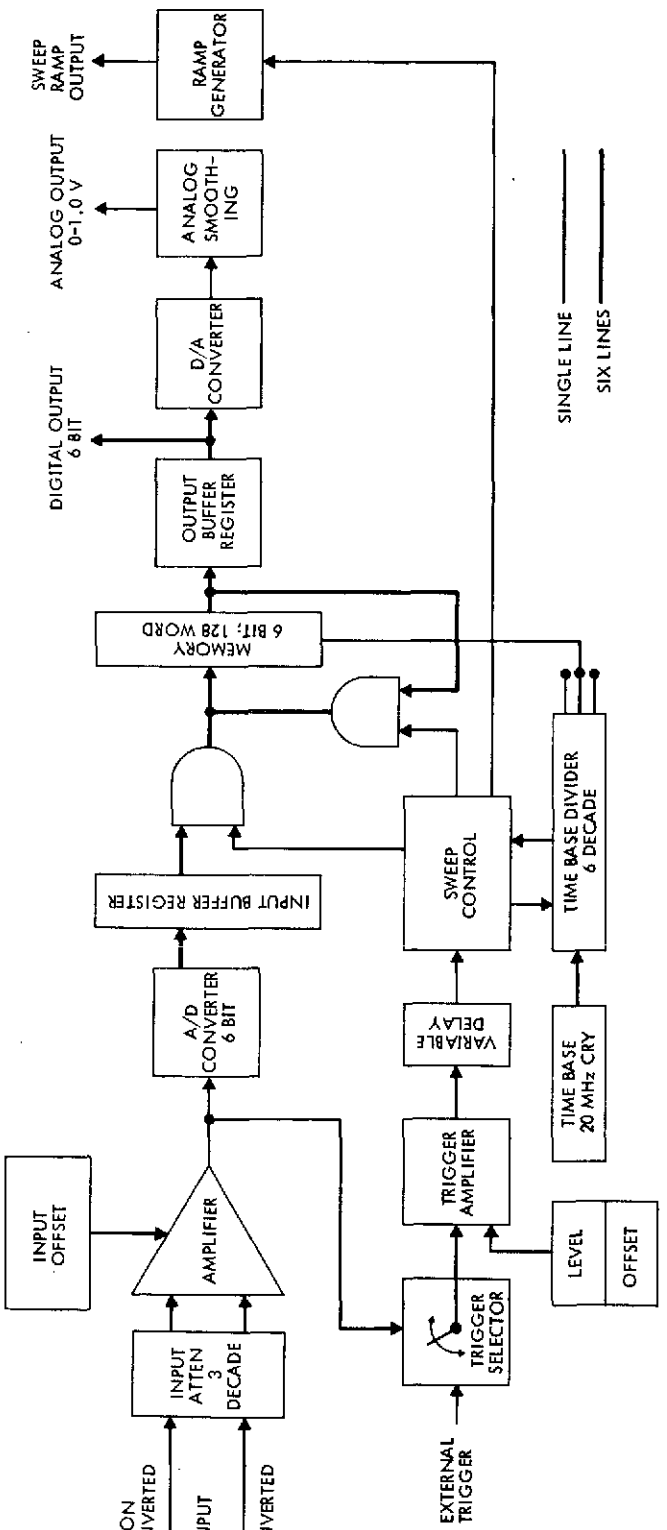

Figure A-2. Flow chart of Biomation Model 610 operation.

APPENDIX B. SCANNING ELECTRON MICROSCOPE ELECTRON BEAM INDUCED CURRENT TECHNIQUES

The scanning electron microscope (SEM), operated in the electron beam induced current (EBIC) mode, was utilized during the course of the experiments to detect certain junction flaws and to simulate localized high doses of X-rays. In the SEM a high energy electron beam impinges on the test device. The electrons in this beam are very similar to the primary photoelectrons produced by X-ray photons absorbed by a sample. They produce electron-hole pairs by collisions until the energy of the initial electrons has been dissipated as phonons, photons, electrons and holes, as explained in Section 2.2 of this report.

The EBIC mode makes use of the electron-hole pairs generated by the beam. In areas of low electric field most of the electron-hole pairs will recombine. In areas of higher electric fields, however, the electrons and holes will be separated, generating an external current. When a junction is reverse-biased, the depletion regions are areas of high electric field, with the remainder of the device subjected to comparatively low fields. Thus, when the electron beam impinges on the sample near a junction, the electron-hole pairs generated form a current, and when the beam is impinging on the sample away from a junction, the carriers recombine before being collected as a current. This electron-beam-induced current that appears at junctions is passed through a specimen current amplifier and used as Z-modulation on a video display. Junction areas appear white, other areas appear dark.

The EBIC signal is not the only signal to affect the current amplifier. If a component of the specimen current is produced by some other mechanism, such as leakage or avalanching, this current will also affect the video display. If one or more areas of the junction breakdown at a lower applied voltage than the remainder of the junction and this area avalanches, such areas will appear

in the video display as a bright dot or a flare located on the junction perimeter. It is these localized breakdown spots for which the devices were examined. Such spots are associated with device flaws which one would like to screen out. A comparison between anomalies located in this manner and anomalous device behavior during X-ray flooding was attempted.

APPENDIX C. TEST DEVICE DESCRIPTIONS

This appendix contains photographs, chip dimensions and abridged data sheets for each device type tested during the course of these investigations.

C.1 2N3810 (REFER TO FIGURE C-1)

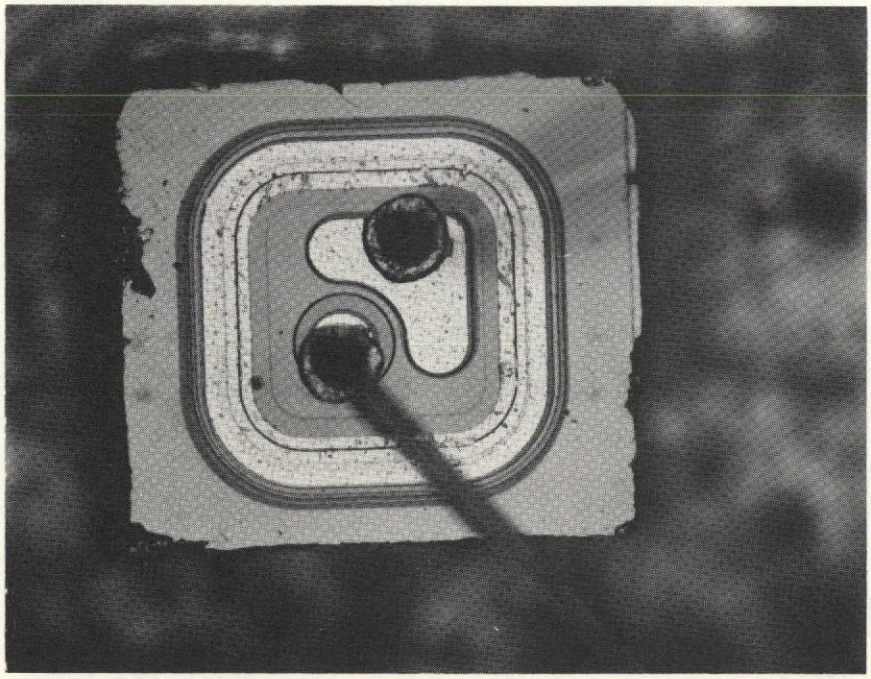

Figure C-1. Photograph of one die in a 2N3810. Both dies are of this configuration; die size is 390 x 370 μm, 15.4 x 14.5 mils (magnification: 172X)

TABLE OF ELECTRICAL SPECIFICATIONS (2N3810)

Characteristic	Symbol	Min	Max	Unit
Off Characteristics				
Collector-Emitter Breakdown Voltage (1) (I_C = 10 mAdc, I_B = 0)	BV_{CEO}	60	-	Vdc
Collector-Base Breakdown Voltage (I_C = 10 μAdc, I_E = 0)	BV_{CBO}	60	-	Vdc
Emitter-Base Breakdown Voltage (I_E = 10 μAdc, I_C = 0)	BV_{EBO}	5.0	-	Vdc
Collector Cutoff Current	I_{CBO}			μAdc
(V_{CB} = 50 Vdc, I_E = 0)		-	0.01	
(V_{CB} = 50 Vdc, I_E = 0, T_A = 150°C)		-	10	
Emitter Cutoff Current	I_{EBO}			nAdc
($V_{BE(off)}$ = 4.0 Vdc, I_C = 0)		-	20	
On Characteristics				
DC Current Gain (1)	h_{FE}			-
(I_C = 10 μAdc, V_{CE} = 5.0 Vdc)		100	-	
(I_C = 100 μAdc, V_{CE} = 5.0 Vdc)		150	450	
(I_C = 100 μAdc, V_{CE} = 5.0 Vdc, T_A = 55°C)		75	-	
(I_C = 500 μAdc, V_{CE} = 5.0 Vdc)		150	450	
(I_C = 1.0 mAdc, V_{CE} = 5.0 Vdc)		150	450	
(I_C = 10 mAdc, V_{CE} = 5.0 Vdc)		125	-	

(Continued next page)

TABLE OF ELECTRICAL SPECIFICATIONS (2N3810) (Continued)

Characteristic	Symbol	Min	Max	Unit
On Characteristics				
Collector-Emitter Saturation Voltage (1)	$V_{CE(sat)}$			Vdc
(I_C = 100 μAdc, I_B = 10 μAdc)		-	0.2	
(I_C = 1.0 mAdc, I_B = 100 μAdc)		-	0.25	
Base-Emitter Saturation Voltage (1)	$V_{BE(sat)}$			Vdc
(I_C = 100 μAdc, I_B = 10 μAdc)		-	0.7	
(I_C = 1.0 mAdc, I_B = 100 μAdc)		-	0.8	
Base-Emitter On Voltage	$V_{BE(on)}$			Vdc
(I_C = 100 μAdc, V_{CE} = 5.0 Vdc)		-	0.7	
Small-Signal Characteristics				
Current Gain - Bandwidth Product	f_T			MHz
(I_C = 500 μAdc, V_{CE} = 5.0 Vdc, f = 30 MHz)		30	-	
(I_C = 1.0 mAdc, V_{CE} = 5.0 Vdc, f = 100 MHz)		100	500	
Small-Signal Current Gain	h_{fe}			
(I_C = 1.0 mAdc, V_{CE} = 10 Vdc, f = 1.0 kHz)		150	600	

(Continued next page)

TABLE OF ELECTRICAL SPECIFICATIONS (2N3810) (Concluded)

Characteristic	Symbol	Min	Max	Unit
Matching Characteristics				
DC Current Gain Ratio[2]	h_{FE1}/h_{FE2}			-
(I_C = 100 μAdc, V_{CE} = 5.0 Vdc)		0.9	1.0	
(I_C = 100 μAdc, V_{CE} = 50 Vdc, T_A = -55 to +125°C)		0.85	1.0	
Base Voltage Differential	$\lvert V_{BE1} - V_{BE2} \rvert$			mVdc
(I_C = 10 μAdc to 10 mAdc, V_{CE} = 5.0 Vdc)		-	5.0	
(I_C = 100 μAdc, V_{CE} = 5.0 Vdc)		-	1.5	
Base Voltage Differential Gradient	$\lvert \Delta V_{BE1} - V_{BE2} \rvert$			mVdc
(I_C = 100 μAdc, V_{CE} = 5.0 Vdc, T_A = -55 to +25°C)		-	0.4	
(I_C = 100 μAdc, V_{CE} = 5.0 Vdc, T_A = +25 to +125°C)		-	0.5	

*Indicates JEDEC Registered Data.
(1) Pulse Test: Pulse Width 300 μs, Duty Cycle 2.0%.
(2) The lowest h_{FE} reading is taken as h_{FE1} for this ratio.

C-2. 2N3767 (REFER TO FIGURES C-2 AND C-3)

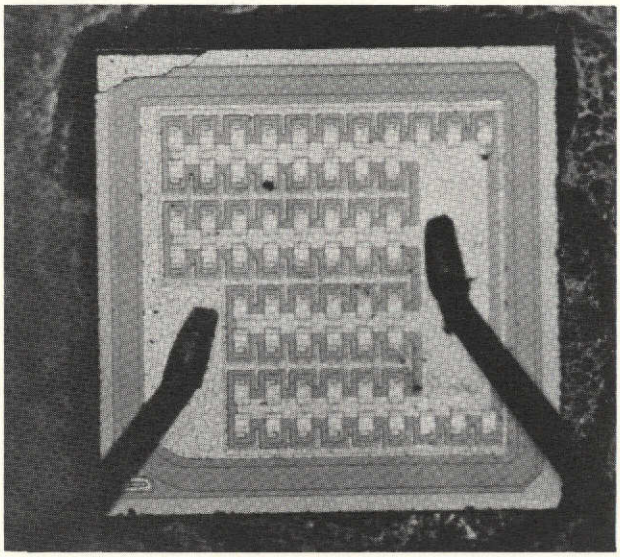

Figure C-2. 2N3767 as manufactured by Fairchild. Die is 1.7 x 1.7 mm (37X).

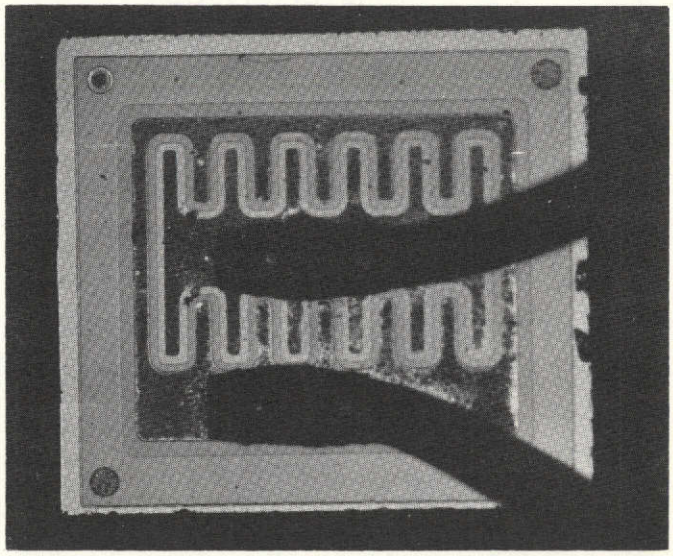

Figure C-3. Solitron 2N3767. Die is 1.8 x 1.7 mm (37X).

SPECIFICATIONS (2N3767)

Collector Current - Continuous Peak	I_C	4.0 4.0		Adc
Base Current	I_B	2.0		Adc
Total Device Dissipation at $T_C = 25^oC$ Derate above 25^oC	P_D	20 0.133		Watts $W/^oC$
Thermal Resistance	θ_{JC}	7.5		$^oC/W$
Operating and Storage Junction Temperature Range	T_J, T_{stg}	-65 to ^{o}175		^oC
Characteristic	Symbol	Min	Max	Unit
Off Characteristics				
Collector-Emitter Voltage (1) (I_C = 100 mAdc, I_B = 0)	BV_{CEO}	80	-	Vdc

(Continued next page)

SPECIFICATIONS (2N3767) (Continued)

Characteristic	Symbol	Min	Max	Unit
Off Characteristics				
Emitter-Base Cutoff Current	I_{EBO}			mAdc
(V_{EB} = 6 Vdc)		-	0.76	
Collector Cutoff Current	I_{CEX}			mAdc
(V_{CE} = 100 Vdc, V_{BE} = 1.5 Vdc)		-	0.1	
(V_{CE} = 70 Vdc, V_{BE} = 1.5 Vdc, T_C = 150°C)		-	1.0	
Collector-Emitter Cutoff Current	I_{CEO}			mAdc
(V_{CE} = 80 Vdc, I_B = 0)		-	0.7	
Collector-Base Cutoff Current	I_{CBO}			mAdc
(V_{CB} = 100 Vdc, I_E = 0)		-	0.1	
On Characteristics				
DC Current Gain	h_{FE}			-
(I_C = 50 mAdc, V_{CE} = 5 Vdc)		30	-	
(I_C = 600 mAdc, V_{CE} = 5 Vdc)		40	160	
(I_C = 1.0 Adc, V_{CE} = 10 Vdc)		20	-	
Collector-Emitter Saturation Voltage	$V_{CE(sat)}$			Vdc
(I_C = 1 Adc, I_B = 0.1 Adc)		-	2.5	
(I_C = 500 mAdc, I_B = 50 mAdc)		-	1.0	
Base-Emitter Voltage	V_{BE}			Vdc
(I_C = 1.0 Adc, V_{CE} = 10 Vdc)		-	1.5	

(Continued next page)

SPECIFICATIONS (2N3767) (Concluded)

Characteristic	Symbol	Min	Max	Unit
Transient Characteristics				
Current-Gain — Bandwidth Product (I_C = 500 mAdc, V_{CE}, 10 Vdc f = 10 MHz)	f_T	10	-	MHz
Common-Base Output Capacitance (V_{CB} = 10 Vdc, I_C = 0 Adc, f = 100 kHz)	C_{ob}	-	50	pF
Small-Signal Current Gain (I_C = 100 mAdc, V_{CE} = 100 Vdc, f = 1 kHz)	h_{fe}	40	-	-
(1) Pulse Test: Pulse Width 300 μs, Duty Cycle ≤ 2.0%.				

C-3. MHT 6424 (REFER TO FIGURE C-4)

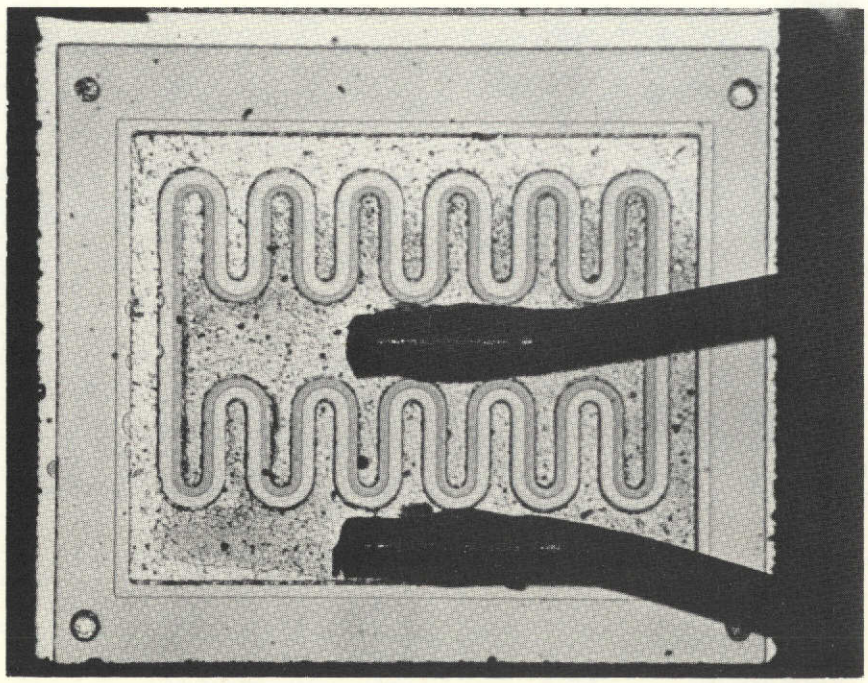

Figure C-4. Die of MHT 6424. Chip size is 2.2 x 1.95 mm (44X).

MAXIMUM RATINGS (MHT 6424)

At T_A = 25°C			At T_C = +100°C	Ambient Temperature Range (°C)		
V_{CEO} (sust) (Vdc)	h_{FE} (At I_C = 1 Adc) Min	h_{FE} (At I_C = 1 Adc) Max	V_{EBO} (Vdc)	① P_c (W)	Operating	Storage	Altitude (feet)
80	100	300	8.0	30	-65 to +175	-65 to +200	Unlimited

ELECTRICAL CHARACTERISTICS (MHT 6424)

Test	Conditions	Symbol	Limits Min	Limits Max	Unit
Breakdown Voltage, Collector to Base	I_C = 10 μAdc I_E = 0	BV_{CBO}	100	-	Vdc
Sustaining Voltage, Collector to Emitter, Open Base	I_C = 100 mAdc I_B = 0	$V_{CEO(sust)}$	80	-	Vdc
Breakdown Voltage, Emitter to Base, Open Collector	I_E = 10 μAdc I_C = 0	BV_{EBO}	8	-	Vdc
Emitter-to-Base Cutoff Current, Open Collector	V_{EB} = 6 Vdc I_C = 0	I_{EBO}	-	1.0	μAdc
Collector-to-Emitter Cutoff Current, Forward-Biased Base	V_{CE} = 30 Vdc V_{BE} = 0.3 Vdc	I_{CEX}	-	10	μAdc
Collector-to-Emitter Saturation Voltage Condition 1	See 4.1(c)* I_C = 1.0 Adc I_B = 25 mAdc	$V_{CE(sat)_1}$	-	0.3	Vdc

(Continued next page)

ELECTRICAL CHARACTERISTICS (MHT 6424) (Concluded)

Test	Conditions	Symbol	Limits		Unit
			Min	Max	
Condition 2	I_C = 500 mAdc I_B = 25 mAdc	$V_{CE(sat)_2}$	-	0.2	Vdc
Base-to-Emitter Saturation Voltage	I_C = 1.0 Adc I_B = 25 mAdc See 4.1(c)	$V_{BE(sat)}$	-	1.1	Vdc
Static Forward-Current Transfer Ratio					
Condition 1	V_{CE} = 2.0 Vdc I_C = 100 mAdc	h_{FE_1}	100	350	-
Condition 2	V_{CE} = 2.0 Vdc I_C = 1.0 Adc	h_{FE_2}	100	300	-
Condition 3	V_{CE} = 0.5 Vdc I_C = 25 mAdc	h_{FE_3}	75	-	-
Condition 4	V_{CE} = 0.5 Vdc I_C = 100 mAdc	h_{FE_4}	85	-	-
Condition 5	V_{CE} = 0.5 Vdc I_C = 500 mAdc	h_{FE_5}	70	-	-
Open-Circuit Output Capacitance	V_{CB} = 10 Vdc I_E = 0 f = 1 Mc	C_{ob}	-	130	pf
Small-Signal Short-Circuit Forward-Current Transfer Ratio	V_{CE} = 10 Vdc I_C = 1 Adc f = 10 Mc	h_{fe}	3	-	-
Pulse Response					
Delay Time Plus Rise Time		$t_d + t_r$	-	0.3	μsec
Storage Time Plus Fall Time		$t_s + t_f$	-	1.8	μsec

C-4. HDIG 1030 (REFER TO FIGURE C-5)

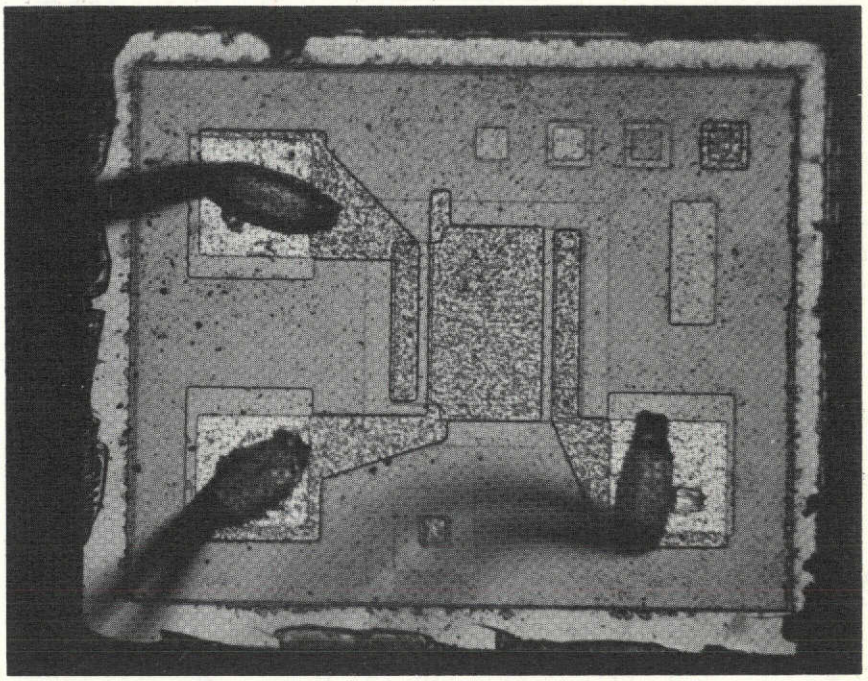

Figure C-5. HDIG 1030 chip. Chip is .64 mm by .51 mm (176X).

ELECTRICAL CHARACTERISTICS (HDIG 1030)

Parameter	Symbol	Conditions	Min.	Type.	Max.	Units
Channel Resistance	R_{ON}	V_{GS} = -10 V I_{DS} = -1 mA		250	330	Ω
Threshold Voltage	V_{TH}	V_{DS} = V_{GS} I_{DS} = -10 μA	-0.7	-2.0	-3.0	V
Gate Breakdown	BV_{GDSB}	V_{DSB} = 0 I_{DSB} = -10 μA	±25			V
Drain Breakdown	BV_{DSB}	V_{GSB} = 0 I_{DSB} = -10 μA	-15	-25		V
Source Breakdown	VB_{SDB}	V_{GDB} = 0 I_{SDB} = -10 μA	-15	-25		V
Gate Leakage	I_{GDSB}	V_{GDSB} = -15V			0.1	nA

(Continued next page)

ELECTRICAL CHARACTERISTICS (HDIG 1030) (Concluded)

Parameter	Symbol	Conditions	Min.	Typ.	Max.	Units
Drain Leakage	I_{DSB}	V_{DSB} = -5V		-0.05	-1.5	nA
Source Leakage	I_{SDB}	V_{SDB} = -5V		-0.05	-1.5	nA
Transconductance	g_m	V_{DSB} = -10 V I_{DS} = -1 mA		1.4		mmhos
Drain-Source Capacitance	C_{GD}	f = 1 MHz		2.0	3.0	pf
Gate-Source Capacitance	C_{GS}	f = 1 MHz		2.0	3.0	pf
Gate-Drain Capacitance	C_{DS}	V_{DSB} = -5V f = 1 MHz		1.7	2.0	pf
Total Gate Capacitance	C_{GDSB}	f = 1 MHz		3.5	4.0	pf

C-5. 2N2222A (REFER TO FIGURES C-6 AND C-7)

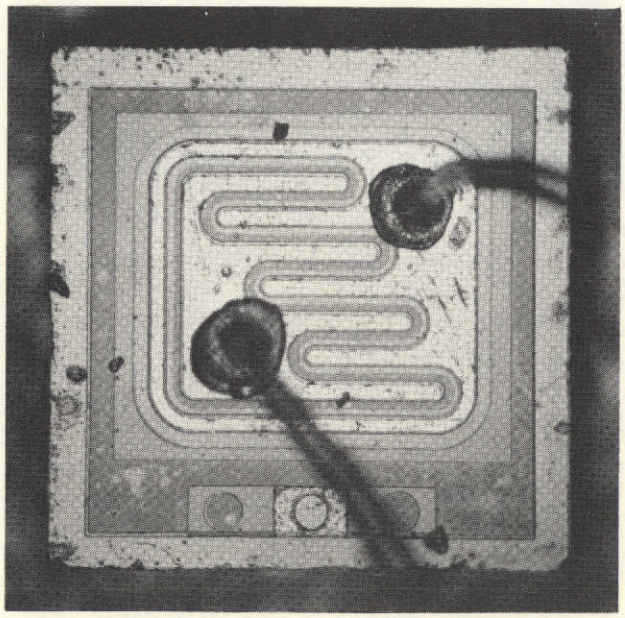

Figure C-6. 2N2222A chip, as used in the control devices and one leaky transistor (#5). Chip is .52 mm by .52 mm (132X).

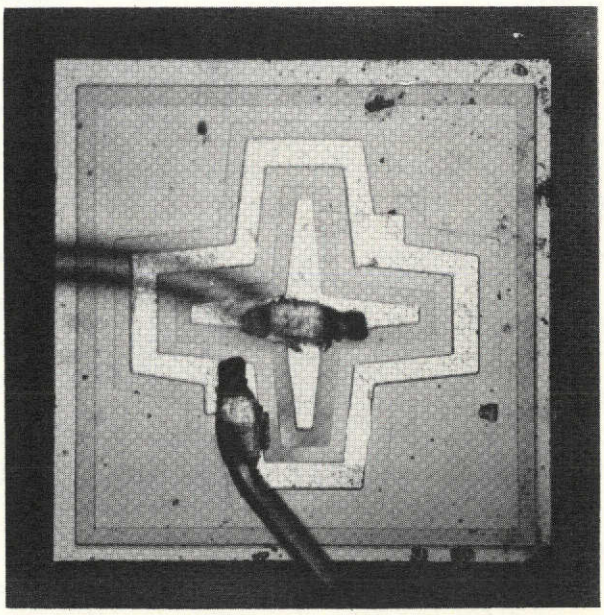

Figure C-7. 2N2222A chip, as used in the leaky transistors numbered 1 through 4. Chip is .50 mm by .50 mm (132X).

ELECTRICAL CHARACTERISTICS (2N2222A)

Test	Conditions	Limits at Temperature			Units
		T_A -55° C	T_A +25° C	T_A +150° C	
BV_{CBO}	I_C = 10 μA, I_E = 0; Cond D		75 min		V
BV_{EBO}	I_E = 10 μA, I_C = 0; Cond D		6 min		V
BV_{CEO}	I_C = 10 mA pulsed, I_B = 0; Cond D		50 min		V
I_{CBO}	V_{CB} = 60 V, I_E = 0; Cond D		0.01 max	10 max	A
I_{EBO}	V_{EB} = 4 V, I_C = 0; Cond D		10 max		nA
$V_{BE(sat)_1}$	I_C = 150 mA, I_B = 15 mA pulsed; Cond A		1.2 max		V
$V_{BE(sat)_2}$	I_C = 500 mA, I_B = 50 mA pulsed; Cond A		2.0 max		V
$V_{CE(sat)_1}$	I_C = 150 mA, I_B = 150 mA pulsed		0.3 max		V
$V_{CE(sat)_2}$	I_C = 500 mA, I_B = 50 mA pulsed		1.0 max		V
h_{FE_1}	V_{CE} = 10 V, I_C = 0.1 mA		50 min		--
h_{FE_2}	V_{CE} = 10 V, I_C = 1.0 mA		75 min		--
h_{FE_3}	V_{CE} = 10 V, I_C = 10 mA pulsed	35 min	100 min		--
h_{FE_4}	V_{CE} = 10 V, I_C = 150 mA pulsed		100/300		min/max
h_{FE_5}	V_{CE} = 10 V, I_C = 500 mA pulsed		30 min		--
h_{fe}	V_{CE} = 10 V, I_C = 1.0 mA f = 1 kHz		50 min		--
$\lvert h_{fe} \rvert$	V_{CE} = 20 V, I_C = 20 mA, f = 100 MHz		2.5 min		--
C_{ibo}	V_{EB} = 0.5 V, I_C = 0; 0.1≤f≤1 MHz		25 max		pf
C_{obo}	V_{CB} = 10 V, I_E = 0; 0.1≤f≤1 MHz		8 max		pf
t_{on}			35max		nsec
t_{off}			300 max		nsec

C-6. CA3018A (REFER TO FIGURE C-8)

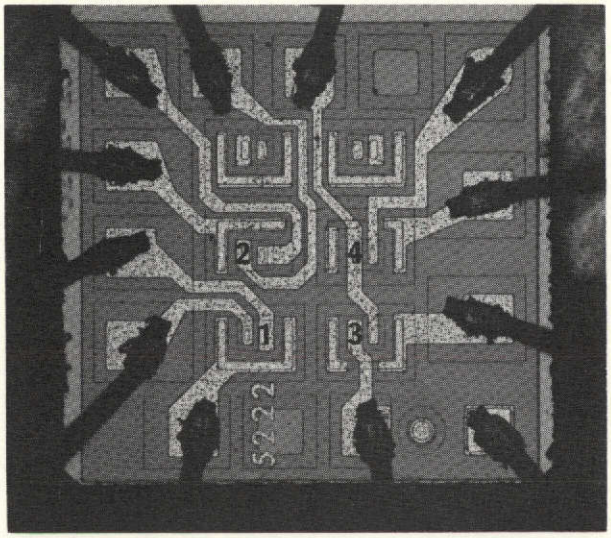

Figure C-8. CA3018A chip. Chip size is 1.06 mm x 1.06 mm (61X). (The transistor numbers appearing in Table III B-4 are as shown on the picture of the chip.)

ELECTRICAL CHARACTERISTICS (CA3018A)

Electrical Characteristics at $T_A = 25^oC$	Symbols	Special Test Conditions	CA3018A Limits			Units
			Min.	Typ.	Max.	
Static Characteristics						
Collector-Cutoff Current	I_{CBO}	$V_{CB} = 10$ V, $I_E = 0$	-	0.002	40	nA
Collector-Cutoff Current	I_{CEO}	$V_{CE} = 10$ V, $I_B = 0$	-		0.5	μA
Collector-Cutoff Current Darlington Pair	I_{CEOD}	$V_{CE} = 10$ V, $I_B = 0$	-	-	5	μA
Collector-to-Emitter Breakdown Voltage	$V_{(BR)CEO}$	$I_C = 1$ mA, $I_B = 0$	15	24	-	V
Collector-to-Base Breakdown Voltage	$V_{(BR)CBO}$	$I_C = 10$ μA, $I_E = 0$	30	60	-	V
Emitter-to-Base Breakdown Voltage	$V_{(BR)EBO}$	$I_E = 10$ μA, $I_C = 0$	5	7	-	V
Collector-to-Substrate Breakdown Voltage	$V_{(BR)CIO}$	$I_C = 10$ μA, $I_{CI} = 0$	40	60	-	V
Collector-to-Emitter Saturation Voltage	V_{CES}	$I_B = 1$ mA, $I_C = 10$ mA	-	0.23	0.5	V
Static Forward Current Transfer Ratio	h_{FE}	$V_{CE} = 3$ V, $I_C = 10$ mA $I_C = 1$ mA $I_C = 10$ μA	50 60 30	100 100 54	- - -	- - -

(Continued next page)

ELECTRICAL CHARACTERISTICS (CA3018A) (Concluded)

Electrical Characteristics at T_A = 25°C	Symbols	Special Test Conditions	CA3018A Limits			Units
			Min.	Type	Max.	
Static Characteristics						
Magnitude of Static-Beta Ratio (Isolated Transistors Q_1 and Q_2)		V_{CE} = 3 V, I_{C1} - I_{C2} = 1 mA	0.9	0.97	-	-
Static Forward Current Transfer Ratio Darlington Pair (Q_3 and Q_4)	h_{FED}	V_{CE} = 3 V, I_C = 1 mA; I_C = 100 µA	2000	5400	-	-
Base-to-Emitter Voltage	V_{BE}	V_{CE} = 3 V, I_E = 1 mA; I_E = 10 mA	0.600	0.715 0.800	0.800 0.900	V
Input Offset Voltage	$\lvert V_{BE_1} - V_{BE_2} \rvert$	V_{CE} = 3 V, I_E = 1 mA	-	0.48	2	mV
Temperature Coefficient: Base-to-Emitter Voltage Q_1 - Q_2	$\frac{\lvert \Delta V_{BE} \rvert}{\Delta T}$	V_{CE} = 3 V, I_E = 1 mA	-	1.9	-	$\frac{mV}{°C}$
Base (Q_3)-to-Emitter (Q_4) Voltage - Darlington Pair	V_{BED} (V_{9-1})	V_{CE} = 3 V; I_E = 10 mA; I_E = 1 mA	- 1.10	1.46 1.32	1.60 1.50	V
Dynamic Characteristics						
Low Frequency Noise Figure	NF	f = 1 KHz, V_{CE} = 3 V, I_C = 100 µA, Source resistance = 1KΩ	-	3.25	-	dB
Low-Frequency, Small Signal Equivalent-Circuit Characteristics:						
Forward Current-Transfer Ratio	h_{fe}		-	110	-	-
Short-Circuit Input Impedance	h_{ie}	f = 1 KHz, V_{CE} = 3 V, I_C = 1 mA	-	3.5	-	K
Open-Circuit Output Impedance	h_{oe}		-	15.6	-	mho
Open-Circuit Reverse Voltage-Transfer Ratio	h_{re}		-	1.8×10^{-4}	-	-
Admittance Characteristics:						
Forward Transfer Admittance	Y_{fe}	f = 1 MHz, V_{CE} = 3 V, I_C = 1 mA	-	31 - j1.5	-	mmho
Input Admittance	Y_{ie}		-	0.3 + j0.04	-	mmho
Output Admittance	Y_{oe}		-	0.001 + j0.03	-	mmho
Reverse Transfer Admittance	Y_{re}					mmho
Gain-Bandwidth Product	f_T	V_{CE} = 3 V, I_C = 3 mA	300	500	-	MHz
Emitter-to-Base Capacitance	C_{EB}	V_{EB} = 3 V, I_E = 0	-	0.6	-	pF
Collector-to-Base Capacitance	C_{CB}	V_{CB} = 3 V, I_C = 0	-	0.58	-	pF
Collector-to-Substrate Capacitance	C_{CI}	V_{CI} = 3 V, I_C = 0	-	2.8	-	pF

C-7. DM54L00 (REFER TO FIGURES C-9 AND C-10)

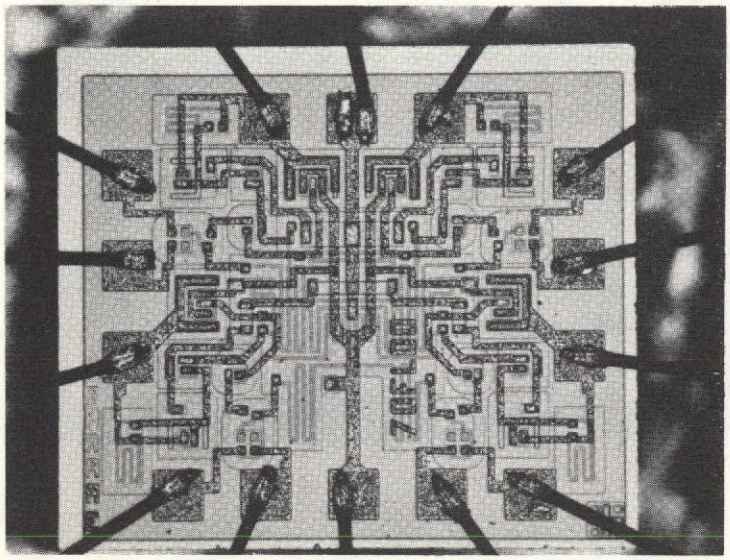

Figure C-9. DM54L00 chip. (The metallization on device No. 67 in Table 3-11 was slightly different as shown in Figure C-10.) Chip size is 1.10 mm by .95 mm (70X).

C 12

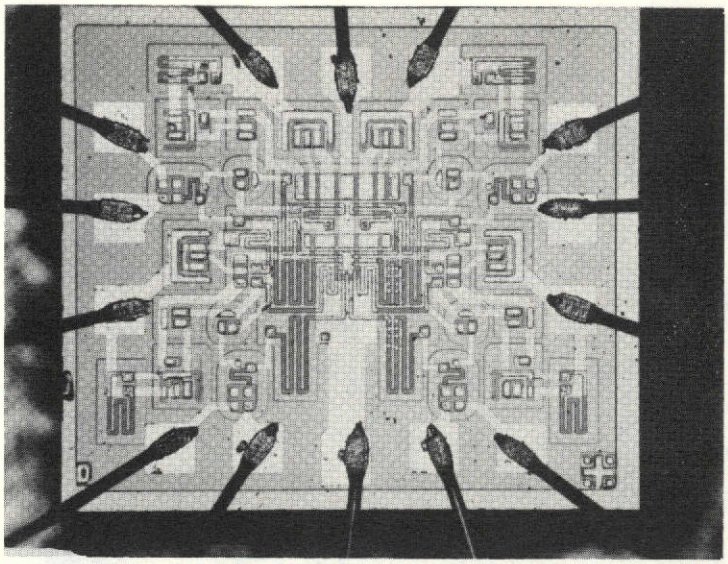

Figure C-10. DM54L00 device No. 67 chip. (The metallization on this device was slightly different from the metallization on the other DM54L00 chips.) Chip size is 1.10 mm x .95 mm (70X).

RECOMMENDED OPERATING CONDITIONS

Power Supply Voltage	4.5V to 5.5V
Operating Temperature	-55°C to 125°C
Absolute Maximum Ratings	
Power Supply Voltage	8.0V
Input Voltage	5.5V
Fan Out Logic "1"	20
Logic "0"	10

DC ELECTRICAL CHARACTERISTICS (DM54L00)

Symbol	Parameter	Conditions	Min	Typ. (Note 1)	Max	Units
$V_{IN(1)}$	Logical "1" Input Voltage	V_{CC} = MIN	2	1.3	0.7	V
$V_{IN(0)}$	Logical "0" Input Voltage	V_{CC} = MIN		1.3	0.7	V
$V_{OUT(1)}$	Logical "1" Output Voltage (Except DM54L01 DM74L01, DM54L03 DM74L03)	V_{CC} = MIN, I_{OUT} = -200 A, V_{IN} = 0.7V, Other Inputs = 2V		2.4	2.8	V
$I_{OUT(1)}$	Output Current DM54L01 DM74L03	V_{IN} = 0.3V, V_{CC} = MIN, V_{OUT} = 5.5V			50	μA
	DM54L01 DM54L03	V_{IN} = 0.6V, V_{CC} = MIN, V_{OUT} = 5.5V			200	μA
	DM74L01 DM74L03	V_{IN} = 0.7V, V_{CC} = MIN, V_{OUT} = 5.5V			200	μA
$V_{OUT(0)}$	Logical "0" Output Voltage	V_{CC} = MIN, I_{OUT} = 2 mA, V_{IN} (All Inputs) = 2V		0.15	0.3	V
		V_{CC} = MAX, V_{IN} = 2.4V		<1	10	μA
$I_{IN(1)}$	Logical "1" Input Current	Other Inputs = 0V				
		V_{CC} = MAX, V_{IN} = 5.5V			100	μA
$I_{IN(0)}$	Logical "0" Input Current	V_{CC} = MAX, V_{IN} = 0.3V, Other Inputs = 4.5V		-120	-180	μA
I_{OS}	Logical "1" Output Short-Circuit Current	V_{CC} = MAX, V_{IN} = 0V, V_{OUT} = 0V	-3	-8	-15	mA
$I_{CC(1)}$	Logical "1" State Power Supply Current (Per Gate)	V_{CC} = MAX, V_{IN} (All Inputs) = 0V, I_{OUT} = 0		120	200	μA
$I_{CC(0)}$	Logical "0" State Power Supply Current (Per Gate)	V_{CC} = MAX, V_{IN} (All Inputs) = 5V, I_{OUT} = 0		300	510	μA

Note 1: All typicals at $T_A = 25^{\circ}C$

AC ELECTRICAL CHARACTERISTICS (DM54L00)

Symbol	Parameter	Conditions	Min	Typ	Max	Units
t_{pd0}	Propagation Delay to a Logical "0" (Except DM54L01 DM74L01 DM54L03 DM74L03) DM54L30 DM74L30	V_{CC} = 5V, C_L = 50 pF T_A = 25 C		30	60	ns
				60	100	ns
t_{pd1}	Propagation Delay to a Logical "1" (Except DM54L01 DM74L01 DM54L03 DM74L03)	V_{CC} = 5V, C_L = 50 pF T_A = 25°C		25	60	ns
t_{pd0}	Propagation Delay to a Logical "0" DM54L01 DM74L01 DM54L03 DM74L03	V_{CC} = 5V, R_L = 4k C_L = 15 pF, T_A = 25°C		25	60	ns
t_{pd1}	Propagation Delay to a Logical "1" DM54L01 DM74L01 DM54L03 DM74L03	V_{CC} = 5V, R_L = 4k C_L = 15 pF, T_A = 25°C		40	90	ns

C-8. RSN54H00 (REFER TO FIGURE C-11)

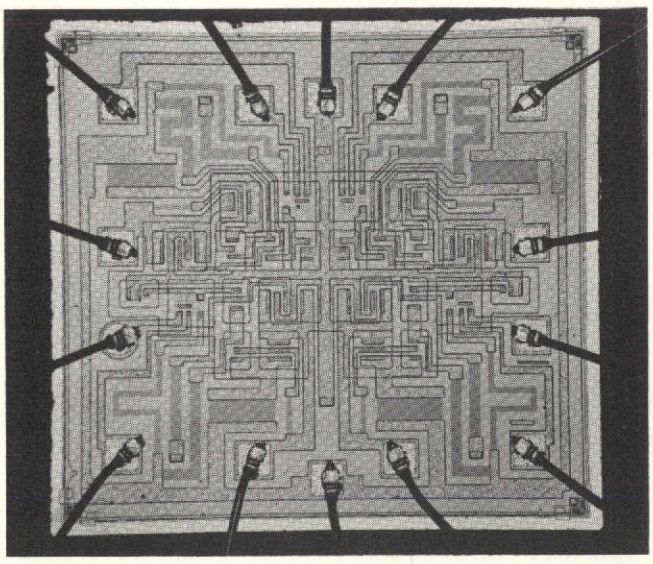

Figure C-11. RSN54H00 chip. Chip size is 1.65 mm x 1.55 mm (44X).

RECOMMENDED OPERATING CHARACTERISTICS

	Min	Nom	Max	Unit
Supply voltage, V_{CC}	4.5	5	5.5	V
Normalized fan-out from each gate, N			10	
High-level output current, I_{OH}			-500	A
Low-level output current, I_{OL}			20	mA
Operating free-air temperature, T_A	-55		125	

ELECTRICAL CHARACTERISTICS OVER RECOMMENDED OPERATING FREE-AIR TEMPERATURE RANGE (UNLESS OTHERWISE NOTED)

Parameter		Test Conditions	Min	Max	Unit
V_{IH}	High-level input voltage		2		V
V_{IL}	Low-level input voltage			0.8	V
V_{OH}	High-level output voltage	V_{CC} = MIN, V_{IL} = 0.8 V, I_{OH} = MAX	2.4		V
V_{OL}	Low-level output voltage	V_{CC} = MIN, V_{IH} = 2 V, I_{OL} = MAX		0.4	V
I_I	Input current at maximum input voltage	V_{CC} = MAX, V_I = 5.5 V		1	mA
I_{IH}	High-level input current	V_{CC} = MAX, V_I = 2.4 V		50	μA
I_{IL}	Low-level input current	V_{CC} = MAX, V_I = 0.4 V		-2	mA
I_{OS}	Short-circuit output current*	V_{CC} = MAX	-40	-120	mA
I_{CCH}	Supply current, high-level output (average per gate)	V_{CC} = MAX, V_I = 0		2.5	mA
I_{CCL}	Supply current, low-level output (average per gate)	V_{CC} = MAX, V_I = 4.5 V		10.8	mA

*Not more than one output should be shorted at a time, and the duration of the short-circuit test should not exceed one second.

SWITCHING CHARACTERISTICS, V_{CC} = 5 V, T_A = 25°C, N = 10

		Test Conditions	Min	Max	Unit
t_{PLH}	Propagation delay time, low-to-high-level output	C_L = 50 pF		12	ns
t_{PHL}	Propagation delay time, high-to-low-level output	C_L = 50 pF		12	ns

C-9. SN5473 (REFER TO FIGURE C-12)

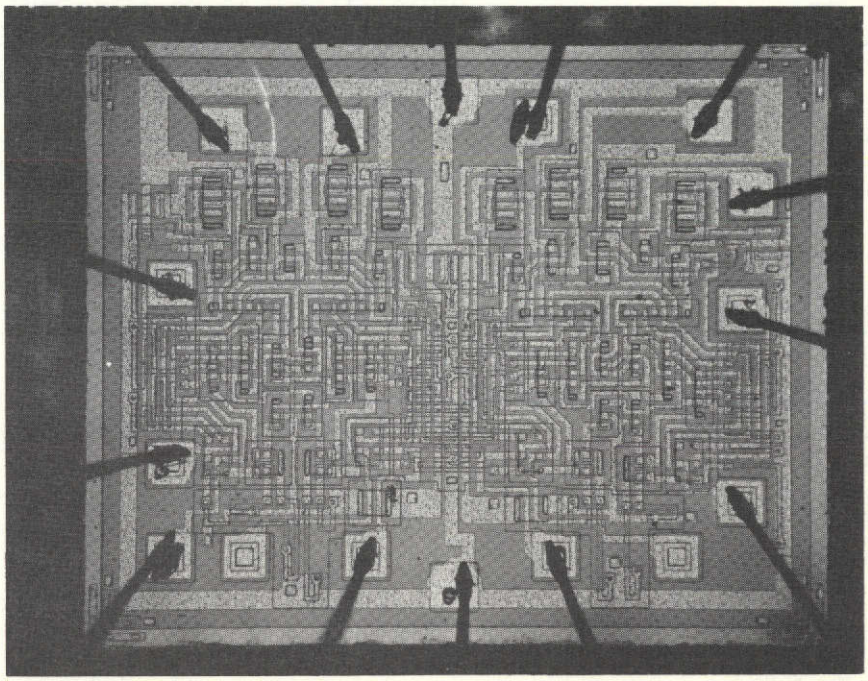

Figure C-12. SN5473 chip. Chip size is 2.34 mm x 1.90 mm (42X).

RECOMMENDED OPERATING CONDITIONS

	Min	Nom	Max	Unit
Supply voltage V_{CC}	4.5	5	5.5	V
Normalized fan-out from each output, N			10	
Width of clock pulse, $t_{p(clock)}$ (See Figure 69)	20			ns
Width of clear pulse, $t_{p(clear)}$ (See Figure 70)	25			ns
Input setup time, t_{setup} (See Figure 69)	$t_{p(clock)}$			
Input hold time, t_{hold}	0			
Operating free-air temperature range, T_A	-55	25	125	°C

ELECTRICAL CHARACTERISTICS

Parameter		Test Conditions	Min	Typ	Max	Unit
$V_{in(1)}$	Input voltage required to ensure logical 1 at any input terminal		2			V
$V_{in(0)}$	Input voltage required to ensure logical 0 at any input terminal				0.8	V
$V_{out(1)}$	Logical 1 output voltage	V_{CC} = MIN, I_{load} = -400 A	2.4	3.5		V
$V_{out(0)}$	Logical 0 output voltage	V_{CC} = MIN, I_{sink} = 16 mA		0.22	0.4	V
$I_{in(0)}$	Logical 0 level input current at J or K	V_{CC} = MAX, V_{in} = 0.4 V			-1.6	mA
$I_{in(0)}$	Logical 0 level input current at clear or clock	V_{CC} = MAX, V_{in} = 0.4 V			-3.2	mA
$I_{in(1)}$	Logical 1 level input current at J or K	V_{CC} = MAX, V_{in} = 2.4 V			40	A
		V_{CC} = MAX, V_{in} = 5.5 V			1	mA
$I_{in(1)}$	Logical 1 level input current at clear or clock	V_{CC} = MAX, V_{in} = 2.4 V			80	A
		V_{CC} = MAX, V_{in} = 5.5 V			1	mA
I_{OS}	Short-circuit output current	V_{CC} = MAX, V_{in} = 0 SN5473, SN54107	-20		-57	mA
		SN7473, SN74107	-18		-57	mA
I_{CC}	Supply current	V_{CC} = MAX		20	40	mA
All typical values are at V_{CC} = 5 V, T_A = 25°C.						

SWITCHING CHARACTERISTICS, V_{CC} = 5 V, T_A = 25°C, N = 10

Parameter		Test Conditions	Min	Typ	Max	Unit
f_{max}	Maximum clock frequency	C_L = 15 pF, R_L = 400Ω	15	20		MHz
t_{pd1}	Propagation delay time to logical 1 level from clear to output	C_L = 15 pF, R_L = 400Ω		16	25	ns
t_{pd0}	Propagation delay time to logical 0 level from clear to output	C_L = 15 pF, R_L = 400Ω		25	40	ns
t_{pd1}	Propagation delay time to logical 1 level from clock to output	C_L = 15 pF, R_L = 400Ω	10	16	25	ns
t_{pd0}	Propagation delay time to logical 0 level from clock to output	C_L = 15 pF, R_L = 400Ω	10	25	40	ns

C-10. RESULTS OF MICROCIRCUIT TESTS ON TEKTRONIX S3260 IC TESTER

Test data for all Maverick devices and representative data for normal devices are shown.

SPECIMEN # 6 (NORMAL)

********** DM54L00 **********

PASS FUNCTIONAL TEST

OUTPUT CHARACTERISTICS

Y	VOH	VOL	IOS
1	3.335 V	160.0 MV	-8.250 MA
2	3.320 V	155.0 MV	-8.250 MA
3	3.310 V	165.0 MV	-8.100 MA
4	3.320 V	165.0 MV	-8.100 MA

INPUT CHARACTERISTICS

A	IIL	IIH1	IIH2	THRESHOLD
1	-40.00 UA	545.0 NA	750.0 NA	1.306 V
2	-44.50 UA	510.0 NA	700.0 NA	1.306 V
3	-47.00 UA	420.0 NA	550.0 NA	1.306 V
4	-47.50 UA	420.0 NA	550.0 NA	1.306 V

B	IIL	IIH1	IIH2	THRESHOLD
1	-41.50 UA	570.0 NA	750.0 NA	1.306 V
2	-54.50 UA	505.0 NA	700.0 NA	1.306 V
3	-43.50 UA	430.0 NA	650.0 NA	1.306 V
4	-48.00 UA	435.0 NA	600.0 NA	1.306 V

ICCH = 395.0 UA ICCL = 1.135 MA

SWITCHING TIME CHARACTERISTICS

Y	TPDL	TPDH	TR	TF
1	46.70 NS	19.30 NS	28.30 NS	14.65 NS
2	46.20 NS	19.60 NS	20.60 NS	11.40 NS
3	46.10 NS	20.05 NS	19.90 NS	12.55 NS
4	46.90 NS	19.45 NS	20.60 NS	12.50 NS

SPECIMEN # 8 (NORMAL)

********** DM54L00 **********

PASS FUNCTIONAL TEST

OUTPUT CHARACTERISTICS

Y	VOH	VOL	IOS
1	3.340 V	165.0 MV	-8.300 MA
2	3.320 V	155.0 MV	-8.300 MA
3	3.315 V	160.0 MV	-7.950 MA
4	3.310 V	165.0 MV	-7.950 MA

INPUT CHARACTERISTICS

A	IIL	IIH1	IIH2	THRESHOLD
1	-42.50 UA	630.0 NA	850.0 NA	1.306 V
2	-45.50 UA	610.0 NA	800.0 NA	1.306 V
3	-49.50 UA	510.0 NA	700.0 NA	1.306 V
4	-49.50 UA	465.0 NA	650.0 NA	1.306 V

B	IIL	IIH1	IIH2	THRESHOLD
1	-42.00 UA	620.0 NA	850.0 NA	1.306 V
2	-55.00 UA	590.0 NA	800.0 NA	1.306 V
3	-44.00 UA	500.0 NA	700.0 NA	1.306 V
4	-51.00 UA	490.0 NA	650.0 NA	1.306 V

ICCH = 395.0 UA ICCL = 1.155 MA

SWITCHING TIME CHARACTERISTICS

Y	TPDL	TPDH	TR	TF
1	46.80 NS	19.00 NS	27.90 NS	15.30 NS
2	46.30 NS	19.85 NS	20.65 NS	11.30 NS
3	45.65 NS	20.40 NS	20.40 NS	12.50 NS
4	46.00 NS	19.30 NS	20.90 NS	12.65 NS

SPECIMEN # 9 (NORMAL)

********** DM54L00 **********

PASS FUNCTIONAL TEST

OUTPUT CHARACTERISTICS

Y	VOH	VOL	IOS
1	3.325 V	155.0 MV	-8.250 MA
2	3.325 V	150.0 MV	-8.350 MA
3	3.320 V	155.0 MV	-8.050 MA
4	3.340 V	155.0 MV	-7.850 MA

INPUT CHARACTERISTICS

A	IIL	IIH1	IIH2	THRESHOLD
1	-38.50 UA	645.0 NA	900.0 NA	1.306 V
2	-43.00 UA	655.0 NA	900.0 NA	1.306 V
3	-46.00 UA	600.0 NA	850.0 NA	1.306 V
4	-46.00 UA	550.0 NA	750.0 NA	1.306 V

B	IIL	IIH1	IIH2	THRESHOLD
1	-36.50 UA	620.0 NA	850.0 NA	1.306 V
2	-54.50 UA	670.0 NA	950.0 NA	1.306 V
3	-41.00 UA	585.0 NA	800.0 NA	1.306 V
4	-46.00 UA	570.0 NA	800.0 NA	1.306 V

ICCH = 375.0 UA ICCL = 1.075 MA

SWITCHING TIME CHARACTERISTICS

Y	TPDL	TPDH	TR	TF
1	47.40 NS	19.85 NS	28.50 NS	14.25 NS
2	44.10 NS	19.95 NS	20.50 NS	10.80 NS
3	44.70 NS	20.90 NS	20.40 NS	11.80 NS
4	46.05 NS	20.30 NS	21.60 NS	11.75 NS

SPECIMEN # 41 (MAVERICK)

********** DM54L00 **********

FAIL FUNCTIONAL TEST ****

OUTPUT CHARACTERISTICS

Y	VOH	VOL	IOS
1	-145.0 MV*	4.975 V*	-100.0 UA*
2	-500.0 MV*	4.975 V*	0.0 A*
3	-90.00 MV*	4.980 V*	-200.0 UA*
4	-230.0 MV*	4.975 V*	-50.00 UA*

INPUT CHARACTERISTICS

A	IIL	IIH1	IIH2	THRESHOLD
1	-1.024 MA*	10.23 UA*	102.3 UA*	618.7 MV
2	500.0 NA*	0.0 A	0.0 A	2.193 V
3	0.0 A	-5.000 NA*	0.0 A	2.193 V
4	-1.024 MA*	10.23 UA*	102.3 UA*	2.193 V

B	IIL	IIH1	IIH2	THRESHOLD
1	0.0 A	-5.000 NA*	0.0 A	2.193 V
2	-1.024 MA*	10.23 UA*	102.3 UA*	2.193 V
3	-1.024 MA*	10.23 UA*	102.3 UA*	2.193 V
4	500.0 NA*	-5.000 NA*	0.0 A	2.193 V

ICCH = 10.23 MA* ICCL = 10.23 MA*

SWITCHING TIME CHARACTERISTICS

Y	TPDL	TPDH	TR	TF
1	1.000 S	-1.400 NS	1.000 S	1.000 S
2	1.000 S	-550.0 PS	0.0 S	-400.0 PS
3	1.000 S	1.250 NS	0.0 S	1.000 S
4	1.000 S	-2.600 NS	0.0 S	-400.0 PS

* DOES NOT MEET SPECIFIED LIMITS

SPECIMEN # 67 (MAVERICK)

********** DM54L00 **********

PASS FUNCTIONAL TEST

OUTPUT CHARACTERISTICS

Y	VOH	VOL	IOS
1	3.255 V	175.0 MV	-9.950 MA
2	3.260 V	175.0 MV	-9.950 MA
3	3.270 V	175.0 MV	-9.550 MA
4	3.240 V	190.0 MV	-9.650 MA

INPUT CHARACTERISTICS

A	IIL	IIH1	IIH2	THRESHOLD
1	-72.00 UA	265.0 NA	350.0 NA	1.293 V
2	-71.00 UA	225.0 NA	300.0 NA	1.218 V
3	-76.00 UA	145.0 NA	200.0 NA	1.293 V
4	-79.00 UA	90.00 NA	150.0 NA	1.256 V

B	IIL	IIH1	IIH2	THRESHOLD
1	-69.50 UA	255.0 NA	350.0 NA	1.293 V
2	-91.00 UA	230.0 NA	300.0 NA	1.243 V
3	-68.00 UA	140.0 NA	200.0 NA	1.218 V
4	-77.50 UA	85.00 NA	100.0 NA	1.256 V

ICCH = 645.0 UA ICCL = 1.815 MA

SWITCHING TIME CHARACTERISTICS

Y	TPDL	TPDH	TR	TF
1	43.60 NS	15.40 NS	21.20 NS	18.65 NS
2	44.00 NS	15.60 NS	16.95 NS	14.30 NS
3	44.60 NS	16.65 NS	16.95 NS	13.70 NS
4	49.40 NS	15.40 NS	16.95 NS	15.75 NS

SPECIMEN # 116 (MAVERICK)

********** DM54L00 **********

PASS FUNCTIONAL TEST

OUTPUT CHARACTERISTICS

Y	VOH	VOL	IOS
1	3.365 V	135.0 MV	-9.250 MA
2	3.345 V	130.0 MV	-9.250 MA
3	3.370 V	130.0 MV	-9.050 MA
4	3.345 V	135.0 MV	-8.950 MA

INPUT CHARACTERISTICS

A	IIL	IIH1	IIH2	THRESHOLD
1	-53.00 UA	1.405 UA	2.100 UA	1.306 V
2	-56.00 UA	1.265 UA	1.900 UA	1.306 V
3	-62.00 UA	1.210 UA	1.850 UA	1.306 V
4	-60.00 UA	1.170 UA	1.750 UA	1.306 V

B	IIL	IIH1	IIH2	THRESHOLD
1	-53.00 UA	1.415 UA	2.150 UA	1.306 V
2	-70.00 UA	1.245 UA	1.900 UA	1.306 V
3	-54.00 UA	1.170 UA	1.750 UA	1.306 V
4	-64.00 UA	1.205 UA	1.850 UA	1.306 V

ICCH = 475.0 UA ICCL = 1.315 MA

SWITCHING TIME CHARACTERISTICS

Y	TPDL	TPDH	TR	TF
1	39.10 NS	18.80 NS	26.55 NS	13.05 NS
2	38.85 NS	19.05 NS	19.65 NS	10.50 NS
3	38.70 NS	19.50 NS	19.00 NS	11.25 NS
4	39.40 NS	19.30 NS	20.35 NS	11.30 NS

SPECIMEN # 123 (MAVERICK)

********** DM54L00 **********

PASS FUNCTIONAL TEST

OUTPUT CHARACTERISTICS

Y	VOH	VOL	IOS
1	3.355 V	145.0 MV	-9.450 MA
2	3.345 V	145.0 MV	-9.500 MA
3	3.345 V	145.0 MV	-9.250 MA
4	3.345 V	150.0 MV	-9.200 MA

INPUT CHARACTERISTICS

A	IIL	IIH1	IIH2	THRESHOLD
1	-62.00 UA	1.160 UA	1.750 UA	1.306 V
2	-65.00 UA	1.095 UA	1.650 UA	1.218 V
3	-69.50 UA	875.0 NA	1.300 UA	1.306 V
4	-69.50 UA	915.0 NA	1.350 UA	1.306 V

B	IIL	IIH1	IIH2	THRESHOLD
1	-62.50 UA	1.180 UA	1.750 UA	1.306 V
2	-60.00 UA	1.070 UA	1.600 UA	1.306 V
3	-65.50 UA	915.0 NA	1.350 UA	1.306 V
4	-76.50 UA	980.0 NA	1.500 UA	1.306 V

ICCH = 550.0 UA ICCL = 1.515 MA

SWITCHING TIME CHARACTERISTICS

Y	TPDL	TPDH	TR	TF
1	32.75 NS	14.75 NS	23.35 NS	11.30 NS
2	32.70 NS	15.00 NS	17.55 NS	9.300 NS
3	32.15 NS	16.05 NS	16.95 NS	9.950 NS
4	31.65 NS	15.10 NS	17.70 NS	10.20 NS

SPECIMEN # 125 (MAVERICK)

********** DM54L00 **********

PASS FUNCTIONAL TEST

OUTPUT CHARACTERISTICS

Y	VOH	VOL	IOS
1	3.305 V	175.0 MV	-7.950 MA
2	3.285 V	170.0 MV	-8.000 MA
3	3.325 V	175.0 MV	-7.300 MA
4	3.315 V	170.0 MV	-7.450 MA

INPUT CHARACTERISTICS

A	IIL	IIH1	IIH2	THRESHOLD
1	-34.00 UA	730.0 NA	1.350 UA	1.206 V
2	-35.00 UA	625.0 NA	1.150 UA	1.206 V
3	-37.50 UA	520.0 NA	900.0 NA	1.206 V
4	-37.00 UA	530.0 NA	950.0 NA	1.206 V

B	IIL	IIH1	IIH2	THRESHOLD
1	-34.00 UA	725.0 NA	1.350 UA	1.206 V
2	-43.00 UA	615.0 NA	1.150 UA	1.206 V
3	-34.50 UA	525.0 NA	950.0 NA	1.206 V
4	-40.50 UA	570.0 NA	1.050 UA	1.206 V

ICCH = 275.0 UA ICCL = 835.0 UA

SWITCHING TIME CHARACTERISTICS

Y	TPDL	TPDH	TR	TF
1	49.40 NS	22.00 NS	30.85 NS	14.85 NS
2	49.55 NS	22.30 NS	22.75 NS	11.85 NS
3	48.20 NS	22.50 NS	23.20 NS	12.50 NS
4	48.80 NS	22.40 NS	24.20 NS	12.70 NS

SPECIMEN # 1 (NORMAL)

********** RSN5400 **********

PASS FUNCTIONAL TEST

OUTPUT CHARACTERISTICS

Y	VOH	VOL	IOS
1	4.370 V	260.0 MV	-51.40 MA
2	4.360 V	260.0 MV	-51.40 MA
3	4.375 V	270.0 MV	-50.90 MA
4	4.365 V	270.0 MV	-51.20 MA

INPUT CHARACTERISTICS

A	IIL	IIH1	IIH2	THRESHOLD
1	-590.0 UA	1.350 UA	1.500 UA	1.406 V
2	-605.0 UA	1.550 UA	2.000 UA	1.418 V
3	-675.0 UA	1.350 UA	1.500 UA	1.406 V
4	-715.0 UA	1.600 UA	2.000 UA	1.418 V

B	IIL	IIH1	IIH2	THRESHOLD
1	-620.0 UA	1.400 UA	2.000 UA	1.418 V
2	-755.0 UA	1.450 UA	2.000 UA	1.418 V
3	-660.0 UA	1.450 UA	2.000 UA	1.406 V
4	-685.0 UA	1.550 UA	2.000 UA	1.418 V

ICCH = 4.900 MA ICCL = 16.60 MA

SWITCHING TIME CHARACTERISTICS

Y	TPDL	TPDH	TR	TF
1	15.95 NS	5.950 NS	1.250 NS	7.950 NS
2	16.50 NS	6.350 NS	100.0 PS	6.000 NS
3	16.60 NS	7.100 NS	50.00 PS	6.300 NS
4	14.90 NS	6.950 NS	2.450 NS	7.250 NS

SPECIMEN # 4 (NORMAL)

********** RSN5400 **********

PASS FUNCTIONAL TEST

OUTPUT CHARACTERISTICS

Y	VOH	VOL	IOS
1	4.440 V	265.0 MV	-52.20 MA
2	4.425 V	265.0 MV	-52.65 MA
3	4.425 V	275.0 MV	-51.80 MA
4	4.425 V	280.0 MV	-52.05 MA

INPUT CHARACTERISTICS

A	IIL	IIH1	IIH2	THRESHOLD
1	-605.0 UA	1.250 UA	1.500 UA	1.418 V
2	-595.0 UA	1.400 UA	2.000 UA	1.406 V
3	-675.0 UA	1.250 UA	1.500 UA	1.418 V
4	-730.0 UA	1.250 UA	1.500 UA	1.418 V

B	IIL	IIH1	IIH2	THRESHOLD
1	-605.0 UA	1.250 UA	1.500 UA	1.431 V
2	-730.0 UA	1.300 UA	1.500 UA	1.418 V
3	-635.0 UA	1.300 UA	1.500 UA	1.418 V
4	-670.0 UA	1.150 UA	1.500 UA	1.418 V

ICCH = 4.900 MA ICCL = 16.60 MA

SWITCHING TIME CHARACTERISTICS

Y	TPDL	TPDH	TR	TF
1	15.40 NS	5.750 NS	1.000 NS	7.500 NS
2	15.80 NS	6.000 NS	100.0 PS	5.800 NS
3	15.50 NS	6.750 NS	0.0 S	6.000 NS
4	13.65 NS	6.550 NS	1.850 NS	7.000 NS

SPECIMEN # 6 (NORMAL)

********** RSN5400 **********

PASS FUNCTIONAL TEST

OUTPUT CHARACTERISTICS

Y	VOH	VOL	IOS
1	4.385 V	250.0 MV	-53.15 MA
2	4.355 V	245.0 MV	-53.35 MA
3	4.360 V	250.0 MV	-52.80 MA
4	4.340 V	260.0 MV	-52.60 MA

INPUT CHARACTERISTICS

A	IIL	IIH1	IIH2	THRESHOLD
1	-635.0 UA	1.050 UA	1.500 UA	1.418 V
2	-645.0 UA	1.000 UA	1.500 UA	1.406 V
3	-720.0 UA	1.000 UA	1.500 UA	1.431 V
4	-760.0 UA	950.0 NA	1.500 UA	1.418 V

B	IIL	IIH1	IIH2	THRESHOLD
1	-640.0 UA	1.050 UA	1.500 UA	1.431 V
2	-805.0 UA	950.0 NA	1.500 UA	1.418 V
3	-690.0 UA	1.050 UA	1.500 UA	1.418 V
4	-720.0 UA	900.0 NA	1.500 UA	1.418 V

ICCH = 5.100 MA ICCL = 15.75 MA

SWITCHING TIME CHARACTERISTICS

Y	TPDL	TPDH	TR	TF
1	15.20 NS	5.500 NS	700.0 PS	7.950 NS
2	15.55 NS	5.950 NS	100.0 PS	5.900 NS
3	15.45 NS	6.550 NS	0.0 S	6.000 NS
4	14.05 NS	6.450 NS	1.800 NS	7.050 NS

SPECIMEN # 12 (NORMAL)

********** RSN5400 **********

PASS FUNCTIONAL TEST

OUTPUT CHARACTERISTICS

Y	VOH	VOL	IOS
1	4.465 V	270.0 MV	-51.65 MA
2	4.445 V	265.0 MV	-51.45 MA
3	4.455 V	270.0 MV	-51.40 MA
4	4.455 V	280.0 MV	-51.40 MA

INPUT CHARACTERISTICS

A	IIL	IIH1	IIH2	THRESHOLD
1	-580.0 UA	1.200 UA	1.500 UA	1.418 V
2	-595.0 UA	1.350 UA	2.000 UA	1.406 V
3	-660.0 UA	1.150 UA	1.500 UA	1.418 V
4	-720.0 UA	1.200 UA	1.500 UA	1.418 V

B	IIL	IIH1	IIH2	THRESHOLD
1	-615.0 UA	1.250 UA	1.500 UA	1.418 V
2	-710.0 UA	1.250 UA	1.500 UA	1.418 V
3	-645.0 UA	1.250 UA	1.500 UA	1.418 V
4	-680.0 UA	1.150 UA	1.500 UA	1.418 V

ICCH = 4.900 MA ICCL = 15.10 MA

SWITCHING TIME CHARACTERISTICS

Y	TPDL	TPDH	TR	TF
1	15.60 NS	5.700 NS	1.000 NS	7.850 NS
2	16.35 NS	6.100 NS	100.0 PS	5.850 NS
3	15.80 NS	6.900 NS	0.0 S	6.050 NS
4	14.00 NS	6.650 NS	1.950 NS	7.000 NS

SPECIMEN # 5 (MAVERICK)

********** RSN5400 **********

PASS FUNCTIONAL TEST

OUTPUT CHARACTERISTICS

Y	VOH	VOL	IOS
1	3.820 V	225.0 MV	-51.45 MA
2	3.815 V	220.0 MV	-51.30 MA
3	3.840 V	215.0 MV	-50.70 MA
4	3.835 V	240.0 MV	-51.20 MA

INPUT CHARACTERISTICS

A	IIL	IIH1	IIH2	THRESHOLD
1	-530.0 UA	1.750 UA	2.500 UA	1.393 V
2	-545.0 UA	1.850 UA	2.500 UA	1.393 V
3	-610.0 UA	1.650 UA	2.000 UA	1.406 V
4	-640.0 UA	1.800 UA	2.500 UA	1.406 V

B	IIL	IIH1	IIH2	THRESHOLD
1	-565.0 UA	1.900 UA	2.500 UA	1.418 V
2	-670.0 UA	1.700 UA	2.000 UA	1.418 V
3	-580.0 UA	1.750 UA	2.500 UA	1.393 V
4	-625.0 UA	1.700 UA	2.000 UA	1.406 V

ICCH = 4.300 MA ICCL = 14.70 MA

SWITCHING TIME CHARACTERISTICS

Y	TPDL	TPDH	TR	TF
1	15.25 NS	5.500 NS	900.0 PS	7.050 NS
2	15.35 NS	5.900 NS	100.0 PS	5.550 NS
3	14.75 NS	6.650 NS	0.0 S	5.450 NS
4	13.15 NS	6.450 NS	1.650 NS	6.700 NS

SPECIMEN # 56 (MAVERICK)

********** RSN5400 **********

PASS FUNCTIONAL TEST

OUTPUT CHARACTERISTICS

Y	VOH	VOL	IOS
1	4.625 V	235.0 MV	-52.00 MA
2	4.795 V	235.0 MV	-51.60 MA
3	4.790 V	240.0 MV	-51.05 MA
4	4.795 V	240.0 MV	-51.75 MA

INPUT CHARACTERISTICS

A	IIL	IIH1	IIH2	THRESHOLD
1	-575.0 UA	4.100 UA	5.500 UA	1.393 V
2	-565.0 UA	4.300 UA	5.500 UA	1.393 V
3	-650.0 UA	4.000 UA	5.000 UA	1.418 V
4	-690.0 UA	4.200 UA	5.500 UA	1.393 V

B	IIL	IIH1	IIH2	THRESHOLD
1	-595.0 UA	4.350 UA	5.500 UA	1.418 V
2	-710.0 UA	4.100 UA	5.500 UA	1.418 V
3	-630.0 UA	4.250 UA	5.500 UA	1.406 V
4	-660.0 UA	3.950 UA	5.000 UA	1.418 V

ICCH = 4.900 MA ICCL = 15.15 MA

SWITCHING TIME CHARACTERISTICS

Y	TPDL	TPDH	TR	TF
1	14.30 NS	5.600 NS	1.050 NS	6.400 NS
2	14.60 NS	6.000 NS	100.0 PS	5.450 NS
3	14.60 NS	7.150 NS	50.00 PS	4.950 NS
4	12.50 NS	6.750 NS	1.750 NS	6.600 NS

SPECIMEN # 93 (MAVERICK)

********** RSN5400 **********

PASS FUNCTIONAL TEST

OUTPUT CHARACTERISTICS

Y	VOH	VOL	IOS
1	4.625 V	270.0 MV	-54.75 MA
2	4.600 V	265.0 MV	-54.75 MA
3	4.615 V	270.0 MV	-53.90 MA
4	4.660 V	270.0 MV	-54.00 MA

INPUT CHARACTERISTICS

A	IIL	IIH1	IIH2	THRESHOLD
1	-620.0 UA	1.850 UA	2.500 UA	1.418 V
2	-720.0 UA	2.450 UA	3.000 UA	1.418 V
3	-700.0 UA	1.900 UA	2.500 UA	1.418 V
4	-825.0 UA	650.0 NA	1.000 UA	1.368 V

B	IIL	IIH1	IIH2	THRESHOLD
1	-730.0 UA	2.300 UA	3.000 UA	1.443 V
2	-780.0 UA	1.900 UA	2.500 UA	1.431 V
3	-760.0 UA	2.300 UA	3.000 UA	1.418 V
4	-720.0 UA	550.0 NA	1.000 UA	1.368 V

ICCH = 5.100 MA ICCL = 19.60 MA

SWITCHING TIME CHARACTERISTICS

Y	TPDL	TPDH	TR	TF
1	13.15 NS	5.200 NS	400.0 PS	6.450 NS
2	13.30 NS	5.600 NS	100.0 PS	5.400 NS
3	13.35 NS	6.500 NS	0.0 S	3.800 NS
4	11.60 NS	6.400 NS	1.300 NS	6.000 NS

SPECIMEN # 99 (MAVERICK)

********** RSN5400 **********

PASS FUNCTIONAL TEST

OUTPUT CHARACTERISTICS

Y	VOH	VOL	IOS
1	3.995 V	270.0 MV	-55.75 MA
2	3.980 V	275.0 MV	-55.75 MA
3	4.005 V	285.0 MV	-55.15 MA
4	3.930 V	285.0 MV	-54.90 MA

INPUT CHARACTERISTICS

A	IIL	IIH1	IIH2	THRESHOLD
1	-650.0 UA	1.350 UA	2.000 UA	1.418 V
2	-660.0 UA	1.500 UA	2.000 UA	1.393 V
3	-740.0 UA	1.400 UA	2.000 UA	1.418 V
4	-790.0 UA	500.0 NA	1.000 UA	1.381 V

B	IIL	IIH1	IIH2	THRESHOLD
1	-685.0 UA	1.450 UA	2.000 UA	1.431 V
2	-810.0 UA	1.400 UA	2.000 UA	1.431 V
3	-710.0 UA	1.500 UA	2.000 UA	1.418 V
4	-735.0 UA	450.0 NA	1.000 UA	1.406 V

ICCH = 5.100 MA ICCL = 19.80 MA

SWITCHING TIME CHARACTERISTICS

Y	TPDL	TPDH	TR	TF
1	14.75 NS	5.350 NS	550.0 PS	7.400 NS
2	15.20 NS	5.800 NS	100.0 PS	5.800 NS
3	15.30 NS	6.550 NS	0.0 S	5.950 NS
4	13.30 NS	6.350 NS	1.550 NS	6.850 NS

SPECIMEN # 7 (NORMAL)

********** SN5473W **********

PASS FUNCTIONAL TEST

MINIMUM CLOCK PULSE WIDTH FOR PROPER OPERATION

CLOCK 1	13.00 NS AT 2.0V	12.00 NS AT 4.5V
CLOCK 2	12.00 NS AT 2.0V	11.00 NS AT 4.5V

OUTPUT CHARACTERISTICS

OUTPUT	VOH	VOL	IOS
Q1	3.580 V	271.0 MV	-19.75 MA*
QN1	3.580 V	277.5 MV	-23.00 MA
Q2	3.580 V	280.5 MV	-19.30 MA*
QN2	3.575 V	289.5 MV	-24.40 MA

INPUT CHARACTERISTICS

INPUT	IIL	IIH1	IIH2	THRESHOLD
CLOCK 1	-1.740 MA	-270.5 UA	4.135 UA	1.387 V
CLOCK 2	-1.725 MA	-271.5 UA	3.955 UA	1.387 V
J1	-927.0 UA	1.015 UA	1.405 UA	1.387 V
K1	-957.5 UA	1.655 UA	2.265 UA	1.437 V
J2	-932.0 UA	1.635 UA	2.265 UA	1.387 V
K2	-948.0 UA	1.015 UA	1.400 UA	1.412 V
CLEAR 1	-932.0 UA	16.00 UA	21.90 UA	1.387 V
CLEAR 2	-923.0 UA	15.50 UA	20.90 UA	1.362 V

SWITCHING TIME CHARACTERISTICS

IN TO OUT	TPDL	TPDH	TR	TF
SPEC LIMIT	40NS	25NS		
CLEAR TO Q1	25.00 NS	----		
CLEAR TO QN1	----	11.60 NS		
CLEAR TO Q2	25.25 NS	----		
CLEAR TO QN2	----	12.40 NS		
CLOCK TO Q1	26.15 NS	13.65 NS	15.35 NS	7.700 NS
CLOCK TO QN1	23.70 NS	15.30 NS	11.40 NS	5.650 NS
CLOCK TO Q2	26.15 NS	14.35 NS	11.90 NS	5.650 NS
CLOCK TO QN2	25.00 NS	15.95 NS	11.30 NS	5.750 NS

POWER SUPPLY CURRENT = 25.25 MA

SPECIMEN # 10 (NORMAL)

********** SN5473W **********

PASS FUNCTIONAL TEST

MINIMUM CLOCK PULSE WIDTH FOR PROPER OPERATION

CLOCK 1	13.00 NS AT 2.0V	12.00 NS AT 4.5V
CLOCK 2	11.00 NS AT 2.0V	11.00 NS AT 4.5V

OUTPUT CHARACTERISTICS

OUTPUT	VOH	VOL	IOS
Q1	3.615 V	255.5 MV	-20.55 MA
QN1	3.615 V	263.5 MV	-24.10 MA
Q2	3.615 V	265.0 MV	-20.10 MA
QN2	3.615 V	275.5 MV	-25.45 MA

INPUT CHARACTERISTICS

INPUT	IIL	IIH1	IIH2	THRESHOLD
CLOCK 1	-1.900 MA	-301.0 UA	4.410 UA	1.162 V
CLOCK 2	-1.900 MA	-306.0 UA	4.250 UA	1.212 V
J1	-1.000 MA	1.040 UA	1.390 UA	1.337 V
K1	-1.010 MA	2.060 UA	2.735 UA	1.362 V
J2	-1.000 MA	2.190 UA	2.925 UA	1.337 V
K2	-1.010 MA	1.035 UA	1.375 UA	1.362 V
CLEAR 1	-1.000 MA	19.00 UA	25.20 UA	1.362 V
CLEAR 2	-989.5 UA	19.50 UA	25.55 UA	1.337 V

SWITCHING TIME CHARACTERISTICS

IN TO OUT	TPDL	TPDH	TR	TF
SPEC LIMIT	40NS	25NS		
CLEAR TO Q1	22.25 NS	----		
CLEAR TO QN1	----	10.90 NS		
CLEAR TO Q2	22.55 NS	----		
CLEAR TO QN2	----	11.60 NS		
CLOCK TO Q1	22.05 NS	12.00 NS	13.00 NS	7.100 NS
CLOCK TO QN1	20.65 NS	12.85 NS	10.20 NS	5.050 NS
CLOCK TO Q2	22.40 NS	12.55 NS	10.40 NS	5.100 NS
CLOCK TO QN2	21.80 NS	13.80 NS	9.850 NS	5.350 NS

POWER SUPPLY CURRENT = 28.00 MA

SPECIMEN # 20 (MAVERICK)

********** SN5473W **********

PASS FUNCTIONAL TEST

MINIMUM CLOCK PULSE WIDTH FOR PROPER OPERATION

CLOCK 1	13.00 NS AT 2.0V	12.00 NS AT 4.5V
CLOCK 2	11.00 NS AT 2.0V	11.00 NS AT 4.5V

OUTPUT CHARACTERISTICS

OUTPUT	VOH	VOL	IOS
Q1	3.615 V	243.5 MV	-20.60 MA
QN1	3.615 V	251.0 MV	-24.05 MA
Q2	3.615 V	253.5 MV	-20.10 MA
QN2	3.615 V	263.5 MV	-25.15 MA

INPUT CHARACTERISTICS

INPUT	IIL	IIH1	IIH2	THRESHOLD
CLOCK 1	-1.870 MA	-291.5 UA	4.645 UA	1.162 V
CLOCK 2	-1.870 MA	-302.0 UA	4.335 UA	1.212 V
J1	-917.0 UA	1.190 UA	1.605 UA	1.312 V
K1	-1.000 MA	1.750 UA	2.325 UA	1.362 V
J2	-990.0 UA	1.770 UA	2.370 UA	1.312 V
K2	-1.006 MA	1.100 UA	1.480 UA	1.362 V
CLEAR 1	-981.0 UA	20.00 UA	26.60 UA	1.362 V
CLEAR 2	-978.0 UA	20.00 UA	26.25 UA	1.337 V

SWITCHING TIME CHARACTERISTICS

IN TO OUT	TPDL	TPDH	TR	TF
SPEC LIMIT	40NS	25NS		
CLEAR TO Q1	22.45 NS	----		
CLEAR TO QN1	----	10.90 NS		
CLEAR TO Q2	22.60 NS	----		
CLEAR TO QN2	----	11.50 NS		
CLOCK TO Q1	22.20 NS	11.85 NS	13.20 NS	7.000 NS
CLOCK TO QN1	20.65 NS	12.85 NS	10.30 NS	5.050 NS
CLOCK TO Q2	22.40 NS	12.45 NS	10.50 NS	5.100 NS
CLOCK TO QN2	21.75 NS	13.75 NS	10.00 NS	5.250 NS

POWER SUPPLY CURRENT = 28.05 MA

SPECIMEN # 43 (MAVERICK)

********** SN5473W **********

PASS FUNCTIONAL TEST

MINIMUM CLOCK PULSE WIDTH FOR PROPER OPERATION

CLOCK 1	13.00 NS AT 2.0V	12.00 NS AT 4.5V
CLOCK 2	11.00 NS AT 2.0V	11.00 NS AT 4.5V

OUTPUT CHARACTERISTICS

OUTPUT	VOH	VOL	IOS
Q1	2.845 V	241.0 MV	-20.30 MA
QN1	3.575 V	247.0 MV	-23.60 MA
Q2	3.590 V	250.0 MV	-19.80 MA*
QN2	2.850 V	257.5 MV	-24.50 MA

INPUT CHARACTERISTICS

INPUT	IIL	IIH1	IIH2	THRESHOLD
CLOCK 1	-1.750 MA	-255.0 UA	5.725 UA	2.187 V
CLOCK 2	-1.725 MA	-257.5 UA	5.460 UA	2.187 V
J1	-948.0 UA	1.340 UA	1.880 UA	2.187 V
K1	-952.5 UA	2.320 UA	3.235 UA	2.187 V
J2	-927.0 UA	2.315 UA	3.250 UA	2.187 V
K2	-953.5 UA	1.355 UA	1.890 UA	2.187 V
CLEAR 1	-946.5 UA	25.50 UA	35.40 UA	1.362 V
CLEAR 2	-912.0 UA	20.00 UA	27.75 UA	2.187 V

SWITCHING TIME CHARACTERISTICS

IN	TO OUT	TPDL	TPDH	TR	TF
SPEC LIMIT		40NS	25NS		
CLEAR	TO Q1	24.40 NS	----		
CLEAR	TO QN1	----	11.30 NS		
CLEAR	TO Q2	24.50 NS	----		
CLEAR	TO QN2	----	12.20 NS		
CLOCK	TO Q1	25.05 NS	12.80 NS	14.65 NS	7.500 NS
CLOCK	TO QN1	22.20 NS	14.65 NS	11.30 NS	-299.9 PS
CLOCK	TO Q2	24.85 NS	13.80 NS	11.60 NS	5.450 NS
CLOCK	TO QN2	23.75 NS	15.30 NS	11.10 NS	5.650 NS

POWER SUPPLY CURRENT = 25.55 MA